ALPHA PARTICLE STATES IN LIGHT NUCLEI

BY

DAVID RONALD GRIGGS

A DISSERTATION PRESENTED TO THE GRADUATE COUNCIL OF
THE UNIVERSITY OF FLORIDA
IN PARTIAL FULFILLMENT OF THE REQUIREMENTS FOR THE
DEGREE OF DOCTOR OF PHILOSOPHY

UNIVERSITY OF FLORIDA

1977

ACKNOWLEDGMENTS

The author would like to thank all those who helped with the performance of the experiments and gave advice: Dr. Henry R. Weller, Dr. Richard A. Blue, Dr. Juan J. Ramirez, and Dr. E. M. Bernstein. Special thanks go to Mr. Gary E. Rochau for all his particularly skillful and personable assistance.

TABLE OF CONTENTS

Page

ACKNOWLEDGMENTS ii

LIST OF TABLES iv

LIST OF FIGURES v

ABSTRACT vii

CHAPTER

I. INTRODUCTION 1

II. EXPERIMENTAL PROCEDURE 9

- A. $^{10}B(p,\alpha_0)^7Be$ and $^{10}B(p,\alpha_1)^7Be^*$ 9
- B. $^{10}B(d,d)^{10}B$ and $^{10}B(d,\alpha)^8Be$ 16
- C. $^{10}B(\alpha,\alpha_0)^{10}B$ 21
- D. $^{10}B(\alpha,\alpha_1)^{10}B^*$ 23

III. THEORY 25

- A. R-Matrix 25
- B. Angular Distributions and Legendre Polynomial Fitting 29
- C. Optical Model 33
- D. APCETS 35

IV. EXPERIMENTAL RESULTS 39

- A. ^{11}C 39
- B. ^{12}C 63
- C. ^{14}N 85

V. CONCLUSION 105

APPENDICES

- A. MULTI 116
- B. ZBAR 120
- C. Target Preparation 125

BIBLIOGRAPHY 127

BIOGRAPHICAL SKETCH 132

LIST OF TABLES

Table | Page

1. Legendre Polynomial Coefficients for Angular Distributions of $^{10}B(p,\alpha_0)^7Be$ Reaction.................................... 48

2. Legendre Polynomial Coefficients for Angular Distributions of $^{10}B(p,\alpha_1)^7Be$ Reaction.................................... 60

3. Optical Model Parameters for the Fit to the 10B(d,d)^{10}B Angular Distribution at E_d = 1.50 MeV.................................... 72

4. Legendre Polynomial Coefficients for Angular Distributions of $^{10}B(d,\alpha_0)^8Be$ Reaction.................................... 79

5. $^{10}B(\alpha,\alpha_0)^{10}B$ Level Parameters, E_α = 2.0 to 4.0 MeV.................................... 87

6. $^{10}B(\alpha,\alpha_0)^{10}B$ Level Parameters, E_α = 4.0 to 9.0 MeV.................................... 94

7. ^{14}N Energy Levels E_x = 14.4 to 18.2 MeV......102

LIST OF FIGURES

Figure Page

1. Possible Alpha Particle Core Excited Threshold States in ^{15}N and ^{15}O 4

2. Excitation Curve for the $^{10}B(p,\alpha_0)^7Be$ and $^{10}B(p,\alpha_1)^7Be^*$ Reactions; from [Ce56] and [Je64].. 6

3. Charged Particle Spectrum from the Proton Bombardment of ^{10}B 12

4. Charged Particle Spectrum from the Proton Bombardment of ^{10}B 15

5. Charged Particle Spectrum from the Deuteron Bombardment of ^{10}B 17

6. Alpha Particle Spectrum Resulting from the Deuteron Bombardment of ^{10}B 20

7. Charged Particle Spectrum from the Alpha Bombardment of ^{10}B 22

8. Charged Particle Spectrum from the Alpha Bombardment of ^{10}B 24

9. Excitation Curves for the $^{10}B(p,\alpha_0)^7Be$ and $^{10}B(p,\alpha_1)^7Be^*$ Reactions between 0.8 Mev and 3.25 MeV 44

10. Measured Angular Distributions and Legendre Polynomial Fits for the $^{10}B(p,\alpha_0)^7Be$ Reaction. 47

11. The Legendre Coefficient Resulting from the Fits to the $^{10}B(p,\alpha_0)^7Be$ Angular Distributions 52

12. Legendre Coefficient Ratios Resulting from the Fits to the $^{10}B(p,\alpha_0)^7Be$ Angular Distributions 54

Figure Page

13. The Measured Angular Distributions and Legendre Polynomial Fits for the $^{10}B(p,\alpha_1)^7Be^*$ Reaction 59

14. The Legendre Coefficients Resulting from the Fits to the $^{10}B(d,\alpha_1)^7Be^*$ Angular Distribution 62

15. Excitation Curve for the $^{10}B(d,d)^{10}B$ Cross Section at $\Theta_{Lab} = 150°$ 66

16. The Measured Angular Distributions for the $^{10}B(d,d)^{10}B$ Reaction 69

17. Measured and Theoretical Angular Distribution for the $^{10}B(d,d)^{10}B$ Reaction at E_d = 1.5 MeV 71

18. Excitation Curves for the $^{10}B(d,\alpha_0)^8Be$ and $^{10}B(d,\alpha_1)^8Be^*$ Reactions 74

19. The Measured Angular Distributions and Legendre Polynomial Fits for the $^{10}B(d,\alpha_0)^8Be$ Reaction 77

20. The Legendre Coefficients for the Fits to the Angular Distributions of $^{10}B(d,\alpha_0)^8Be$... 81

21. Excitation Curves for the $^{10}B(\alpha,\alpha_1)^{10}B^*$ Reaction 89

22. Excitation Curves and R-matrix Fits for the $^{10}B(\alpha,\alpha_0)^{10}B$ Reaction 94

23. Results of Calculation of Level Shape Dependence on r_0 100

24. APCETS Identification of Levels in ^{11}C and ^{12}C 108

25. Level Diagram of ^{14}N 112

26. Energy Conversion Scales: E_{LAB} to E_x 115

Abstract of Disseration Presented to the Graduate Council
of the University of Florida
in Partial Fulfillment of the Requirements for the
Degree of Doctor of Philosophy

ALPHA PARTICLE STATES IN LIGHT NUCLEI

By David Ronald Griggs

August, 1977

Chairman: Henry R. Weller
Major Department: Physics and Astronomy

We have measured the reaction cross-sections for the reaction $^{10}B(p,\alpha)^{7}Be$ for proton energies from 0.8 to 2.5 MeV, the $^{10}B(d,\alpha)^{8}Be$ reaction for deuteron energies of 0.8 to 4.0 MeV, and the $^{10}B(\alpha,\alpha)$ reaction for alpha energies from 4.0 to 9.0 MeV. In each case resonances are observed which might suggest the existence of alpha-particle configurations in the appropriate compound nucleus. In the case of ^{11}C, we see two states which appear to be $^{7}Be + \alpha$ and $^{7}Be^{*}_{.43} + \alpha$. In ^{12}C, we again see two states which might be interpreted as $^{8}Be + \alpha$ and $^{8}Be^{*}_{2.9} + \alpha$ configurations. The present measurement of the reaction $^{10}B(\alpha,\alpha)$ extends the previous measurements to higher energies.
The data for $4 < E_{\alpha} < 7$ MeV are dominated by several strong resonances which have been fitted using an R-matrix calculation.

CHAPTER I

INTRODUCTION

It is well known that the ^{4}He nucleus or alpha particle is a strongly bound low mass nuclear system. This fact has led to the development of "cluster models" with the hope of simplifying the explanations of level structures in certain nuclei (e.g., [Wi66]). The most successful applications of this model have been in dealing with alpha-particle nuclei, i.e., those light even-even nuclei which have atomic numbers evenly divisible by four, such as ^{12}C or ^{20}Ne. As an extension of this picture, it has been suggested that as soon as the excitation of a compound system is high enough to allow alpha decay, there may be a tendency for the formation of a relatively stable alpha cluster outside an A-4 core, with any excess energy used in exciting the core of remaining nucleons. If this configuration does occur, we might expect to observe resonances of definite spin and parity in the alpha particle exit channel at relatively high excitation energies which might be explained as the coupling of an alpha particle with orbital angular momentum L to the low-lying energy levels of the remaining A-4 nucleus (see Section III, D.). Structures which can be explained on the basis of the alpha-particle core-excited threshold states (APCETS) model have indeed been observed in ^{15}O, ^{15}N and ^{19}Ne.

In the mass fifteen case, studied by Weller, et al [We69, Ja71, Ra70, Ot71], multiplets of states have been found in the compound nuclei. In both ^{15}O and ^{15}N, the multiplets can be explained as the coupling of an $L = 1$ alpha particle to the low lying state of ^{11}C and ^{11}B, respectively, as shown in Figure 1. In the case of ^{19}Ne, the levels found in the region of 10.0 to 13.0 MeV excitation had a one-to-one correspondence to the low lying levels of ^{15}O states coupled to an $L = 0$ alpha particle. The success of the APCETS model in these cases [We72] gave impetus to find other examples where it might be applicable.

The reactions of $^{10}B(p,\alpha_0)^7Be$ and $^{10}B(p,\alpha_1)^7Be^*$ had been previously measured by Cronin [Cr56]. Excitation curves for the α_0 and α_1 exit channels (Figure 2) in the excitation region 9.7 to 10.2 MeV indicated that the possibility that two states seen in ^{11}C might be described as an alpha particle with $L = 0$ coupled to the ground $(3/2^-)$ and first excited $(1/2^-, 0.43$ MeV$)$ states of ^7Be. Higher values of angular momentum were ruled out because of the apparent absence of multiplets which should result if the orbital angular momentum of the alpha particle was greater than zero. Since these data were inconclusive, the experiment was reperformed in hopes of obtaining enough data to allow the extraction of a more definite conclusion.

The reaction $^{10}B(\alpha,\alpha_0)^{10}B$ had been measured for alpha energies of 1.0 to 4.3 MeV by Mo and Weller [Mo73]. In this excitation region (see Figure 26 for conversions between

Figure 1. Possible Alpha Particle Core Excited Threshold States in ^{15}N and ^{15}O; from [We72]

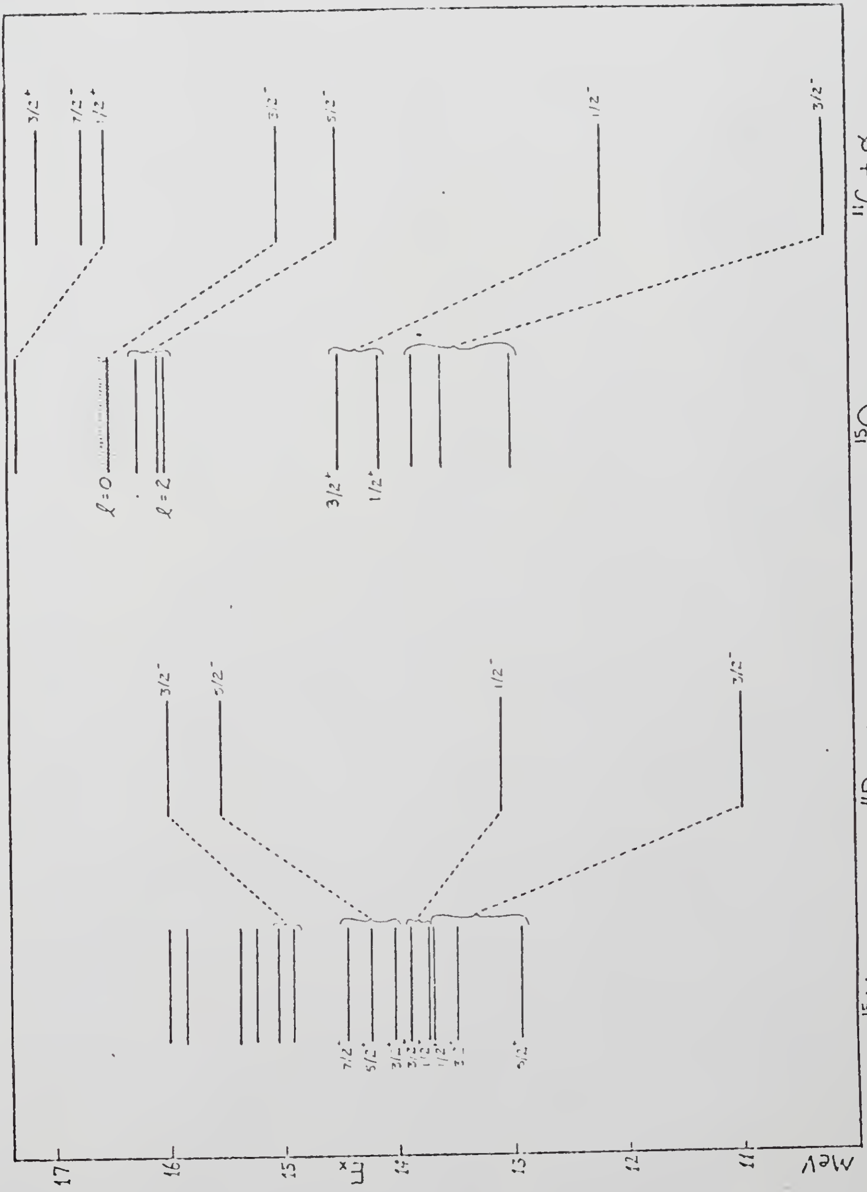
MeV
E_x
17
16
15
14
13
12
11
^{15}N
$^{11}B + \alpha$
^{15}O
$^{11}C + \alpha$
7/2⁺
5/2⁺
3/2⁺
1/2⁺
5/2⁺
3/2⁻
5/2⁻
1/2⁻
3/2⁺
1/2⁺
ℓ = 0
ℓ = 2
7/2⁻
1/2⁺

Figure 2. Excitation Curve for the $^{10}B(p,\alpha_0)^7Be$ and $^{10}B(p,\alpha_1)^7Be^*$ Reactions; from [Ce56] and [Je64]

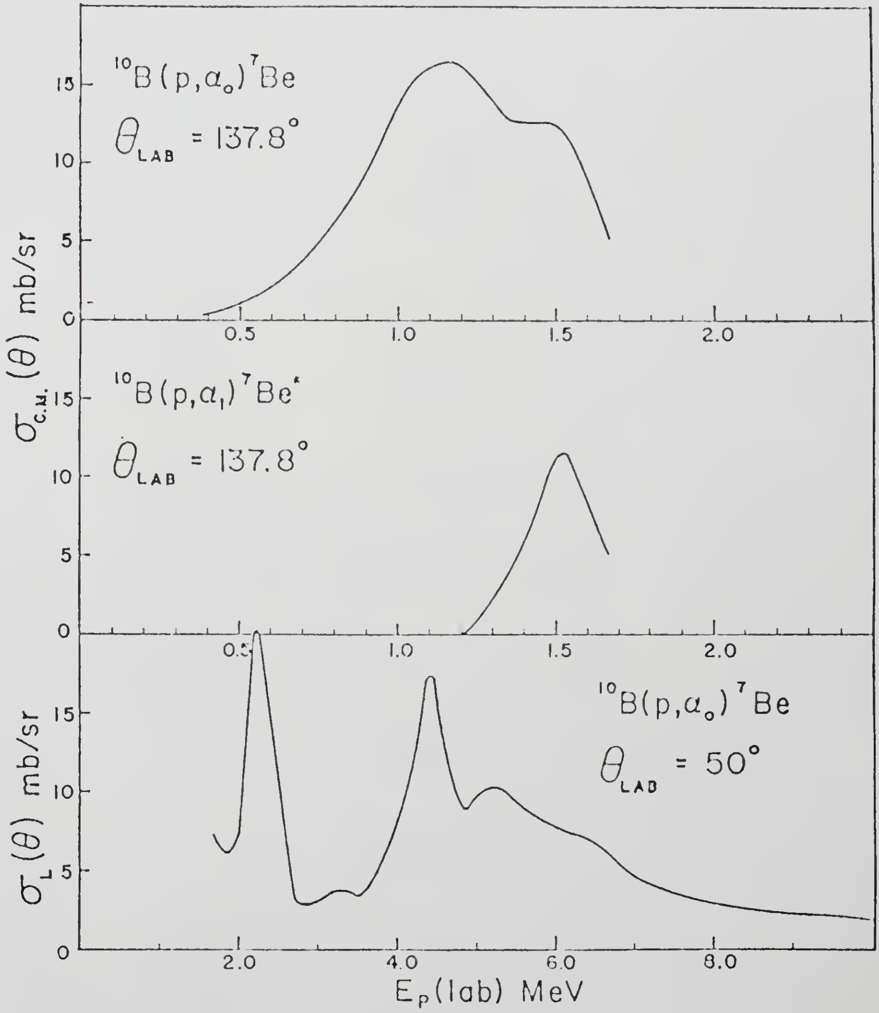
$^{10}B(p,\alpha_0)^7Be$
$\theta_{LAB} = 137.8°$
$^{10}B(p,\alpha_1)^7Be^*$
$\theta_{LAB} = 137.8°$
$^{10}B(p,\alpha_0)^7Be$
$\theta_{LAB} = 50°$
$\sigma_{c.m.}(\theta)$ mb/sr
$\sigma_L(\theta)$ mb/sr
0
5
10
15
0.5
1.0
1.5
2.0
2.0
4.0
6.0
8.0
E_p(lab) MeV

laboratory bombarding energy and center-of-mass excitation energy), states were seen which fit a description of an L = 0 alpha particle coupled to the ground state (3^+) and first excited state (1^+, 0.717 MeV) of ^{10}B. Therefore, this reaction was extended to alpha energies of 9.0 MeV, and the reaction $^{10}B(\alpha,\alpha_1)^{10}B^*_{.72}$ was measured for alpha energies of 2.7 to 3.2 MeV to look for correlations in the inelastic channel with known states [Ga69].

Finally, some of the previously measured data indicated that the APCETS model might give a relatively simple description of some of the excited states in ^{12}C observed via the $^{10}B(d,\alpha_0)^8Be$ and $^{10}B(d,\alpha_1)^8Be^*_{2.90}$ reactions. Further measurements in the energy region of these states was considered worthwhile in order to better determine the character of the states.

This work presents a report on the above experiments $^{10}B(p,\alpha)^7Be$, $^{10}B(d,d)^{10}B$, $^{10}B(d,\alpha)^8Be$, and $^{10}B(\alpha,\alpha)^{10}B$, which were motivated by the considerations of the preceding paragraphs and the analysis of the data acquired. Three nuclei were studied, ^{11}C, ^{12}C, and ^{14}N with the intention of applying the APCETS model.

Experimental techniques and equipment will be discussed in Chapter II. In Chapter III, the theories employed in the analysis of the data will be discussed. The topics covered will include the general R-matrix formalism, angular distribution fitting using Legendre polynomials and the angular-momentum coupling $\overline{Z}$ factors, a note on the optical model, and a discussion of the details and appropriateness of the APCETS model to these studies. Chapter IV will present the experimental results and describe how the formalisms were used to extract the significant parameters for comparison with the model. The final chapter will consider the comparison of the results with the predictions of the model and a conclusion concerning the applicability of the APCETS model.

CHAPTER II

EXPERIMENTAL PROCEDURE

All of the reactions performed for this work used thin, self-supporting target foils, composed of ^{10}B of 95% enrichment as supplied by the Stable Isotope Division of Oak Ridge National Laboratory. These targets were made by electron beam evaporation (see Appendix C) and had thicknesses of the order of $60 \mu g/cm^2$ as measured by the energy loss of the 5.48 MeV alpha particles from an ^{241}Am source. The main target contaminants were the naturally occurring ^{11}B, ^{12}C from the beam line, and atmospheric ^{14}N and ^{16}O, all identified by kinematic considerations.

The proton and deuteron induced experiments were performed using the University of Florida 4 MV Van de Graaff accelerator. The beam current on target, measured by an insulated Faraday cup, was 350 to 400 nanoamperes for protons and less than 100 nanoamperes for deuterons. More current was available but the preservation of the target was taken into consideration. Neutron radiation levels while using a deuteron beam also placed a limitation on the current used.

A. $^{10}B(p,\alpha_0)^7Be$ and $^{10}B(p,\alpha_1)^7Be^*$

Special problems were encountered in performing these two reactions. The $^{10}B(p,\alpha_0)^7Be$ reaction has a Q-value of

1.15 MeV, while the α_1 Q-value is only 0.72 MeV [Aj68]. These low Q-values have the effect that the exiting alpha particles have energies only slightly greater than the elastically scattered protons. The situation is further complicated by the greater energy loss of the alpha particles as they pass through the target material. These two facts result in an overlap in the energy spectrum between the elastic protons and the alpha particle groups at low bombarding energies when measured using a full energy (300 μ-thick) silicone surface barrier detector. In order to partially alleviate the problem, a 25 μ-thick silicon surface barrier transmission detector was employed. By varying the bias voltage and thereby adjusting the sensitive layer in the detector, a larger difference in the signal sizes resulting from the protons and alpha particles was obtained. The thickness of the detector was chosen such that protons in the energy range we were considering were transmitted by the detector while the alpha particles were stopped and gave full energy peaks. Figure 3 shows a comparison between a spectrum using the transmission detector and one resulting from the thicker full-energy detector. The better resolution of the elastically-scattered protons is obvious in the full energy spectrum, whereas the elastic protons are smeared into one group by the transmission detector. The thinner detector, though, allowed separation of the alpha groups from the elastic protons at lower energies and more backward (>90°) detection angles.

Figure 3. Charged Particle Spectram from the Proton Bombardment of ^{10}B; Counts/Channel versus Channel Number and $[E_{p(Lab)}] = 2.50$ MeV

a) Elastic Proton Spectrum using Transmission Detector at $\Theta_L = 60°$

b) Elastic Proton Spectrum using Full Energy Detector at $\Theta_L = 45°$. Peaks are due to the scattering from the labeled nuclei; solid line is to guide the eye.

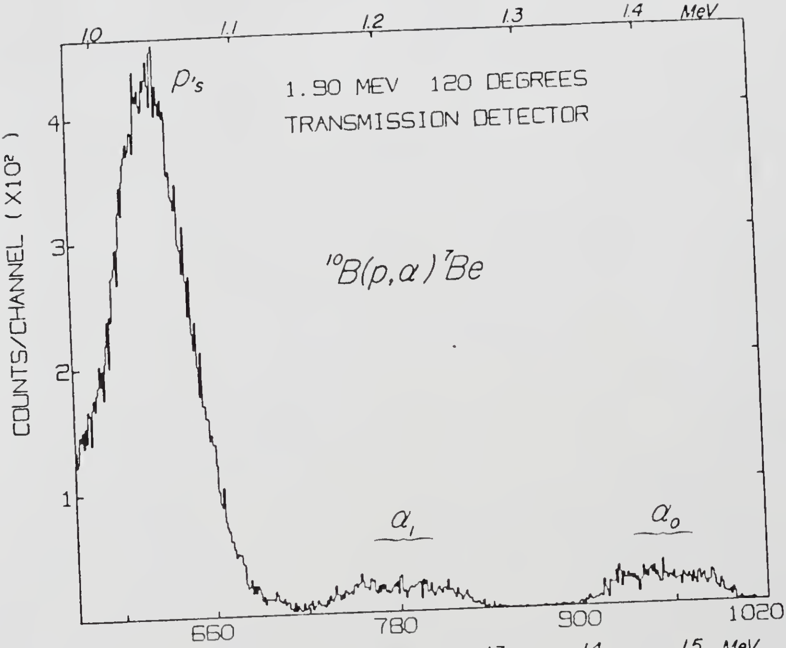
1.0
1.1
1.2
1.3
1.4
MeV
p's
1. 90 MEV 120 DEGREES
TRANSMISSION DETECTOR
$^{10}B(p,\alpha)^{7}Be$
COUNTS/CHANNEL (X10²)
4
3
2
1
α_1
α_0
660
780
900
1020

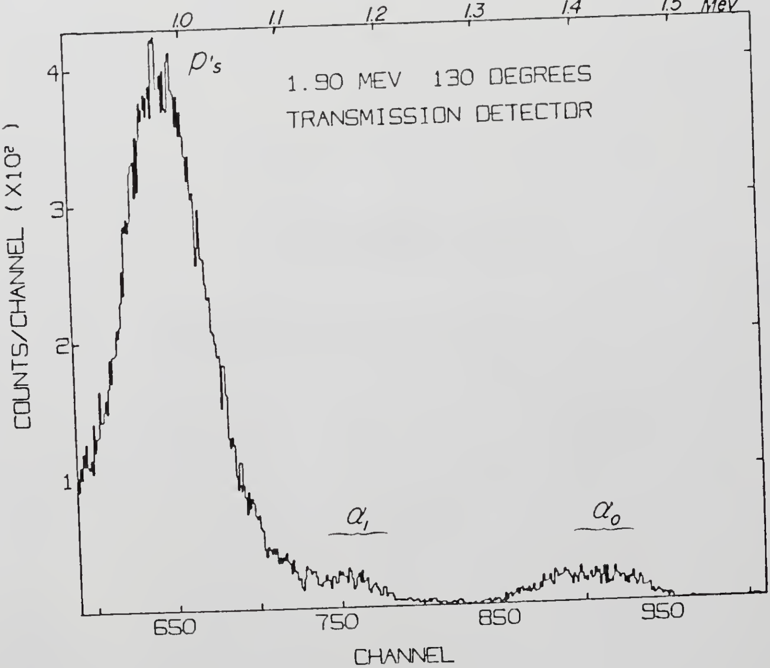
1.0
1.1
1.2
1.3
1.4
1.5
MeV
p's
1. 90 MEV 130 DEGREES
TRANSMISSION DETECTOR
COUNTS/CHANNEL (X10²)
4
3
2
1
α_1
α_0
650
750
850
950
CHANNEL

The reactions were studied for incident proton energies of 0.8 to 3.2 MeV in 50 keV steps. Excitation curves were taken at the four laboratory angles of 45°, 50°, 60°, and 90°. Nine α_0 angular distributions were measured at proton energies of 1.10, 1.30, 1.45, 1.60, 1.90, 2.10, 2.20, 2.30, and 2.50 MeV. The range of angles measured was, for most energies, from 40° to 150° or 160° in 10° steps; higher energy distributions were extended to more backward angles. The α_1 group angular distributions could be measured only at the six higher energies. The limitation in detection angle is pictured in Figure 4. As the detection angle is increased, kinematic effects result in the alpha groups decreasing in energy more rapidly than the protons, thereby resulting in an overlap between the peaks. At 120°, both the α_0 and α_1 groups are well separated from the protons, but at 130°, the α_1 group overlaps the proton peak. Any further increase in angle results in an even greater overlap, and eventually the α_0 group also is obscured by the proton peaks.

Beam energy calibration was done using the ^{7}Li(p,n)^{7}Be threshold at $E_p = 1.881$ MeV. The absolute energy was determined to an accuracy of ±20 keV. Cross-sections were calculated by normalization to the $^{10}B(p,\alpha_0)^7Be$ measurements made by Overley and Whaling [Ov62] using the 2.2 MeV resonance seen in both experiments. Including the 10% error of the previous experiment, we estimate that the present cross-sections are accurate to ±15%.

Throughout the measurement of the angular distributions,

Figure 4. Charged Particle Spectrum from the Proton Bombardment of ^{10}B; Count/Channel versus Channel Number [and $E_{p(Lab)}$]

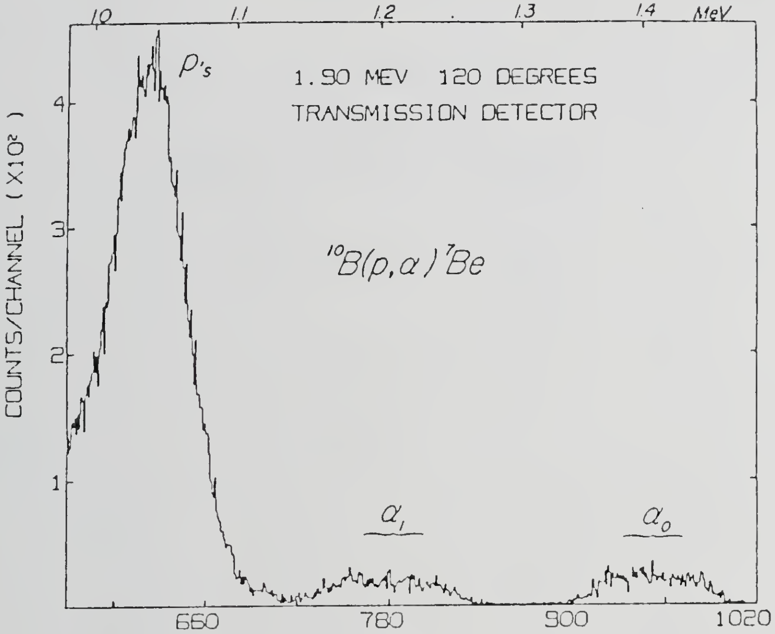
10
1.1
1.2
1.3
1.4
MeV
p's
1.90 MEV 120 DEGREES
TRANSMISSION DETECTOR
$^{10}B(p,\alpha)^{7}Be$
α_1
α_0
COUNTS/CHANNEL (X10^2)
1
2
3
4
660
780
900
1020

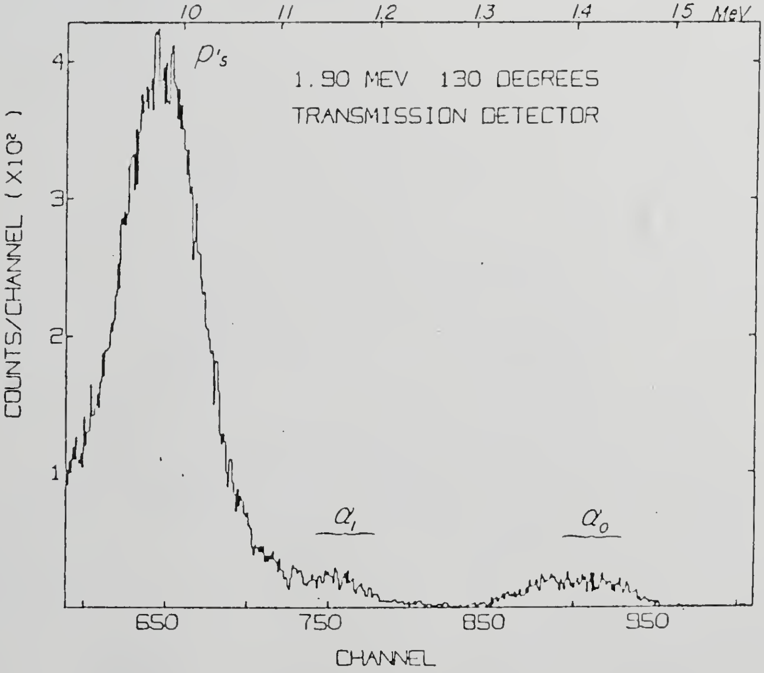
10
11
1.2
1.3
1.4
15
MeV
p's
1.90 MEV 130 DEGREES
TRANSMISSION DETECTOR
α_1
α_0
COUNTS/CHANNEL (X10^2)
1
2
3
4
650
750
850
950
CHANNEL

a monitor detector set at 40° to the beam direction was used; the protons elastically scattered from ^{10}B were summed and used to provide consistency of measurements as the target was rotated to allow forward and backward angle measurements. All detectors were collimated using tantalum collimators with 0.32cm apertures set at a distance of approximately 12cm from the target.

Detector signals were processed by the usual preamplifier-amplifier circuits and the resultant pulses fed into a 1024-channel ADC in use with the University of Florida General Automation 18/30 computer. The particle spectra were plotted, and the peaks of interest were summed on line. The accumulated spectra were subsequently written on magnetic tape for storage. Contaminants caused no problems with the summing.

B. $^{10}B(d,d)^{10}B$ and $^{10}B(d,\alpha)^{8}Be$

The elastic scattering of deuterons was performed for incident energies of 0.8 to 4.0 MeV at laboratory angles of 60°, 75°, 90°, 105°, 135°, and 150° in energy steps of 50 keV. Two silicon surface barrier detectors were used simultaneously, and their signals were amplified and routed into a 512-channel analyzer set to operate as two 256-channel analyzers. The pulse height spectra were punched on paper tape and listed for later summation. Beam currents of 10 to 50 nanoamperes were used depending on energy and accelerator condition. The deuterons scattered from ^{10}B were easily resolvable from those scattered from any

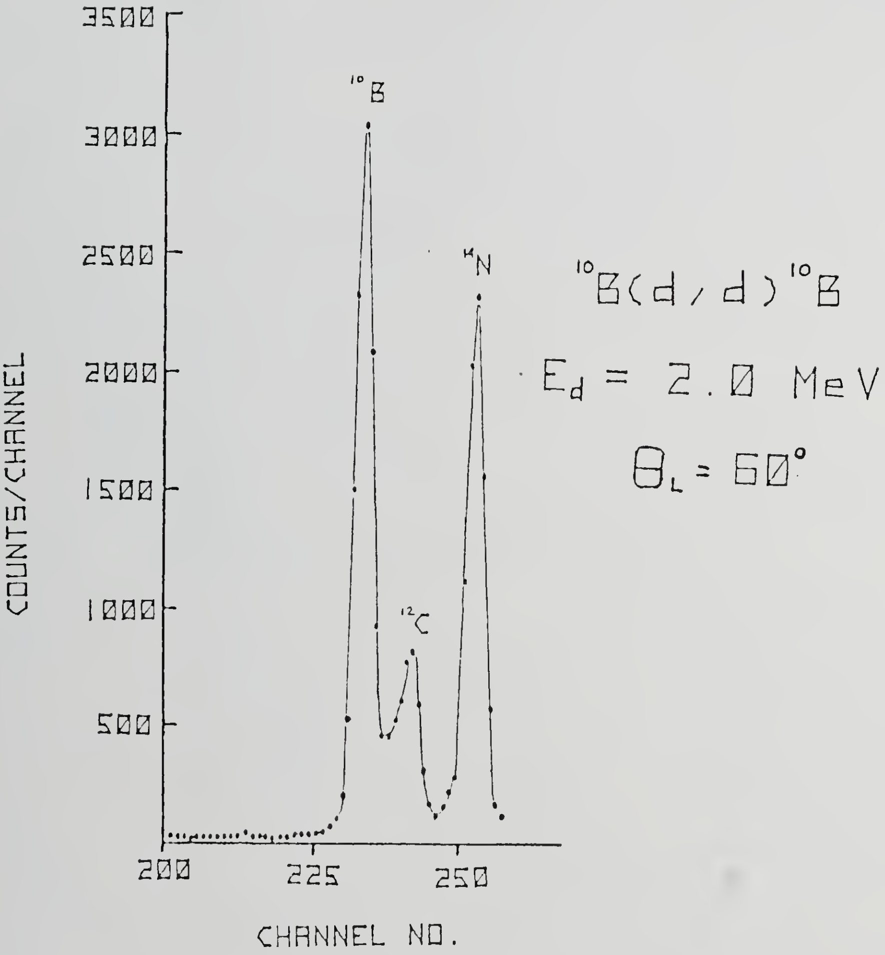

Figure 5. Charged Particle Spectrum from the Deuteron Bombardment of ^{10}B; Peaks are Due to the Elastic Scattering of Deuterons from the Labeled Nuclei

contaminants. Angular distributions were also measured at incident energies of 1.5, 2.0, 2.5, 3.0, 3.5 and 4.0 MeV for laboratory angles of 60° to 160° in 10° steps.

The $^{10}B(d,\alpha_0)^8Be$ and $^{10}B(d,\alpha_1)^8Be^*$ reactions were performed using a similar experimental set-up. Since the Q-value for the α_0 reaction is 17.82 MeV and for the α_1 reaction, 14.92 MeV, the alpha groups were easily identified; no other exit particle had as much energy. A biased amplifier was used in order to spread the region of interest of the spectrum over the available number of channels. Excitation curves were measured for laboratory angles of 70°, 90°, 150°, and 170° for incident energies of 0.8 to 4.0 MeV in 50 keV steps. Eleven angular distributions for the α_0 group were measured for laboratory angles of 40° to 170° in 10° steps. Beam energy was again calibrated using the $^7Li(p,n)$ threshold. Experimental yields were converted to center-of-mass cross-sections by measuring the 2.2 MeV elastic proton resonance as measured by Overley and Whaling [Ov62] and comparing their cross-sections to our yields. Their relative error is approximately 10%. Including the statistical errors, our absolute cross-sections are estimated to be accurate to ±20%.

A typical pulse height spectrum is shown in Figure 6. The α_0 group was easily summed, but because of the relatively small yield, the statistical errors were greater than 5%. Larger statistical errors in the α_1 yields resulted from background subtraction. The background was

Figure 6. Alpha Particle Spectrum Resulting from the Deuteron Bombardment of ^{10}B; Counts Channel versus E_α(Lab). Solid lines are approximate level shapes to guide the eye. Dotted line indicates approximate background subtracted from α_1 peak.

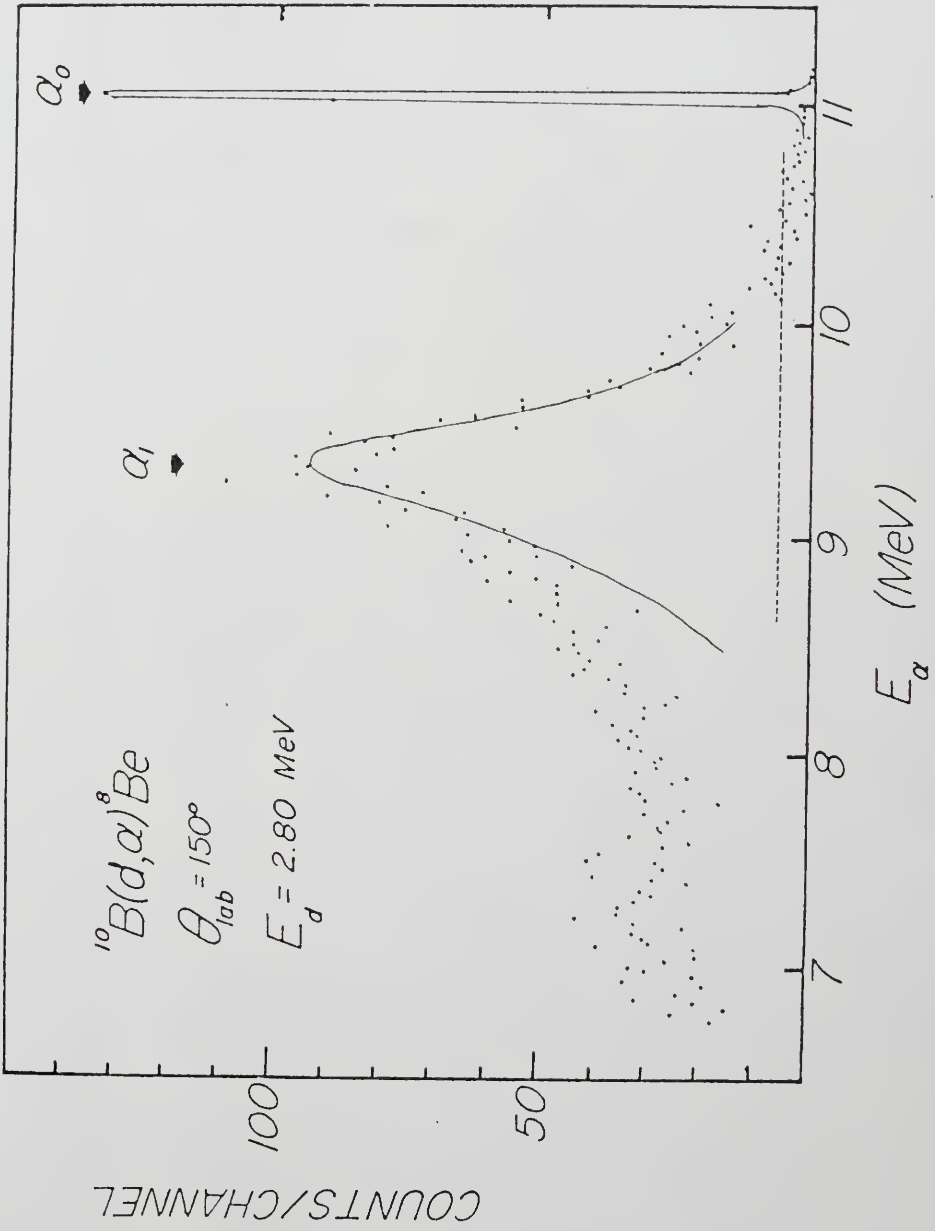
$^{10}B(d,\alpha)^8Be$
$\theta_{lab} = 150°$
$E_d = 2.80$ MeV
α_0
α_1
E_α (MeV)
7
8
9
10
11
50
100
COUNTS/CHANNEL

energy dependent and resulted in an asymmetrical peak shape. In order to simplify the peak summation, the raw channel sums were made only on the high half of the peak. These sums were then multiplied by two, assuming the higher half of the peak gave the correct shape. An assumed straight background was subtracted (see Figure 6).

C. $^{10}B(\alpha,\alpha_0)^{10}B$

The elastic scattering of alpha particles from ^{10}B had been performed by Mo and Weller [Mo73] in the energy region E_α = 1.0 to 4.2 MeV. This reaction was extended in energy for alpha energies of 4.0 to 9.0 MeV using the EN tandem Van de Graaff at Western Michigan University. The usual charged-particle detection system was used, and the amplified detector signals were fed into a PDP-15 computer for analysis. A typical spectrum is shown in Fig. 7. The ^{10}B elastic peak was summed on-line with a straight background subtraction. Four excitation curves were measured over the full energy region at laboratory angles of 68°, 98°, 150°, and 165°. Energy increments were 30 keV from 4 to 6 MeV and 50 keV from 6 to 9 MeV. No angular distributions were measured.

The yields were converted to center-of-mass cross-sections by comparison of the resonance yield at 4.15 MeV to the same resonance as measured by Mo and Weller. The error in the absolute cross-section is estimated to be less than 10%.

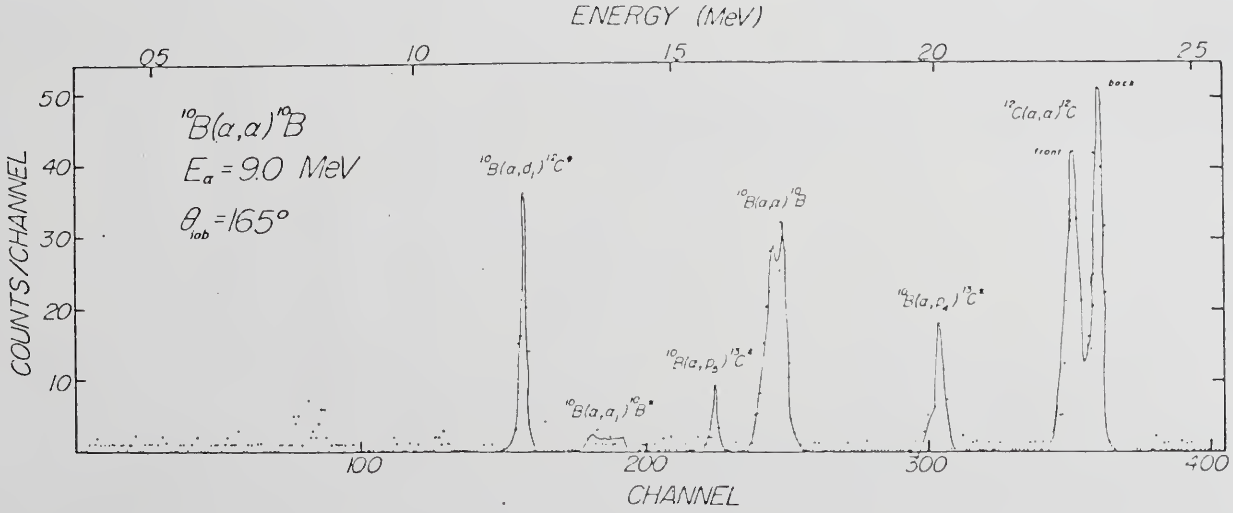

Figure 7. Charged Particle Spectrum from the Alpha Bombardment of ^{10}B; Counts/Channel versus Channel Number and [E_α(Lab)]. Solid line is to guide eye.

D. $^{10}B(\alpha,\alpha_1)^{10}B^*$

The inelastic scattering of alpha particles for the first excited state of ^{10}B was measured using the 4 MV University of Florida Van de Graaff accelerator. Two 300 μm silicon surface barrier detectors were used. Two excitation curves were measured at laboratory angles of 45° and 60° in 50 keV steps for incident alpha energies of 2.7 → 3.3 MeV. Absolute cross-sections were obtained from the yields by assuming that low energy (1.0 MeV), small angle (≈40°) scattering of alpha particles off ^{10}B could be described as almost purely Rutherford scattering. The cross-sections are accurate to ±20% and are in agreement within errors with those deduced from the corresponding $^{10}B(\alpha,\alpha_0)^{10}B$ cross-sections. A typical spectrum is shown in Figure 8.

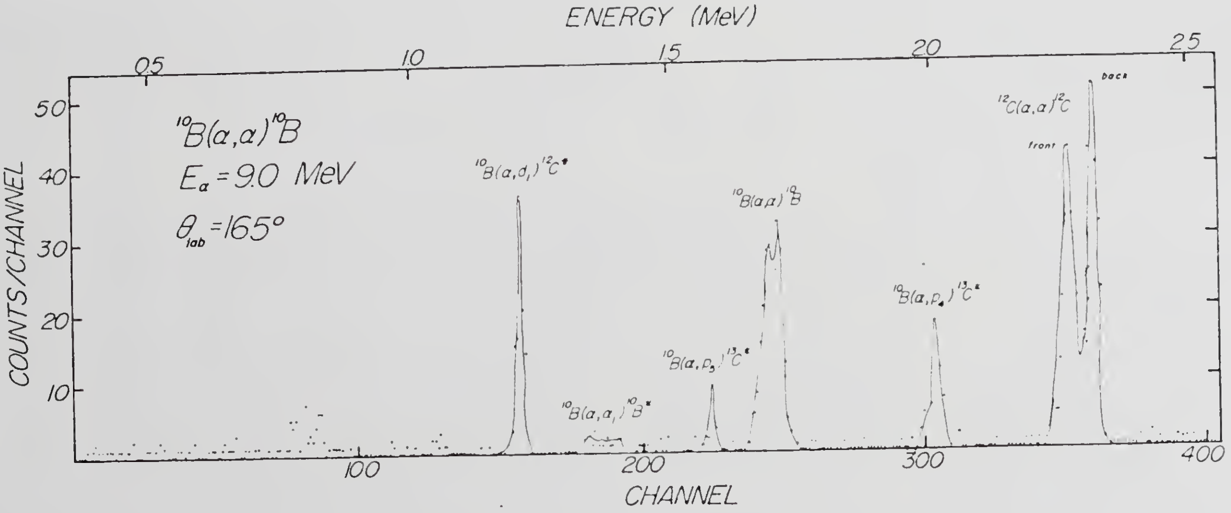

Figure 8. Charged Particle Spectrum from the Alpha Bombardment of ^{10}B: Counts/Channel versus Channel Number and [E_α(Lab)]. Solid line is to guide eye.

CHAPTER III

THEORY

A. R-matrix

One of the general formalisms used in the analysis of the data is the R-matrix formalism. This formalism was used in the analysis of the $^{10}B(\alpha,\alpha_0)^{10}B$, $^{10}B(p,p)^{10}B$, and $^{10}B(p,\alpha)^{7}Be$ results, and could have been applied to all the reactions. A brief review of this formalism will be given; for more details the complete review article by Lane and Thomas [La58] should be consulted. A more recent treatment of the basic development of this formalism can be found in McCarthy [Mc68], while a good review has been written by Vogt [Vo62]. Many variations of the R-matrix theory have been proposed, but the one described by Lane and Thomas was first set forth by Wigner and Eisenbud [Wi47]. This formulation of the theory has the advantage over the reaction formalism of Kapur and Peierls [Ka38] in that the energy dependence of all the expressions is made as explicit as possible. Wigner's variation has energy independent boundary conditions but is equivalent to Kapur and Peierls.

Any discussion of R-matrix theory must begin with a list of the basic assumptions. Though a thorough discussion of the implications of these assumptions can be found in Lane and Thomas, they will be listed here for completeness.

1) The usual Hamiltonian equation $H\Psi=E\Psi$ is applicable where H is the sum of kinetic and potential operators. This Hamiltonian is defined in all space and its use implies the validity of non-relativistic quantum mechanics.

2) It is assumed that any reaction resulting in more than two product nuclei is nonexistent or unimportant. The situation where three or more products are produced could be dealt with as a two step process.

3) It is assumed that all processes of annilhilation or creation are unimportant or absent. This assumption excludes the possibility of gamma decay, but the restriction can be removed by using a perturbation treatment of coupling nuclear particles to the electromagnetic field.

4) The existence of some finite radial separation (channel or interaction radius) between any pair of nuclei beyond which neither nucleus experiences any polarizing potential from the other is assumed. This radial distance differs for each pair of nuclei and is usually taken to be the sum of the radii of the pair, as a minimum. Other than this restriction, the choice of channel radii is largely arbitrary. This assumption allows each channel (i.e., each possible reaction process) to be orthogonal to all others.

The choice of an interaction radius immediately divides the interactions into problems in two separate regions. In the exterior region ($r>r_c$), the form of the interactions is known and the wave functions for the nuclei can be found exactly. In the interior region ($r \leq$ channel radius), the interactions are not specifically known and a unique solution to the problem cannot be found. In the interior region, therefore, standing wave solutions to the Schroedinger equations using some potential are found. The complete set of solutions X_λ (λ is the level index) is used to expand the actual wave function for $r \leq r_c$. These X_λ's are not, however, identifiable as the wave functions of bound states of the nucleus but only as a basis set for the expansion of an arbitrary wave function. Boundary conditions are applied at the nuclear surface S, a surface chosen to satisfy the orthonormality conditions. The R-matrix is designed to connect the external solutions to the internal region using the boundary conditions applied at S.

If the entire external wave function is written as a channel sum over both incoming waves I_c and outgoing waves as

$$\Psi = \sum_c Y_c I_c + X_c O_c ,$$

where X_c and Y_c are the amplitudes of the outgoing and incoming waves respectively, then the X_c should be uniquely determined by the interactions occurring in the internal region. If this is the case, then it should be possible to express the amplitudes of the outgoing waves in terms of the amplitudes of the incoming waves, i.e.,

$$X_{c'} = -\sum_c U_{c'c} Y_c$$

or

$$\underset{\sim}{X} = -\underset{\sim}{U}\underset{\sim}{Y}$$

where $\underset{\sim}{X}$, $\underset{\sim}{U}$ and $\underset{\sim}{Y}$ are matrices. The quantity $\underset{\sim}{U}$ is called the collision or scattering matrix and connects the outgoing amplitudes to the known incoming amplitudes; it contains all of the desired physical information. The experimentally observed cross-sections should be expressable in terms of this collision matrix.

Since the collision matrix actually specifies the wave function outside the internal region, some connection must be made to the internal region. With the boundary conditions on S,

$$r\frac{d\chi_\lambda}{dr}\bigg|_{r=r_c} = b_c\chi_\lambda\bigg|_{r=r_c}$$

where the χ_λ's are the elements of the complete orthonormal set previously mentioned, and the b_c's are arbitrary constants, we can generate an expansion which relates the value of the total wave function to its derivatives at the surface. The coefficients in this expansion are the elements of the R-matrix

$$R_{cc'} = R_0 + \sum_\lambda \gamma_{\lambda c}\gamma_{\lambda c'}/(E_\lambda - E).$$

Here, R_0 gives rise to a "background" in a reaction. Various forms can be used for R_0, but the simplest case is usually used, that is R_0 is set to zero. The $\gamma_{\lambda c}$'s are the reduced width amplitude and are related to the overlap integral of the χ_λ and the exterior wave function on the surface S_c; they characterize the rate of decay of the level λ of the compound system into the channel c. The γ_λ's are related to the observed level width by

$$\Gamma_{\lambda c} = 2P_c\gamma_{\lambda c}^2$$

where P_c is the penetrability for the channel c. The penetrability along with other important parameters are discussed in more detail in Appendix A. The R-matrix code MULTI is also discussed in detail there.

As a final note, the choice of the channel radius is largely arbitrary but probably should correspond in some way to the physical configuration of the interacting nuclei. The radius parameter is usually taken as

$$r_c = r_0(A_1^{1/3} + A_2^{1/3}).$$

In this expression, r_0 is a constant whose value is usually near 1.40fm. A_1 and A_2 are the atomic numbers of the interacting particles. The calculated cross-section independent on the choice of r_0. Details of the R-matrix code MULTI are found in Appendix A.

B. Angular Distributions and Legendre Polynomial Fitting

In dealing with angular distributions, that is, cross-sections measured at a constant incident laboratory energy as a function of laboratory angle, a concise theoretical expression can be written, as derived by Wigner and Eisenbud [Wi47] and Blatt and Biedenharn [Bl52] and corrected by Huby [Hu54]. In terms of center-of-mass variables,

$$\frac{d\sigma}{d\Omega}(\alpha'|\alpha) = \frac{\bar{\lambda}^2}{4}\Sigma\frac{(-1)^{s-s'}}{(2I+1)(2i+1)}\bar{Z}(\ell_1 J_1 \ell_2 J_2;sL)\bar{Z}(\ell'_1 J_1 \ell'_2 J_2;s'L)$$

$$\times \mathrm{Re}\mathcal{T}(\alpha'\ell'_1 s'|\alpha\ell_1 s|J_1\Pi_1)\mathcal{T}^*(\alpha'\ell'_2 s'|\alpha\ell_2 s|J_2\Pi_2) \times P_L(\cos\Theta).$$

[Fe60]

In this formula, Θ is the angle between the emergent particle direction and the beam direction and s and s' are the initial and final channel spins. The initial channel spin $\vec{s} = \vec{I}+\vec{i}$, where $\vec{I}$ and $\vec{i}$ are the target and projectile spin quantum numbers, and $\vec{s}'=\vec{I}'+\vec{i}'$, where $\vec{I}'$ and $\vec{i}'$ refer to the residual nucleus and product spins. $\lambda\!\!\!^{-}$ is $\hbar c/(E)^{1/2}$. The quantity $\mathcal{T}(\alpha'\ell_1's'|\alpha\ell_1 s|J_1\Pi_1)$ is the transition matrix element describing the transition from state α with channel spin s to the state α' with channel spin s' through the compound system having a total angular momentum J_1 and parity Π_1. The ℓ_1 is the incident particle relative angular momentum quantum number and ℓ_1' is the emergent particle relative angular momentum quantum number; $\mathcal{T}^*(\alpha'\ell_2's'|\alpha\ell_2 s|J_2\Pi_2)$ is the complex conjugate of a similar matrix element for another or the same possible set of production and decay quantum numbers.

The $\mathcal{T}$ elements contain most of the physics of the interaction, other than angular momentum considerations. The $\mathcal{T}$'s can be broken up into two terms, one of which varies smoothly with energy, the other having a rapid fluctuation with energy as is necessary in the description of resonances:

$$\mathcal{T}(\alpha'\ell's'|\alpha\ell s|J\Pi) = \mathcal{T}_P(\alpha'\ell's'|\alpha\ell s|J\Pi)+\mathcal{T}_R(\alpha'\ell's'|\alpha\ell s|J\Pi).$$

For cases where $\alpha'=\alpha$, $\mathcal{T}_P$ describes the potential scattering. When $\alpha' \neq \alpha$, $\mathcal{T}_P$ is the non-resonant, smoothly-varying part of the reaction amplitude representing the effect of all levels other than those in $\mathcal{T}_R$. Here $\mathcal{T}_R$ is the resonant amplitude explicitly containing resonant effects and can be written in the Breit-Wigner form

$$T(\alpha'\ell'\ s'|\alpha\ell s|J\Pi) = \frac{i\Gamma^{\frac{1}{2}}(\alpha'\ell's'|J\Pi)\ \Gamma^{\frac{1}{2}}(\alpha\ell s|J\Pi)}{(E-E_{J\Pi}) + \frac{i\Gamma_{J\Pi}}{2}}$$

where $\Gamma(\alpha\ell s|J\Pi)$ and $\Gamma(\alpha'\ell's'|J\Pi)$ are the partial widths for the entrance and decay channels respectively (see Chapter III-A). Here E is the excitation energy, $E_{J\Pi}$ is the resonance energy, and $\Gamma_{J\Pi}$ is the total resonance width.

By performing the division of the T amplitudes into potential (non-resonant) and resonant parts, the cross-section can be written

$$\frac{d\sigma}{d\Omega}(\alpha'|\alpha) = \frac{d\sigma_P(\alpha'|\alpha)}{d\Omega} + \frac{d\sigma_R(\alpha'|\alpha)}{d\Omega} + \frac{d\sigma_I(\alpha'|\alpha)}{d\Omega}$$

where I refers to the interference between resonant and non-resonant parts. Such a decomposition is important when resonances are widely spaced relative to their widths. In the region between the resonances, the slowly varying non-resonant cross-section $d\sigma_P/d\Omega$ is the major term, while right at resonance, it provides a background on which the resonance structure is superimposed. The interference term is quite important, especially if the resonant and non-resonant amplitudes are comparable.

The $\bar{Z}$ factors are kinematical, i.e., they do not depend on the nuclear interaction but only on the decomposition of the initial plane wave into states of given J,Π,ℓ, and s, and they decay into the final state with quantum numbers ℓ' and s'. [See Appendix B.]

In order to obtain some information concerning the J^{Π} values of resonances seen in excitation curves, the angular distributions measured around the resonance energy are fitted to a Legendre polynomial expansion $d\sigma/d\Omega=\Sigma A_L P_L(\cos\Theta)$ using the code LEGFIT, which employs Legendre polynomials up to order eight. The fitting is done by minimizing the chi-squared criterion

$$\chi^2 = \Sigma\frac{|\sigma_{exp}(i)-\sigma_{th}(i)|^2}{|\Delta\sigma_{exp}(i)|^2}$$

where σ_{exp} and σ_{th} are the experimental and theoretical values of the cross-sections respectively, and $\Delta\sigma_{exp}$ is the statistical uncertainty in the experimental cross-section.

The fits to the angular distributions yield a set of coefficients, A_L, of the Legendre polynomials, $P_L(\cos\Theta)$, which can be examined as a function of energy. This examination can give definite clues to the possible spins and parities of resonances by comparision to an analysis of the $\overline{Z}$ coefficients (see Appendix B).

Though an examination of the Legendre coefficients can give some clues to the ℓ and J^Π values of a resonance, other consideration must be made. The appearance of a correlated resonant-type behavior in a Legendre coefficient places a definite limit as to possible angular momentum values (Appendix B), non-appearance of such behavior can be the result of factors other than angular momentum coupling. The amplitudes Γ which appear in the $\mathcal{T}$ elements and which depend on variables other than angular momentum quantum numbers, can themsevles be zero for certain configurations. Therefore, the Legendre polynomial fitting procedure is only one part of a complete analysis required for a confident determination of resonance parameters.

C. Optical Model

The simplest model of a nucleon-nucleus interaction ignores any structure and replaces it by a simple real potential well characterized by a depth and a radius. This model has had some success in describing scattering processes. The optical model resulted from the addition to the real well of an imaginary component to account for absorption. The initial development of the optical model was due to Fernbach, Serber, and Taylor [Fe49] in analyzing reactions due to 90 MeV neutrons. They found that the nucleus was quite transparent to the neutrons and proposed that the elastic scattering of nucleons be compared with the scattering of light by a refractive and absorbing sphere. Classically, this situation can be represented by a complex index of refraction.

It was natural to extend this semi-classical picture and apply quantum-mechanical techniques. The solution to the Schroedinger equation with a complex potential was first done at low energies by LeLevier and Saxon [Le52]. While a generally good account of nucleon scattering can be obtained [Ho63], it is natural to extend it to scattering of composite particles, such as deuterons, helium-3 nuclei, and alpha particles.

The approach of the optical model is to replace all interactions between the projectile and target nucleus by an average potential in the Schroedinger equation and then solve the scattering problem. The real part of the potential gives rise to elastic scattering while the imaginary part results in absorption. This technique has been most successful at higher excitation energies where many overlapping levels are found. Extensions of this method where resonances were included have also been fruitful [We68,Ot71].

In order to calculate the elastic scattering cross-section, we must find the amplitude of the outgoing waves in the elastic channel. We begin by solving the Schroedinger equation

$$\nabla^2\Psi+\frac{2\mu}{\hbar^2}(E-V)\Psi = 0.$$

The optical potential is taken to have the form

$$V(r) = V_c(r)-V_0 f(r,R_r,a_r)+i4Wa_w\frac{d}{dr}f(r,R_w,a_w)$$

where

$$f(r,R,a) = (1+e^{(r-R)/a})^{-1}$$

$$V_c(r) = \begin{cases} \dfrac{zZe^2}{2R_c}\left\{3-\left(\dfrac{r}{R_c}\right)^2\right\} & r\leq r_0A^{1/3} \\ \dfrac{zZe^2}{r} & r>r_0A^{1/3} \end{cases}$$

$V_c(r)$ is the Coulomb potential with z and Z being the projectile and target atomic numbers respectively; f is the Woods-Saxon [Wo54] well shape; V_0 and W are the real and imaginary optical model potential strengths. The imaginary potential is taken to be a derivative Woods-Saxon and results in surface (as opposed to volume) absorption. The R_r and R_W are the radius parameters for the real and imaginary wells, respectively; a_r and a_W are the corresponding diffuseness parameters.

The code JUPITOR2 [Ta67] was used for the optical model fitting.

D. APCETS

The core-excited threshold state model is one which is widely used in calculating properties of energy levels in nuclei. It is usually applied to a nearly closed-shell system where the nucleus in question can be depicted as a closed-shell nucleus plus a particle or hole (e.g., Th66). Interactions between the particle or hole and remaining nucleus are generally expressed as a product of tensor operators of order k:

$$H_{INT} = \sum_k \tilde{T}_c^{(k)} \cdot \tilde{T}_p^{(k)}$$

where $\tilde{T}_c^{(k)}$ operates only the degrees of freedom of the core and $\tilde{T}_p^{(k)}$ operates on the particle (hole) degrees of freedom. Specific choices of the tensor operators are made in order to discover the energy eigenvalues with this term added to the Hamiltonian. Usual choices include first order (e.g., $\vec{J}^{(1)}$) or second order ($\tilde{Q}^{(2)}$) tensor [Th65].

In dealing with a core-excited model where the extra-core particle is a ^{4}He nucleus, the usual choice for the interaction is $\vec{I} \cdot \vec{L}$, where $\vec{I}$ is the spin of the target (core nucleus) and $\vec{L}$ is the orbital angular momentum of the alpha particle. This interaction is a result of summing of the usual one nucleon spin orbit $\vec{\ell} \cdot \vec{S}$ interaction over the core nucleus [Ra72].

The results of such an interaction between an alpha particle and a core nucleus have been seen, e.g., [We69].

In cases previously considered [We72], the alpha particle possessed $\vec{L} = 1$. This value can lead to the formation of multiplets in the compound system. For example, if an $\vec{L} = 1$ alpha particle is coupled to the ground state ($3/2^-$) of ^{11}B, we might expect a $5/2^+$, $3/2^+$, $1/2^+$ triplet in ^{15}N; such a triplet is seen. If the alpha particle is coupled to the first excited state ($1/2^-$) of ^{11}B, a $1/2^+$, $3/2^+$ doublet is expected and seen. An $\vec{L} = 0$ alpha particle coupling would not result in multiplets, but in singlets based on the core states as in ^{19}Ne [Ot71]. The energy separation between the centers of gravity [La57] of the multiplets should roughly correspond to the energy separation of the core states on which they are built.

Inversion of the level order in multiplets, such as the $1/2^+$, $3/2^+$ doublet in ^{15}N (the order, in increasing energy, should be $3/2^+$, $1/2^+$), suggests deformation of the core, probably by the alpha particle. A detailed investigation of the $\vec{I} \cdot \vec{L}$ alpha particle core interaction which leads to the level inversion has been made by Rawitcher [Ra72]. This interaction has been successfully used in calculations on ^{15}N and ^{15}O by Purcell and Meder [Pu74] where an alpha particle is coupled to the low lying levels of ^{11}B and ^{11}C, respectively. These levels were previously described in terms of the shell model [Me74].

A third effect is also seen in ^{15}N, where multiplet spacing is strongly compressed as compared to ^{15}O. This compression might be explained as a broadening of the effective core potential to a greater extent by the interaction with the alpha particle.

Though this model has been successful in accounting for observed level schemes in several nuclei, it should not be taken too literally. The states tentatively identified as alpha particle core-excited threshold states are obviously not purely an alpha particle coupled to an excited core. In most instances, the states are observed in reaction channels other than α scattering, such as (p,α), (d,α), $(^3He,\alpha)$, etc., indicating that the states have partial widths other than just Γ_α. The other partial widths [such a Γ_p for the (p,α) reaction] are probably small compared to Γ_α. This relation would result in states being seen in a (p,α) reaction and less likely to be observed in a (p,p) or a $(p,^3He)$ reaction. By inspecting the usual Breit-Wigner resonance form where the cross-section for any reaction $C \rightarrow C'$ is proportional to the product of the partial widths Γ_C, $\Gamma_{C'}$, we can see that if $\Gamma_C < \Gamma_\alpha$ ($C' = \alpha$ channel), the cross-section will be less prominent when the α particle state is formed through a non-alpha channel.

Another question to be dealt with is the appearance in the elastic α channel (or α_0 channel) of states which the APCETS model would say were the first excited state of the core nucleus coupled to an alpha particle. If this picture was actually true, then these states would not be seen in α_0 channel. There are at least two possible pictures of what may occur. One, the configuration consisting of the first excited state of the core nucleus plus an alpha particle may be mixed by some interaction within the nucleus. Such a mixing might lead to decays by α_0 emission of a state which mostly consists of the first excited state coupled to an alpha particle, but has some ground state strength. Two, the reaction may take place as a two (or more) step process where the incident particle first excites the core nucleus and is then captured to form the intermediate state. Such a process might be more formally dealt with by using the concept of doorway states [Fe66]. Here, the open (incident or exit channel Ψ_p), excites directly through the full Hamiltonian opeator some part of the internal (closed) channel amplitude. The rest of the possible closed channel wave function is generated by some residual interaction with the excited portion. The intermediate step wave function is called a doorway state. Though both of these pictures (and others) should result in the same physics, further investigation is necessary.

Further investigation is also necessary to explain the reasons for the L-value of the extra-core alpha particle. A detailed model which would predict the L-value of the threshold states is not available, though the value might be related to the lowest energy shell model configuration available to the four nucleons comprising the alpha particle.

CHAPTER IV

EXPERIMENTAL RESULTS

A. ^{11}C

Neutron groups, observed in the stripping reaction $^{10}B(d,n)^{11}C$, indicate the existence of states in ^{11}C at 9.69±.03, 10.09±.02, 10.69±.02, and 10.89±.02 MeV [Ce56], [Ov63]. This energy region has also been previously investigated through the reactions $^{10}B(p,\alpha_0)^7Be$, $^{10}B(p,\alpha_1)^7Be^*$, and $^{10}B(p,\alpha)^{11}C$ [see references below], but uncertainties remain concerning the spins and parities (and existence) of some of the reported states. The $^{10}B + p$ reactions have indicated the existence of 9.69, 10.09, and 10.69 MeV states, but conflicting spin assignments remain.

The yield of gamma rays to the ground state of $^{11}C(J^{\pi} = 3/2^-)$ for proton energies of less than 3 MeV exhibits a strong resonance of width approximately 500 keV at E_p = 1.14 MeV indicating a state in ^{11}C at 9.74 MeV [Da 54, Ch56, Hu57]. Observations have been made of γ-cascade radiation from this excitation region (around E_x = 9.8 MeV) to states with excitation energies of 6.48 and 4.32 MeV thought to have spins of $7/2^-$ and $5/2^-$, respectively [Ja61]. Examination of the relative intensities of these γ transitions, along with the observation of no forward-backward asymmetry, indicates that the transitions all derive from a single parent state. Absolute intensities indicate that the γ-rays have the same multipolarity, limiting the spin of the parent state to 5/2. Analysis of the angular distributions of γ-radiation supported the spin and parity of the 9.74 MeV state in ^{11}C is set at $5/2^-$ [Ch56, Ja61].

Using the $^{10}B(p,\alpha)^7Be$ reaction the α- particle decay to the ground state of $^7Be(J^\pi = 3/2^-)$ has been investigated for proton energies from $E_p = 0.8$ MeV to $E_p = 1.65$ MeV [Cr56, Br51]. Broad resonances were seen near $E_p = 1.17$ MeV and $E_p = 1.5$ MeV, hereafter called resonances I and II, respectively. The α-particle angular distributions were nearly isotropic below 1.2 MeV but showed a dependence of $P_1(\cos\Theta)$ and $P_3(\cos\Theta)$, peaking near $E_p = 1.36$ MeV. The apparent presence of odd Legendre polynomials was interpreted as an indication that the two states have opposite parities. Examination of the total cross-section at resonance placed minimum values on the spins of $J_{min} \geq 3/2$ for the lower energy resonance (resonance I) and $J_{min} \geq 5/2$ for the upper (resonance II) resonance. Legendre coefficients obtained from fitting the measured angular distributions gave support to the assignment of $3/2^-$ and $7/2^+$, respectively, as the spins of the two resonances.

The α_1 decay to the first excited state of ^{7}Be($J^{\pi} = 1/2^{-}$), which has been studied for proton energies up to 3.0 MeV through the reactions ^{10}B(p,α)^{7}Be* [Cr56] and ^{10}B(p,$\alpha\gamma$)^{7}Be [Hu57], is resonant only at Ep = 1.5 MeV. The preferred assignment for this state [Ex = 10.09 MeV] is $7/2^{+}$, formed by s- and d-wave protons and decaying by $\ell = 3$ α-particles. A $7/2^{+}$ state can decay to both the ground and first excited state of ^{7}Be by the emission of $\ell = 3$ alpha particles. Thus, from angular momentum considerations alone, roughly equal decays might be expected. The same argument might also be valid to explain the non-observance of γ transitions to the ground state of ^{11}C, a transition which would have to be quadrupole.

The elastic scattering excitation curves for protons on ^{10}B for energies of 0.15 MeV to 3.0 MeV [Ov62] exhibited a conspicuous anomaly at Ep = 1.5 MeV along with some structure around Ep = 1.2 MeV. Analysis of the angular distributions measured in this region indicated that the scattering was primarily s-wave. The anomaly was satisfactorily reproduced [Ov62] using level assignments of $5/2^{+}$ and $7/2^{+}$ for resonances I and II, respectively, though values of $5/2^{-}$ and $3/2^{-}$ for the spin of resonance I were not eliminated.

The observation of these two resonances near the threshold for α-particle production, both of which α-decay to the ground state of ^{7}Be, while only the higher energy one decays to the first excited state of ^{7}Be, led to the hypothesis that the states might be describable using the APCETS model. The most straight forward possibility was that resonance I corresponded to the ground state of ^{7}Be coupled to an alpha particle while resonance II was the first excited state ($J^\pi = 1/2^-$, 0.43 MeV) coupled to an alpha particle. The energy separation of the observed states (≈0.33 MeV) was close to the first excited state energy and gave credence to the hypotheses. This model would predict that the states should have spins of $3/2^-$ and $1/2^-$, respectively. These assignments assume the extra-core alpha particle to have zero relative angular momentum to eliminate the possibility of multiplets. Because of the existing ambiguities and desire to test the model, the reactions $^{10}B(p,\alpha_0)^7Be$ and $^{10}B(p,\alpha_1)^7Be$ were measured for proton energies from 0.8 MeV to 3.25 MeV. The excitation curves are shown in Figure 9. The broad peak centered near E_p = 1.4 MeV is recognizable as being composed of two overlapping resonances, especially obvious at Θ_L = 45°. In order to facilitate the analysis of these resonances (tentatively identified with the previously discussed resonances I and II), α_0 angular distributions were measured at incident proton energies of 1.10, 1.30, 1.45, 1.60, and 1.90 MeV; these distributions are shown in Figure 10.

Figure 9. Excitation Curves for the $^{10}B(p,\alpha_0)^7Be$ and $^{10}B(p,\alpha_1)^7Be^*$ Reactions between E_p = 0.8 MeV and 3.25 MeV. Center-of-Mass Differential Cross Section versus E_p(Lab). Solid lines are to guide the eye. Statistical Errors are less than the size of the points.

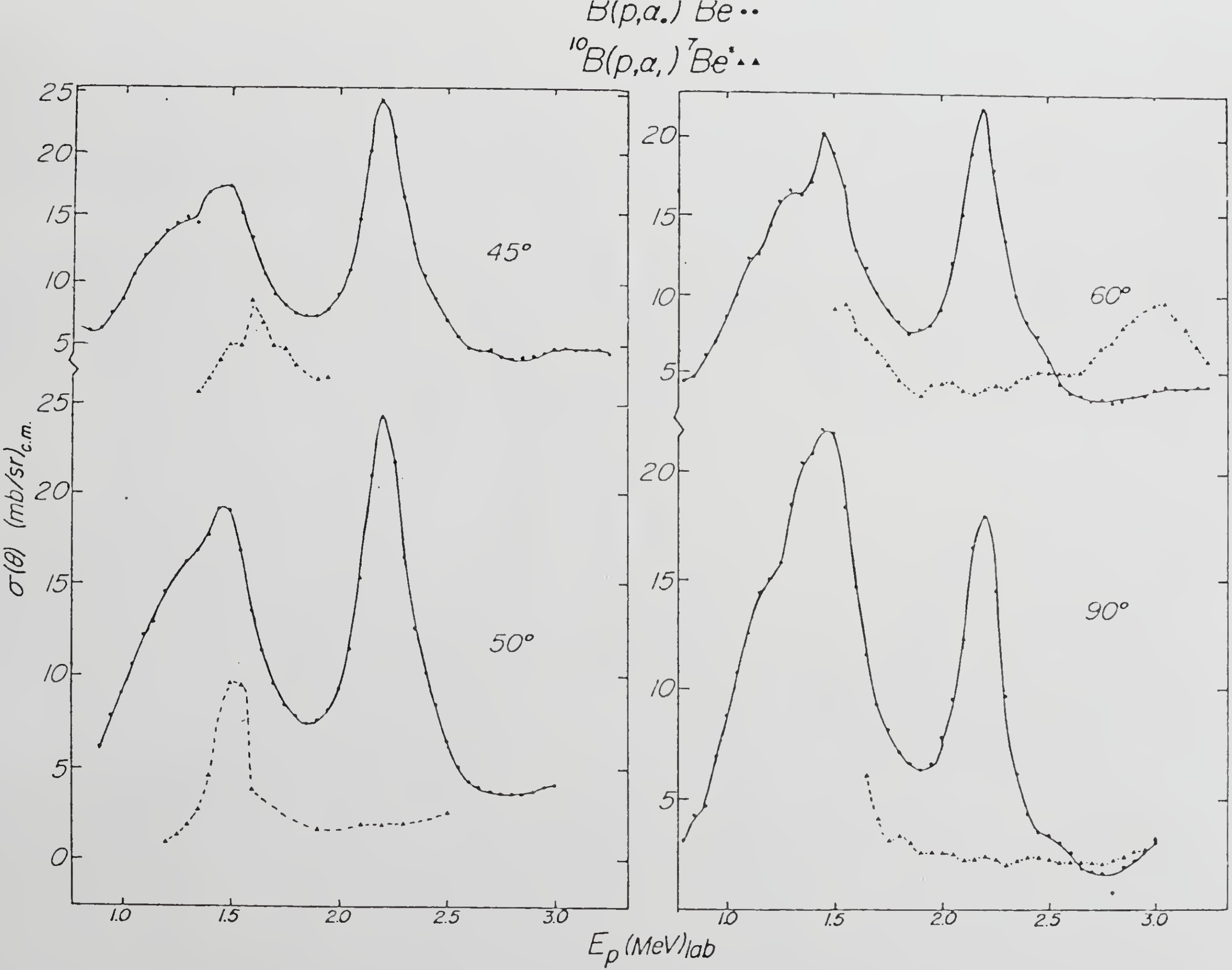
B(p,α₀) Be ••
¹⁰B(p,α₁) ⁷Be* ▲▲
σ(θ) (mb/sr)c.m.
Ep (MeV)lab
45°
50°
60°
90°
25
20
15
10
5
0
1.0
1.5
2.0
2.5
3.0

The angular distributions were fitted using a Legendre polynomial expansion as previously discussed. Initial examination of the χ^2 measure of goodness-of-fit indicated that polynomials only through P_4 (cosΘ) were required. A pure resonance would be symmetric around 90° and would require only the even polynomials (P_0,P_2,P_4) for description of its angular distribution. Any resonance effects are more pronounced in the back (>90°) angles where direct processes are normally small, and so these points were fitted using only even polynomials. Most of the angular structure was thus accounted for using P_0, P_2, and P_4; the χ^2 measure of the quality of fit did not indicate the need for the addition of a P_3 (cosΘ) term. The angular distributions in their entirety were not symmetric around 90° but showed a slight forward-to-backward tilt, which indicated the need for P_1 (cosΘ). Therefore, the angular distributions in the region E_p = 1.10 to 1.90 MeV were fitted using only P_0, P_1, P_2, and P_4. The Legendre coefficients resulting from this fitting procedure are given in Table 1 and shown in Figure 11. At 1.1 MeV, the χ^2 criterion indicated that P_2 and P_4 were unnecessary; their coefficients were zero within error. At 1.30 MeV, the coefficient of P_4 was also zero. These values are marked with a cross.

In the region E_p = 1.1 to 1.9 MeV, there is no obvious peaking of the odd Legendre coefficients (A_1) as reported by Cronin [Cr56]. The energy dependence of Cronin's

Figure 10. Measured Angular Distributions for the $^{10}B(p,\alpha_0)^7Be$ Reaction at Selected Proton Energies. Solid lines are the Legendre polynomial least-squares fits. Statistical errors are less than the size of the points.

$^{10}B(p,\alpha_0)^7Be$

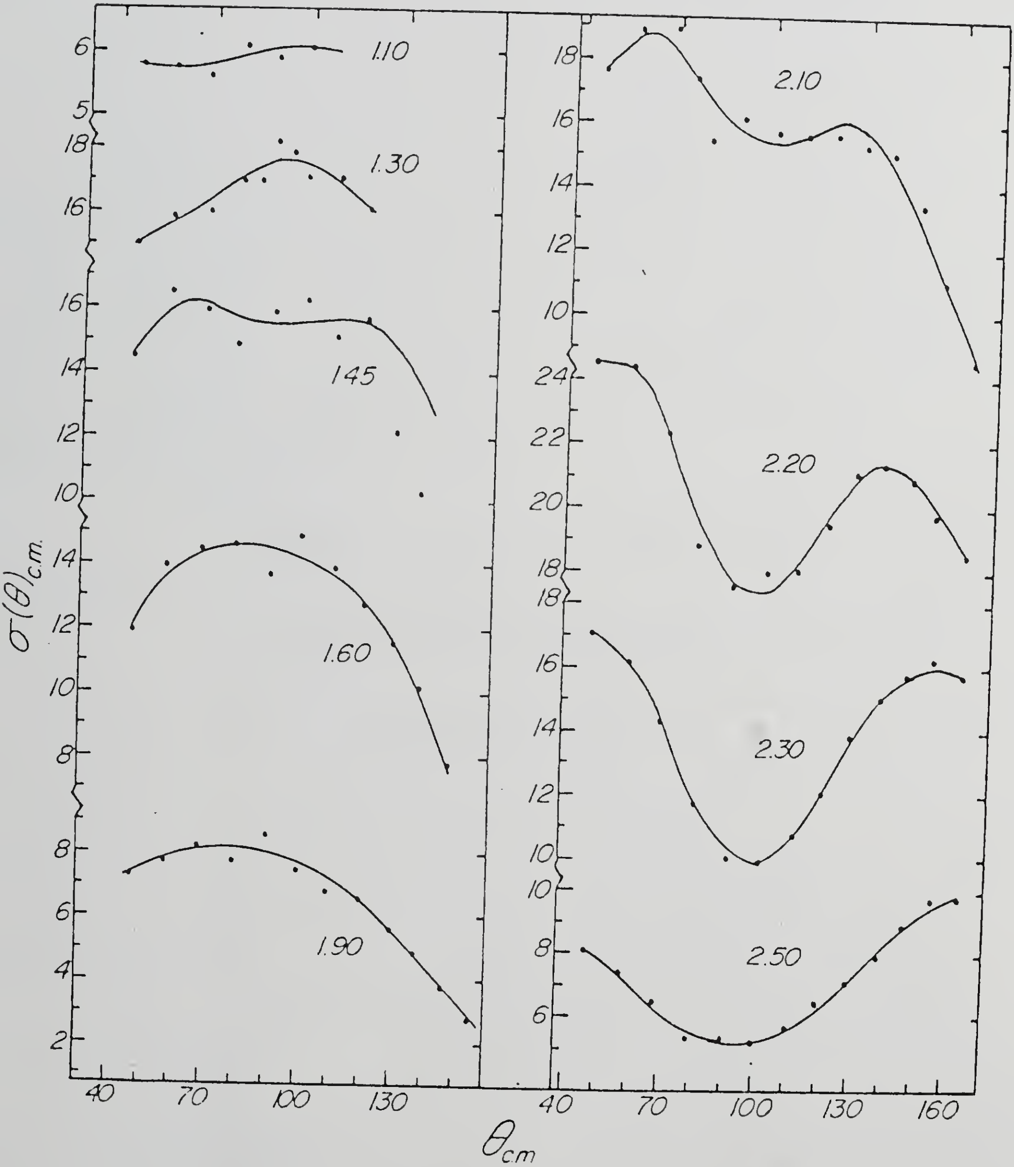

TABLE 1

Legendre Polynomial Coefficients for Angular Distributions of $^{10}B(p,\alpha_0)^7Be$ Reaction

E_p	A_0	A_1	A_2	A_3	A_4
1.1	5.99 ±.05	-0.43±.12	--	--	--
1.3	15.8 ±.1	-0.3 ±.2	-3.3 ±.4	--	--
1.45	13.9 ±.1	0.54±.2	-6.2 ±.1	--	-4.05±.7
1.5	12.0 ±.1	0.90±.1	-6.6 ±.3	--	-2.1 ±.3
1.9	6.65 ±.1	1.32±.2	-3.2 ±.3	-0.06±.3	-0.68±.26
2.1	15.3 ±.1	0.77±.3	-4.7 ±.4	-2.4 ±.5	-5.4 ±.4
2.2	20.3 ±.1	1.2 ±.3	0.63±.45	-3.50±.5	-6.0 ±.4
2.3	13.5 ±.1	0.8 ±.3	3.35±.35	-3.57±.5	-3.9 ±.3
2.5	7.3 ±.1	0.19±.2	3.13±.3	-0.8 ±.3	-0.6 ±.2

coefficients can basically be reproduced by fitting the angular distributions using all the polynomials P_0 through P_4. The observed peaking of the odd coefficient near E_p = 1.4 MeV is, therefore, probably a result of the fitting procedure and not due to any angular momentum considerations.

If the APCETS model is correct, the resonances I and II should have spins of $3/2^-$ and $1/2^-$, respectively. The lower energy resonance would be expected to decay by an $L = 0$ alpha particle and would thus only result in an A_0 coefficient in its Legendre fit. This expectation is consistent with our results, not considering the small A_1 value which will be discussed later. A $1/2^-$ state (for resonance II) decaying to the $3/2^-$ ground state of ^7Be would be expected to require P_2 for its description. We obtain a significant A_2 value in this region ($E_p \sim 1.5$ MeV) but we also have A_4 being non-zero along with the small A_1.

The smooth energy dependence of A_1 indicates that there are some background processes of opposite (+) parity occurring, a not unreasonable possibility. The necessity of P_4 in fitting the angular distributions around the higher energy resonance might be caused by some process other than alpha-particle cluster state formation. Another level which does not fit into the APCETS scheme might exist in this energy region (another level has been postulated by Overley and Whaling), or some other process might be taking place. Support is given to the possibility of alternative explanations by close examination of the energy dependence of the coefficients.

The A_2 coefficient does not appear to peak exactly at the energy of the upper resonance (E_p = 1.5 MeV, see Figure 9), indicating that it is not entirely a result of that resonance. Secondly, the A_4 coefficient, though it does appear to peak at this resonance (II) energy, peaks as a result of only one point (one angular distribution) and, if the A_4/A_0 ratio is examined (Figure 12), the energy dependence is fairly smooth when the error bars are taken into consideration. We cannot therefore rule out, from our data, the possibility that the two states seen near E_p = 1.20 MeV and 1.50 MeV are APCETS and have spins of $3/2^-$ and $1/2^-$, respectively.

Computation of the $\overline{Z}$ amplitudes (See Sect. III, B.) for the assignments made by Overley and Whaling [Ov62] indicates that the signs and, to the first order, the magnitudes of the experimental A_L/A_0 ratios are consistent with their assignments. Those authors calculated the $^{10}B(p,p)^{10}B$ cross-section using a simplified R-matrix formalism with the resonance parameters $J^\pi = 5/2^+$, E_R = 1.17 MeV, Γ_p = 45 keV, Γ_α = 225 keV, Γ_{TOT} = 300 keV, and $J^\pi = 7/2^+$, E_R = 1.50 MeV, Γ_p = 90 keV, Γ_α = 100 kev, Γ_T = 250 keV. The parameters for the $7/2^+$ (II) states are consistent with Cronin, though the $5/2^+$ state parameters are not. Both states would be produced by s-wave protons with channel spins $5/2^+$ and $7/2^+$, respectively, although no interference effects were included in their calculations.

Figure 11. The Legendre Coefficient Resulting from the Fits to the $^{10}B(p,\alpha_0)^7Be$ Angular Distributions; Coefficients of Polynomials P_0 through P_4. Calculated errors are shown. The solid line represents a smooth curve drawn through the data points. A_3 and A_4 = 0.

* - p_2 not used in fit; x - p_3 not used in fit; ⊗ - p_4 not used in fit.

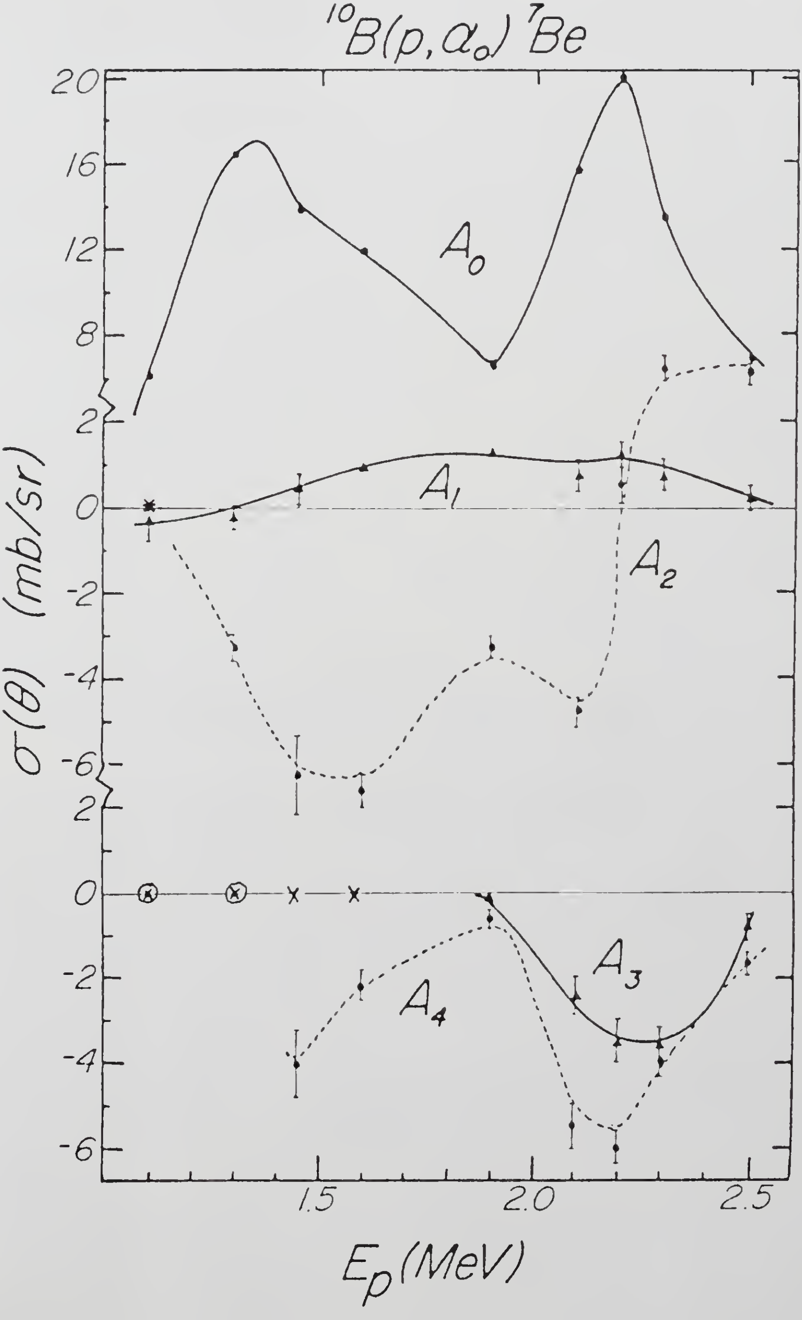
$^{10}B(p,\alpha_0)^7Be$
A_0
A_1
A_2
A_3
A_4
$\sigma(\theta)$ (mb/sr)
E_p(MeV)
20
16
12
8
2
0
-2
-4
-6
2
0
-2
-4
-6
1.5
2.0
2.5

Figure 12. Legendre Coefficient Ratios Resulting from the fits to the $^{10}B(p, \alpha)^{7}Be$ Angular Distributions. The solid line represents a smooth curve drawn through the data points. Errors are shown.

$^{10}B(p,\alpha_0)^7Be$

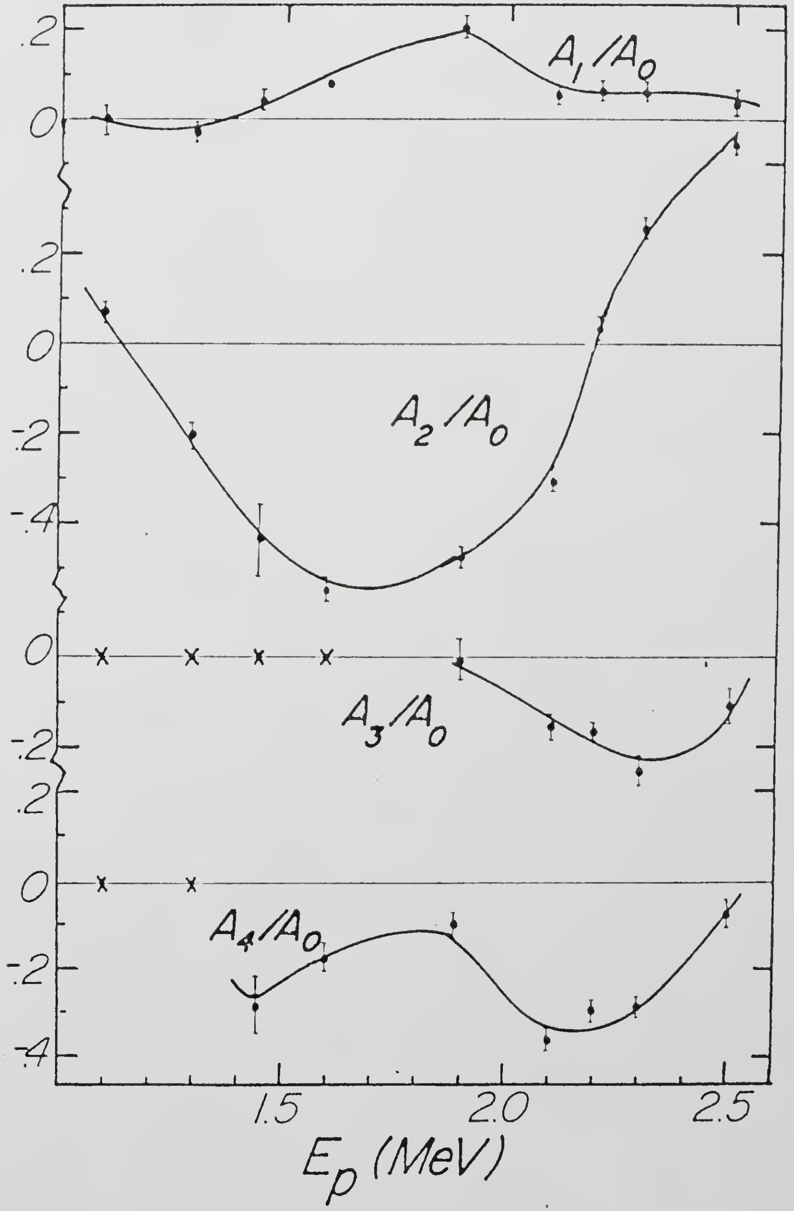

Overley and Whaling state that above E_p = 1.3 MeV, higher ℓ-values are actually needed to describe the proton scattering. If the states seen in the (p,p) scattering are the same as those in the (p,α_0) reaction, then the requirement for higher ℓ-values might be an indication of the existence of an opposite-parity background, as previously discussed concerning the APCETS prediction.

Attempts to reproduce both our alpha particle data and the elastic proton data simultaneously with Overley and Whaling's parameters using the full R-matrix formalism were not successful. This failure does cast some doubt on their parameter assignments, which are inconsistent with the APCETS model.

The Overley and Whaling spin assignments of $5/2^+$ and $7/2^+$ for resonances I and II are also not consistent with the γ-ray decay rate [Ch56, Ja61], which requires a negative parity state at 1.17 MeV. It is possible that the (p,γ) reaction is populating a different state from the (p,α) reaction; the reported energies and total widths are slightly different: E_p = 1.14 MeV and $\Gamma_{TOT} \simeq 540$ keV in the (p,γ) reaction [Ch56]; E_p = 1.17 MeV and $\Gamma_{TOT} \simeq 300$ keV in the (p,α) reaction. Our Legendre fitting information is not inconsistent with some negative parity assignments, the same parity as predicted by the APCETS scheme. Our data also show that the 10.09 MeV state (II) decays by α_1 emission, while the lower level shows no such decay. This fact gives strong support to the APCETS model since we would expect this state to be strongly coupled to the first excited state of ^{7}Be. Though the predictions of the APCETS model ($3/2^-$, $1/2^-$) and the assignments of Overley and Whaling ($5/2^+$, $7/2^+$) are not consistent, our data cannot rule out either set. For the most part, this inconsistency seems to stem from incomplete data. The original γ-ray and (p,γ) work included no rigorous calculations. More work needs to be done, especially in the (p,γ) reaction, in order to clear up the confusion.

In the energy region E_p = 1.9 to 3.0 MeV, the proton elastic scattering and α_0 yields are dominated by a large resonance centered at E_p = 2.2 MeV (E_x = 1.068 MeV). Overley and Whaling [Ov62] examined the angular distributions around this energy and concluded that the resonance was formed predominantly by $\ell = 2$ protons. Of the spin values which can be formed by coupling the spin of the ground state of ^{10}B($J^\pi = 3^+$) with d-wave protons, only $9/2^+$ and $11/2^+$ can be made exclusively by this coupling, though the possible values are $1/2^+$ through $11/2^+$. The maximum cross-section of the elastically scattered peak limited the spin to values larger than 5/2 [Ov62]. The spin value $11/2^+$ can probably be discarded since it would require $\ell' = 5$ for the observed α_0 decay to the ground state in ^{7}Be. Therefore, the choice of $7/2^+$ or $9/2^+$ remains. The choice of $9/2^+$ is more favored for several reasons: first, a $7/2^+$ state could decay by $\ell' = 3$ α-emission to both the ground state and first excited state ($J^\pi = 1/2^-$) of ^{7}Be, but for a $9/2^+$

assignment, ℓ' can be 3 for the α_0 group while it must be 5 for the α_1 group, thus predicting a lower liklihood for the α_1 decay; our data show no evidence for the α_1 decay. Second, calculation of the appropriate $\overline{Z}$ amplitudes favors $9/2^+$ over $7/2^+$ because of the experimentally observed negative value of A_4 in this energy region as shown in Figure 10. Third, the R-matrix calculation using $9/2^+$ as the spin value done both by Overley and Whaling and in this present work, reproduces the basic characteristics of this resonance in both the proton and alpha exit channels. Overley and Whaling did find it necessary to postulate the existence of a $7/2^+$ state at $E_p = 2.8$ MeV in order to satisfactorily fit their data; our data show no evidence for the existence of such a state. Overley and Whaling display no firm experimental evidence other than a better fit to lower energy data.

This resonance at 10.68 MeV was also measured by Jenkin et al [Je64]. The cross-section at 90° for the $^{10}B(p,\alpha_0)$ reaction in Jenkins measurement is approximately 50% of that of Overley and Whaling; no reason for this discrepancy is apparent. A very narrow state at $E_p = 2.189$ MeV observed by Bernstein [Be65] in the reaction $^{10}B(p,\alpha_0)^7Be$ is very weak and not readily identified with the state in question because of its width (<50 keV) as compared to the width as measured by Overley and Whaling of 200 keV.

Again in this energy region, as in the lower energy

Figure 13. Measured Angular Distributions for the $^{10}B(p,\alpha_1)^7Be^*$ Reaction at Selected Proton Laboratory Energies. Solid lines are the Legendre polynomial least-squares fits. Statistical errors are less than the size of the points.

$^{10}B(p,\alpha_1)^7Be^*$

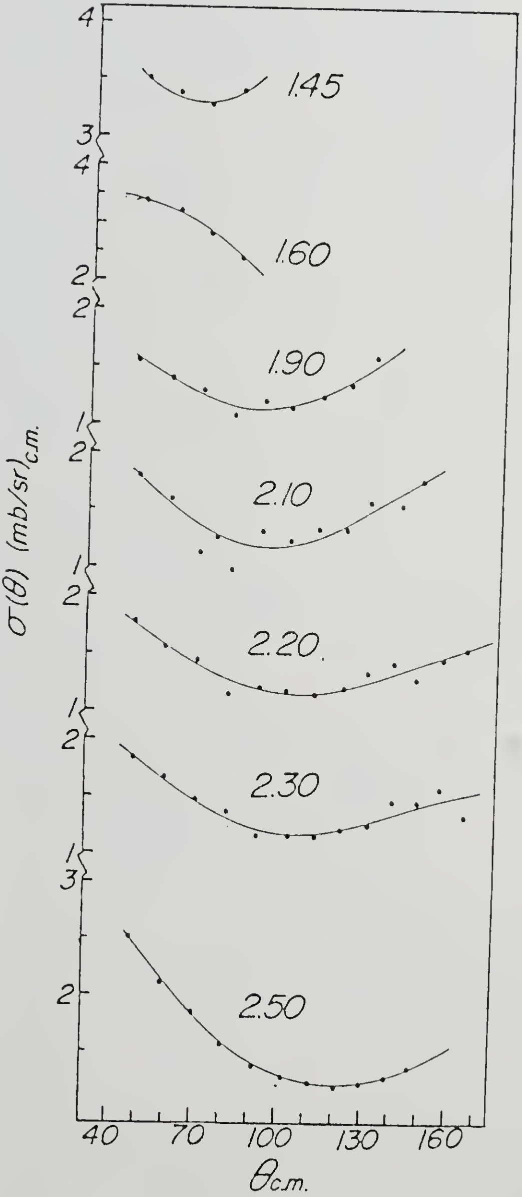

TABLE 2

Legendre Polynomial Coefficients for Angular Distributions of $^{10}B(p,\alpha_1)^7Be$ Reaction

E_p	A_0	A_1	A_2
1.45	4.55 .5	-2.01 .9	1.76 .7
1.60	1.18 .4	3.64 .7	-1.28 .6
1.9	1.45 .02	0.02 .03	0.64 .05
2.1	1.55 .01	0.19 .03	0.74 .04
2.2	1.43 .01	0.35 .02	0.49 .03
2.3	1.43 .01	0.43 .02	0.51 .03
2.5	1.75 .01	0.93. 03	0.67 .04

Figure 14. The Legendre Coefficients Resulting from the Fits to the $^{10}B(p,\alpha_1)^7Be^*$ Angular Distributions. The solid line represents a smooth curve drawn through the data points.

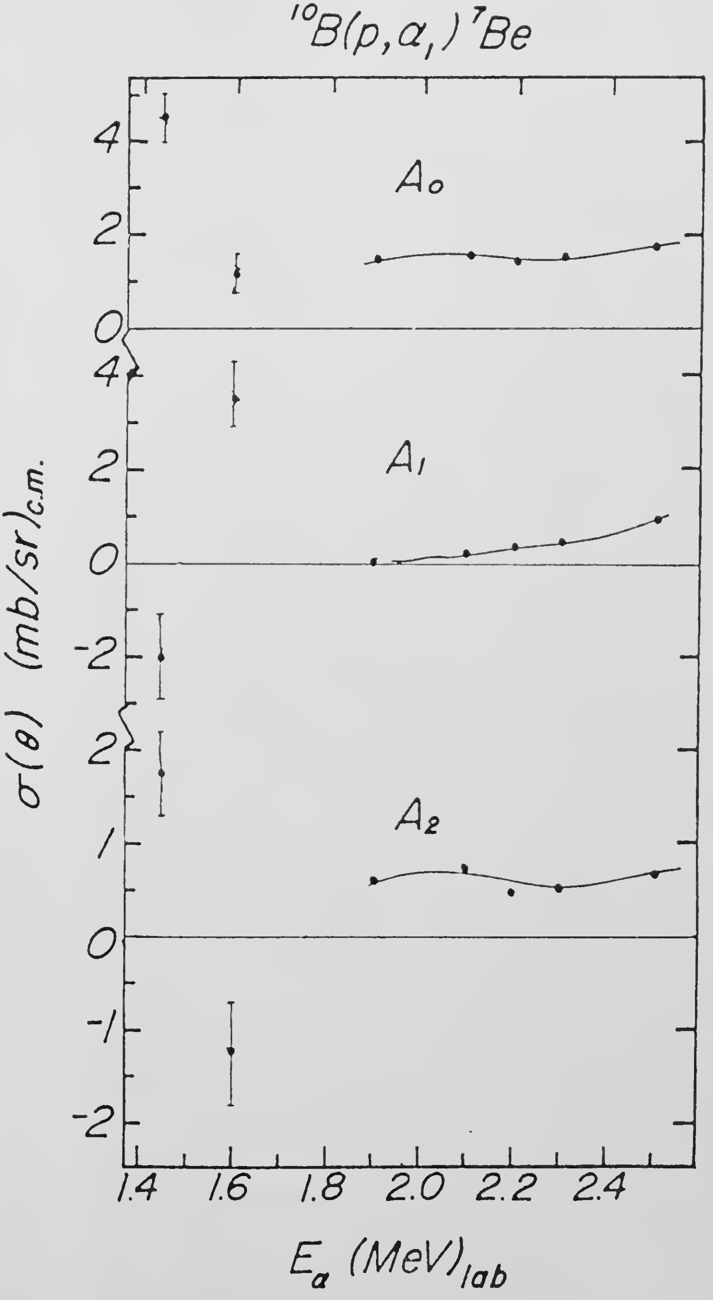

$^{10}B(p,\alpha_1)^7Be$
A₀
A₁
A₂
4
2
0
4
2
0
-2
2
1
0
-1
-2
σ(θ) (mb/sr)c.m.
1.4
1.6
1.8
2.0
2.2
2.4
E_α (MeV)lab

region, some odd order polynomials were necessary for the fit of the angular distributions. In fact, the χ^2 criterion indicated that both P_1 and P_3 were necessary, as shown in Figure 11. If the spin assignments are correct ($9/2^+$ for the E_p = 2.2 MeV resonance, and $7/2^+$ for the postulated 2.8 MeV resonance), then no odd polynomials should be necessary since odd order polynomials result from interference of states of opposite parity. The appearance of the odd order polynomials suggests that there is an unidentified smooth negative parity background. Negative parity states (or processes) which comprise this background may be the cause of the seemingly inconsistent γ decay data. Only further experiments will tell. Our present data are not inconsistent with the Overley and Whaling parameters of E_R = 2.18±.02 MeV, $J^\pi = 9/2^+$, and Γ_{TOT} cm = 200±20 keV; we have no measure of the partial widths of this state.

B. ^{12}C

Carbon-12 is a nucleus on which numerous experimental and theoretical studies have been performed. The reasons for this situation are many: it is a light, stable, even-even nucleus where both the neutron and proton $P_{3/2}$ shells are filled; the six protons and six neutrons lend themselves to both cluster and alpha particle models; it is an important member of the chain in certain astrophysical processes, and it is a readily available target.

In order to populate the energy levels in ^{12}C above excitations of 25 MeV, one must use protons of energy 10

MeV or greater impinging on ^{11}B. The reaction ^{9}B + ^{3}He can form states above 26.3 MeV while the reactions in ^{10}B + d and ^{6}Li + ^{6}Li can form states in excitation above 27.37 MeV and 28.175 MeV, respectively. In this work, we explore the energy region of 25.8 to 28.5 MeV through the reaction ^{10}B + d.

The region of excitation between 25.2 MeV and 28.6 MeV holds great interest because of the formation of T ≠ 0 states. A T = 1, 2^+ state at 27.9 MeV was predicted using a shell model formalism by Vinh-Mau and Brown [Vi62]. A T = 1, $J^\pi = 1^-$ state has been seen through the reaction ^{9}Be(^{3}He,γ)^{12}C by Blatt et al. [Bl72], interpreted as a 3p - 3h state. The existence of the lowest lying T = 2 state in ^{12}C was found by Nettles, et al. [Ne71] to occur at E_x = 27.595±.02 MeV and was confirmed by Goosman et al. [Go74]. In other work in this energy region above the giant dipole resonance (which occurs at E_x = 22.5 MeV) states have been reported at E_x = 27.4 MeV [Gr64].

In the present experiment, the energy region in ^{12}C from 25.8 to 28.5 MeV was studied through the reactions ^{10}B(d,d)^{10}B, ^{10}B(d,α_0)^{8}Be, and ^{10}B(d,α_1)^{8}Be$^{*}_{2.94}$ using incident deuteron energies of 0.8 MeV to 4.0 MeV. Some of this energy region had been previously explored using these same reactions by Purser et al. [Pu63], Din et al. [Di67], Black et al. [Bl70], and Friedland and Verleger [Fr68].

A typical excitation curve for the elastically scattered deuterons is shown in Figure 15. This curve shows

Figure 15. Excitation Curve for the $^{10}B(d,d)^{10}B$ Reaction Cross Section at $\Theta_{Lab} = 150°$ Differential Cross Section (mb/sr) versus Ed(Lab). Solid line is to guide the eye. Sample statistical errors are shown.

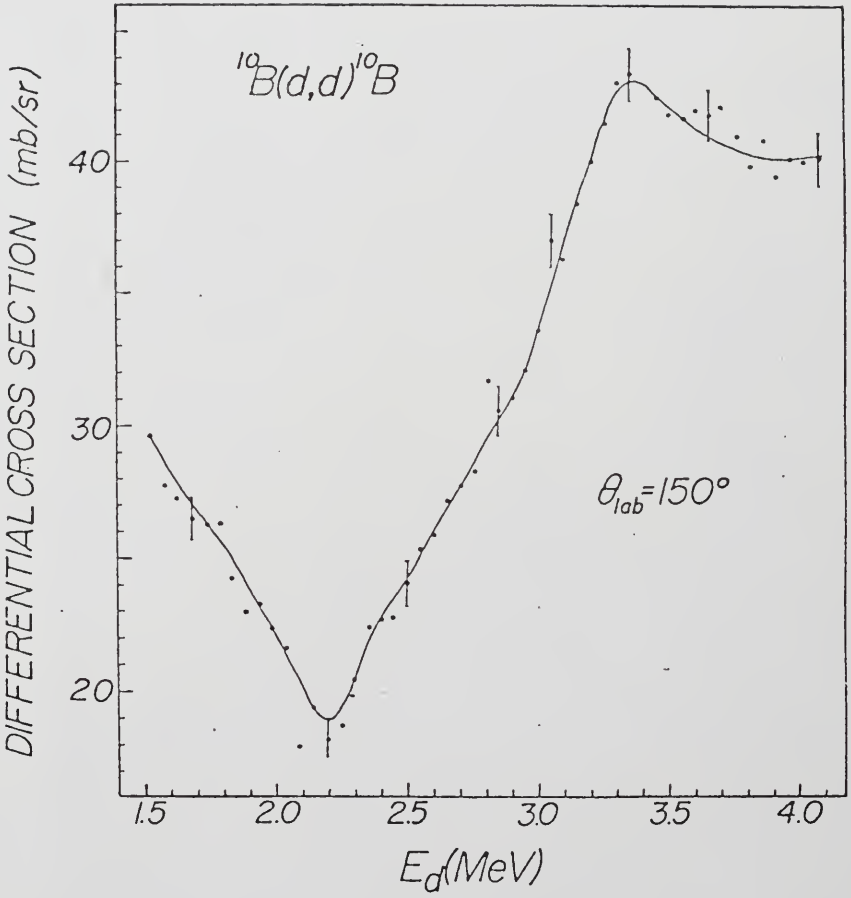
$^{10}B(d,d)^{10}B$
DIFFERENTIAL CROSS SECTION (mb/sr)
40
30
20
$\theta_{lab}=150°$
1.5
2.0
2.5
3.0
3.5
4.0
E_d(MeV)

a minimum occurring at E_d = 2.2 MeV, then a gradual increase to a maximum in the cross-section at E_d = 3.3 MeV. The data points were taken in 50 keV steps from 1.5 to 4.0 MeV. Figure 16 shows the angular distributions which were measured at six energies in this region. They show a smooth energy dependence and little angular structure.

It was decided that the use of the optical model might give some insight into this reaction. Using the code JUPITOR2 [Ta67], the optical model parameters were adjusted to obtain a reproduction of the angular distributions for this elastic scattering reaction. A typical fit is shown in Figure 17 for the distribution resulting from incident deuterons of energy 1.5 MeV (E_x = 26.4 MeV). The optical model parameters which resulted in this fit are listed in Table 3. These parameters are close to those used for other light nuclei [Pa68].

The energy dependence of the well depths was smooth throughout this region. Since the optical model was successful in reproducing most of the significant features in the angular distributions, it was unnecessary to include any resonance effects.

The reactions $^{10}B(d,\alpha_0)^7Be$ (Q = 17.82 MeV) and $^{10}B(d,\alpha_1)^8Be^*$ (Q = 14.88 MeV) were performed for incident deuteron energies of 0.8 to 4.0 MeV. Typical excitation curves are shown in Figure 18. The α_0 yield curve is dominated by two distinct resonances centered around laboratory energies E_d = 1.0 MeV and E_d = 2.0 MeV. The

Figure 16. Measured angular Distributions for the $^{10}B(d,d)^{10}B$ Reaction at Selected Deuteron Laboratory Energies. The solid line represents a smooth curve drawn through the data points. Statistical errors are less than the size of the points.

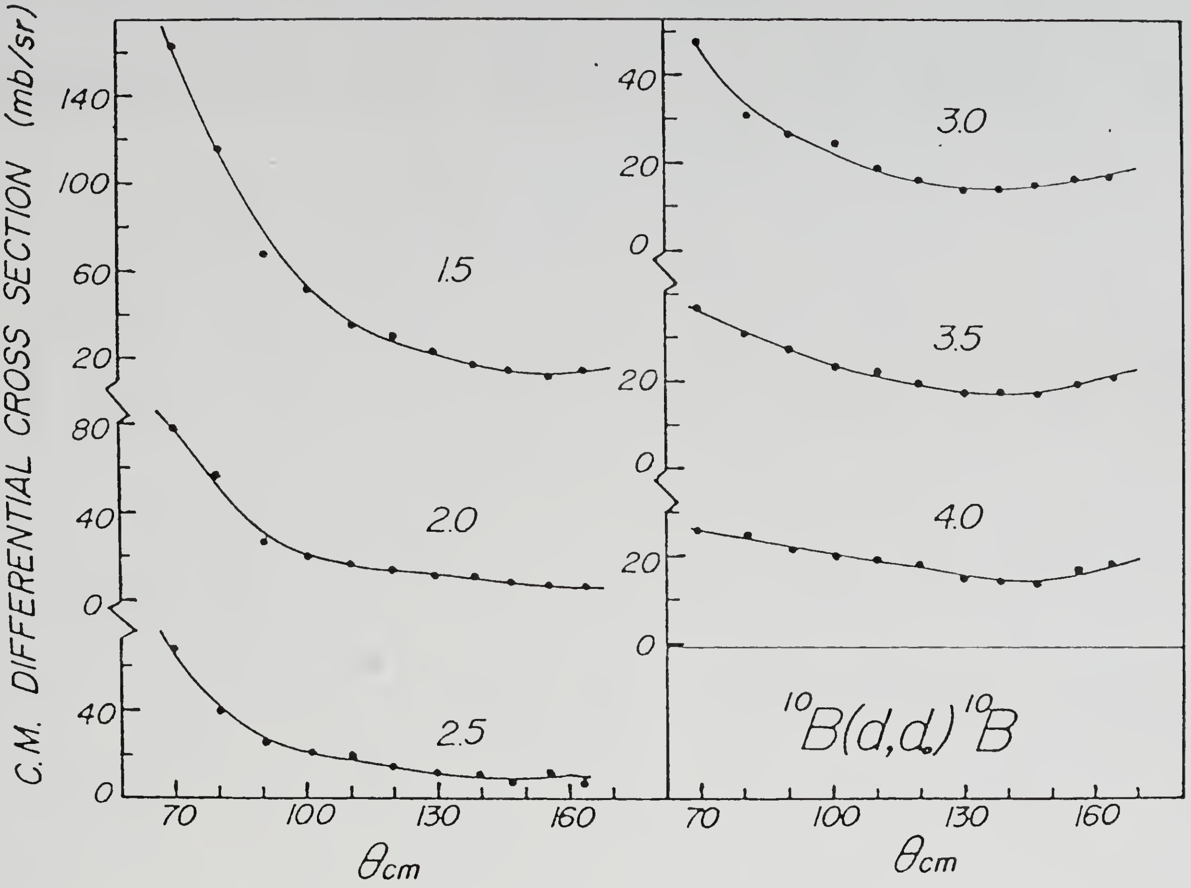
C.M. DIFFERENTIAL CROSS SECTION (mb/sr)
140
100
60
20
80
40
0
40
0
70
100
130
160
θ_{cm}
1.5
2.0
2.5
40
20
0
20
0
20
0
3.0
3.5
4.0
70
100
130
160
θ_{cm}
$^{10}B(d,d_0)^{10}B$

Figure 17. Measured Angular Distribution for the $^{10}B(d,d)^{10}B$ Reaction at a Deuteron Laboratory Energy of 1.50 MeV. Solid line is optical model fit. Statistical errors are shown.

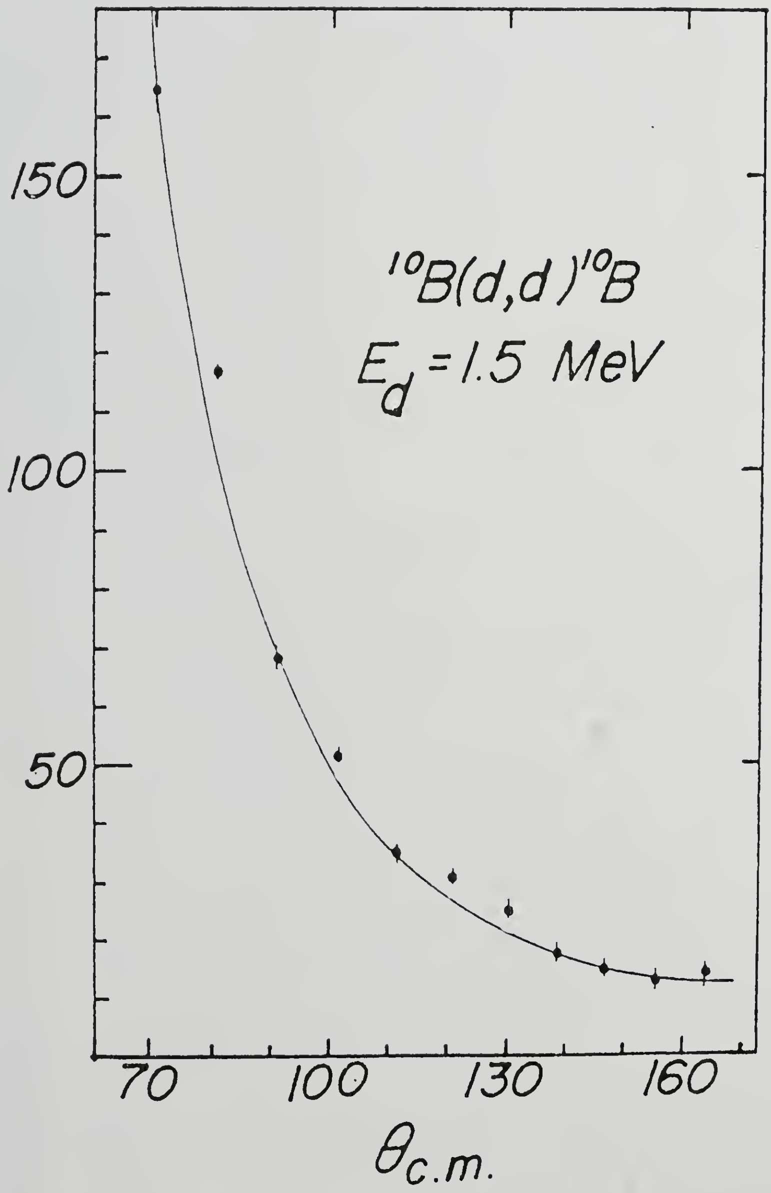
$^{10}B(d,d)^{10}B$
$E_d = 1.5$ MeV
$\sigma(\theta)$ (mb/sr)$_{c.m.}$
150
100
50
70
100
130
160
$\theta_{c.m.}$

TABLE 3

Optical Model Parameters for the Fit to the $^{10}B(d,d)^{10}B$ Angular Distribution at E_d = 1.50 MeV

V_0 = 94.4 MeV (25)	Real well depth
W_s = 32.1 MeV (11)	Imaginary well depth (surface)
A_r = 0.74 fm (.72)	Real well diffuseness
A_s = 1.24 fm (1.2)	Imaginary well diffuseness
R_o = 1.24 fm (1.85)	Real well radius
R_s = 1.2 fm (1.2)	Imaginary well radius
V_{so} = 0 MeV (0)	Spin-orbit well depth
W_v = 0 MeV (0)	Volume imagined well depth

All non-zero parameters (except R_s) were varied in order to obtain a fit to the angular distributions. Also given (in parentheses) are the initial parameters used in the search.

Figure 18. a) Excitation Curve for the $^{10}B(d,\alpha_0)^8Be$ Reaction at Θ_{Lab} = 90° for Laboratory Deuteron Energies of 0.8 MeV to 4.0 MeV

b) Excitation Curve for the $^{10}B(d,\alpha_1)^8Be^*$ Reaction at Θ_{Lab} = 150° for Laboratory Deuteron Energies of 0.8 MeV to 4.0 MeV.

Both curves are laboratory yield versus deuteron energy. Statistical errors are shown. Solid lines are to guide the eye.

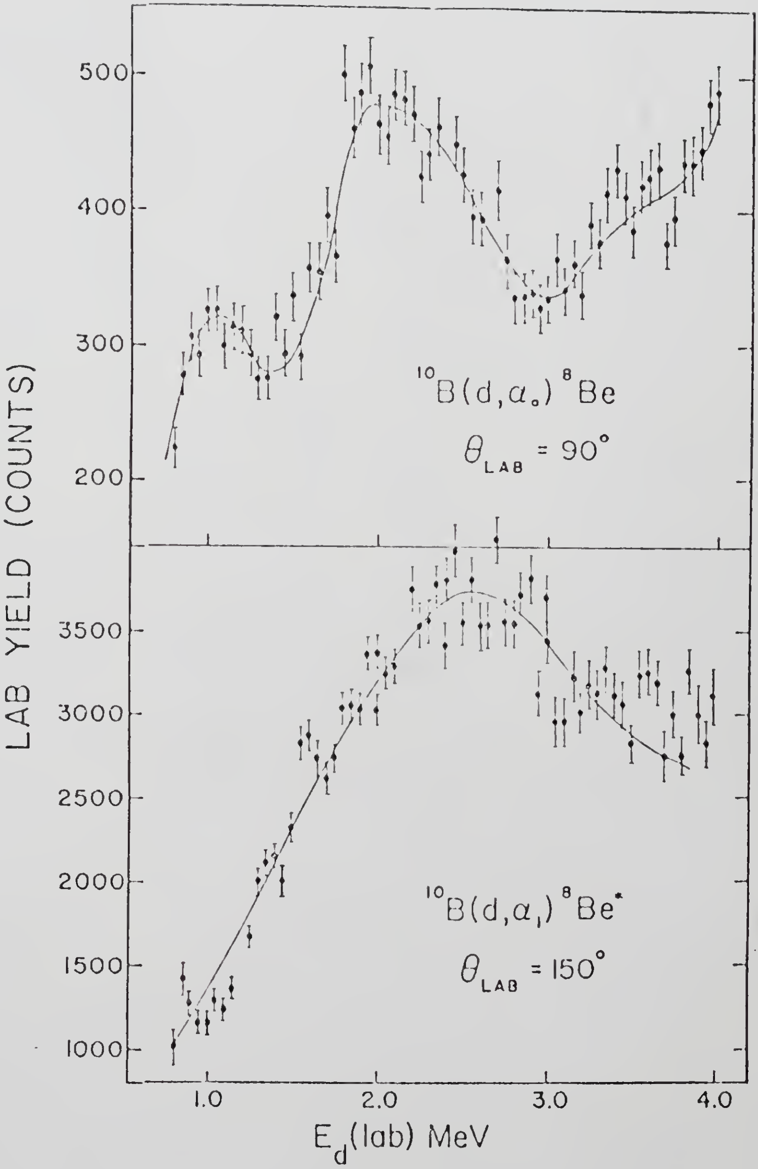
LAB YIELD (COUNTS)
500
400
300
200
$^{10}B(d,\alpha_0)^8Be$
$\theta_{LAB} = 90°$
3500
3000
2500
2000
1500
1000
$^{10}B(d,\alpha_1)^8Be^*$
$\theta_{LAB} = 150°$
1.0
2.0
3.0
4.0
E_d(lab) MeV

lower energy resonance is narrower than the higher energy one. The α_1 excitation curve exhibits one large resonance near $E_d = 2.1$ MeV. The structure of these curves suggested the application of the APCETS model.

The residual nucleus, ^{8}Be, has a ground state with $J^\pi = 0^+$, $T = 0$ and a first excited state with $J^\pi = 2^+$ at 2.94 MeV. The first excited state is relatively broad (1.5 MeV) compared to the ground state and, like the ground state, is unstable to decay. In this experiment, the appearance of two states in the α_0 decay channel separated by 1 MeV with the upper one relatively broad suggested that these levels might be identified, within the APCETS model, with the ground and first excited states of ^{8}Be. The measurement of a resonance in the α_1 decay channel at nearly the same energy as the upper resonance in the α_0 channel gave more support to this identification.

In order to attempt to make spin-parity assignments to these two levels, angular distributions were measured at 11 energies in this region; these distributions are shown in Figure 19. The usual least-square fitting procedure using Legendre polynomials was performed, with the resulting fits also shown in Figure 19. It was found that the fit to the five lowest energy distributions ($E_d = 0.85$, 0.9, 0.95, 1.05, and 1.20 MeV) required only polynomials P_0 through P_4; higher order polynomials were judged necessary using the χ^2 criterion. The six remaining distributions were found to require the addition of P_5 (cosΘ) to attain a

Figure 19. Measured Angular Distributions for the $^{10}B(d,\alpha_0)^8Be$ Reaction at Selected Deuteron Laboratory Energies. Solid lines are the Legendre polynomial least-square fits. Statistical errors are shown.

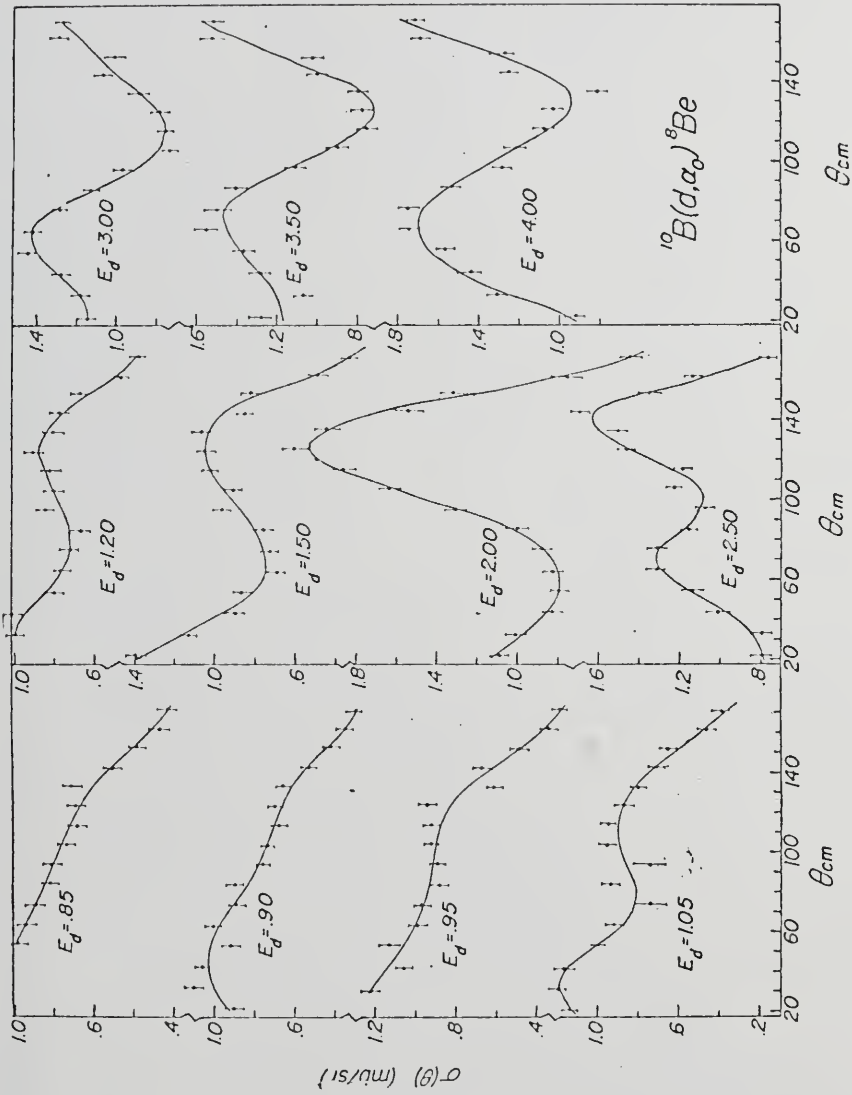
$^{10}B(d,\alpha_0)^8Be$
E_d=.85
E_d=.90
E_d=.95
E_d=1.05
E_d=1.20
E_d=1.50
E_d=2.00
E_d=2.50
E_d=3.00
E_d=3.50
E_d=4.00
θ_{cm}
20
60
100
140
$\sigma(\theta)$ (mb/sr)
1.0
.6
.4
1.0
.6
1.2
.8
.4
1.0
.6
.2
1.0
.6
1.4
1.0
.6
1.8
1.4
1.0
1.6
1.2
.8
1.4
1.0
1.6
1.2
.8
1.8
1.4
1.0

satisfactory χ^2. The coefficients of the polynomials are listed in Table 4 and plotted as a function of energy in Figure 20.

According to the APCETS model, these two states should have $J^\pi = 0^+$ for the state at $E_d = 1.0$ MeV and $J^\pi = 2^+$ for the state at $E_d = 2.1$ MeV, the same J's of the ground state and first excited state in ^{8}Be. These assignments are consistent with the behavior of the even Legendre coefficients of Figure 20. Namely, only A_0 is involved in the 0^+ level at $E_d = 1.0$ MeV, whereas A_0, A_2 and A_4 are involved in the 2^+ level at $E_d = 2.1$ MeV. Both of these assignments have positive parity and therefore, the measured angular distributions should, in a pure two-level representation, require no odd polynomials for the description of the angular distributions. The necessity for the use of the odd Legendre polynomials, P_1, P_3 and P_5, indicates that some interference effects are occurring. Whatever the background or other level effects are, those effects must have negative parity components to account for the odd polynomials.

Within the context of this experiment, the rise in the cross-section beginning around $E_d = 3.5$ MeV suggested the existence of another level at higher energy. If this level had negative parity and was broad enough to extend down in energy to the region of the other two levels in question, then the requirement for odd Legendre polynomials might be explained. In fact, the shape of the excitation curve (Figure 18) does suggest that such a level might have a low-energy "tail" which would underlie the other two levels. The existence of the A_5 coefficient indicates that the spin of this level would need to be at least J = 3 if

TABLE 4

Legendre Polynomial Coeficients for Angular Distributions of $^{10}B(d,\alpha_0)^8Be$ Reaction

E_d	A_0	A_1	A_2	A_3	A_4	A_5
0.85	.77±.04	.26±.1	-.17±.13	.002±.13	-.145±.07	---
0.90	.79±.01	.30±.02	-.10±.03	0 ± .03	-.12 ± .03	---
0.95	.91±.02	.34±.03	-.07±.04	.2 ± .05	-.05 ± .04	---
1.05	.90±.02	.33±.02	.02±.04	.2 ± .04	-.13 ± .04	---
1.20	.82±.01	.13±.02	.06±.03	.26 ± .04	-.13 ± .04	---
1.50	.91±.01	.08±.02	.12±.03	.49 ± .03	-.06 ± .04	.12±.04
2.00	1.26±.02	-.49±.02	-.1 ± .03	.84 ± .04	-.39 ± .04	.12±.05
2.50	1.21±.02	-.24±.02	-.10±.03	-.08 ± .04	-.31 ± .04	.40±.05
3.00	1.10±.02	-.24±.02	.07±.03	-.46 ± .04	.02 ± .04	.12±.05
3.50	1.17±.02	.25±.02	-.05±.03	-.49 ± .04	.35 ± .05	.17±.05
4.00	1.34±.02	.15±.02	-.24±.03	-.65 ± .04	.12 ± .05	-.13±.06

Figure 20. The Legendre Coefficient for the Fits to the Angular Distributions of $^{10}B(d,\alpha_0)^8Be$. Calculated errors are shown. The solid line represents a smooth curve drawn through the data points.

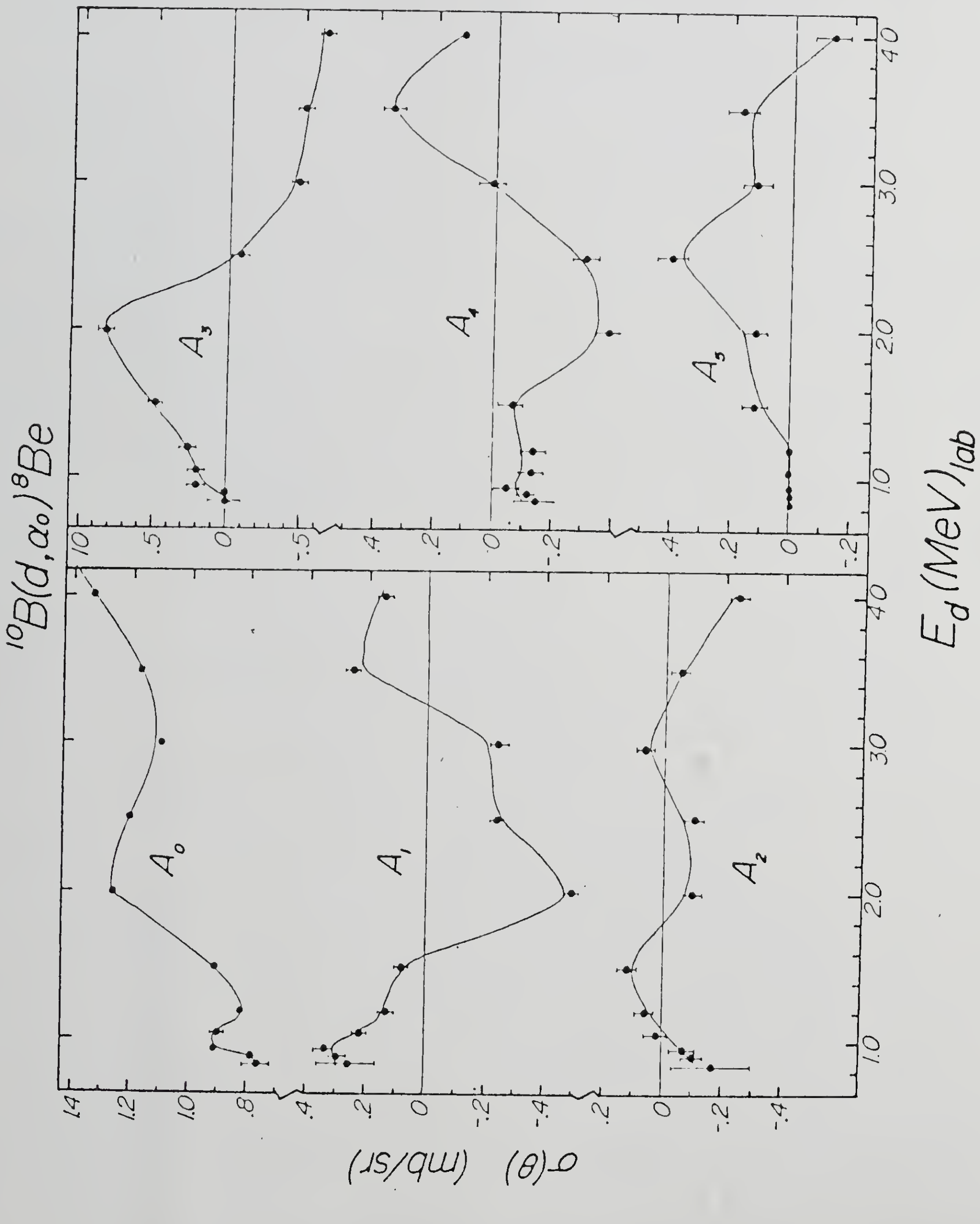
$^{10}B(d,\alpha_0)^8Be$
A_0
A_1
A_2
A_3
A_4
A_5
$\sigma(\theta)$ (mb/sr)
E_d (MeV)$_{lab}$
1.4
1.2
1.0
.8
.4
.2
0
-.2
-.4
.2
0
-.2
-.4
1.0
.5
0
-.5
.4
.2
0
-.2
.4
.2
0
-.2
1.0
2.0
3.0
4.0

the level at E_d = 2.1 MeV were a J = 2 level. The interference between a $J^\pi = 2^+$ and a $J^\pi = 3^-$ level might exhibit itself in A_1, A_3, and A_5 coefficients, all of which are present in the data. The interference between the postulated $J^\pi = 0^+$ and $J^\pi = 3^-$ levels would only be exhibited in the A_3 coefficients; while no strong effect can be identified in any of the odd coefficients around E_d = 1.0 MeV, the interference effects would be expected to be small because of the large energy separation between the two levels.

In order to more fully explore these possible assignments, the $\overline{Z}$ coefficient products, as appear in the equation given in Sect. III, B., were calculated. These products can be made to agree with those expected for the $0^+ - 2^+ - 3^-$ assignments for a suitable choice of magnitude and phases of the $\mathcal{T}$-matrix elements. So we can conclude that these data can be interpreted to be consistent with the assignment of spins and parities of 0^+ and 2^+ to the two states at E_d = 1.0 and 2.1 MeV.

The experimental appearance in the α_0 channel of a state which the APCETS model identifies as the first excited state of ^{8}Be coupled to an alpha particle is inconsistent with the pure APCETS model. Obviously, the wave function of the 2^+ state (tentatively assigned) must contain some ground-state-plus-alpha component along with a first-excited-state-plus-alpha component. A measure of the relative strengths of these components can be obtained from the reduced width, γ_c^2, for each channel. We can obtain a ratio for the reduced widths from the experimental data.

Assuming a Breit-Wigner form for the reaction C' → C given by

$$\sigma_{CC'} = \pi \lambda\!\!\!^{-2} \frac{2J+1}{(2I+1)(2i+1)} \frac{\Gamma_C \Gamma_{C'}}{\frac{\Gamma^2_{TOT}}{9} + (E-E_R)^2} \qquad [Fe60]$$

where $\lambda\!\!\!^{-}$ is the wave number, J is the angular momentum of the resonance, I is the spin of the target, i is the spin of the projectile, Γ_C and $\Gamma_{C'}$ are the partial widths of the respective channels, Γ^2_{TOT} is the total width, and E_R is the resonance energy, we can obtain the required ratio. The total width is the sum of the partial widths, each of which can be written as

$$\Gamma_C = 2P_C \gamma^2_C .$$

Here P_C is the penetrability and γ^2_C is the reduced width which is a measure of the probability of forming the channel, C, from the total nuclear wave function. If we take the ratio of resonance cross-section for two exit channels, C' and C", formed by the same incident channel, C, (as is the case), we obtain

$$\frac{\sigma_{C'C}}{\sigma_{C''C}} = \frac{\Gamma_{C'} \Gamma_C}{\Gamma_{C''} \Gamma_C} = \frac{2P_{C'} \gamma^2_{C'} \cdot 2P_C \gamma^2_C}{2P_{C''} \gamma^2_{C''} \cdot 2P_C \gamma^2_C}$$

which reduces to

$$\frac{\sigma_{C'C}}{\sigma_{C''C}} = \frac{2P_{C'} \gamma^2_{C'}}{2P_{C''} \gamma^2_{C''}} .$$

If we have a value for the left side of the equation [which we obtain from the measured integrated cross-section for α_0 at 2.0 MeV corrected for non-resonance background and from the data of Figure 18 for α_1 by assuming an isotropic ($\ell = 0$) angular distribution at 2.0 MeV] and can calculate the penetrabilities (which we can), we can then get a value for the ratio of the reduced widths.

In the present case, extracting from the resonance yields, we find that the yield for the tentative 2^+ state in the α_1 channel is at least three times the yield in the α_0 channel. If we define C' = α_0 and C" = α_1, then

$$\frac{\sigma_{\alpha_0}}{\sigma_{\alpha_1}} = \frac{1}{7} = \frac{P_{\alpha_0}\gamma^2_{\alpha_0}}{P_{\alpha_1}\gamma_{\alpha_1}} .$$

The penetrabilities have the values

$$P_{\alpha_0} = 7 \times 10^{-3}, (\ell=2)$$

$$\text{and} \quad P_{\alpha_1} = 7 \times 10^{-4}, (\ell=0)$$

using $r_0 = 1.4$ fm.

We therefore obtain a ratio of reduced widths

$$\frac{\gamma^2_{\alpha_0}}{\gamma^2_{\alpha_1}} = .01 .$$

This small value indicates that, although the 2^+ state appears in the α_0 channel, the wave function describing this state is composed mainly of the first excited state of ^{8}Be plus an alpha particle.

In the pure APCETS picture, this ratio should be zero. The fact that it is not might be explained in at least two ways (Also see Sect. III, D.): The wave function of this state may have two components, alpha particle plus ground state and alpha particle plus first excited state as

$$\Psi \simeq A|\alpha_0, {}^8\mathrm{Be}> + B|\alpha_1, {}^8\mathrm{Be}^*>$$

where the mixing is caused by some residual interaction. A second explanation could describe the formation of this state as a two-step process where the alpha particle interacts with the ground state of ^{8}Be, exciting it and then falling into a new orbit itself. These two pictures have different points of view as to the actual process, but, in detail, they should be equivalent.

This result lends more support to the identification of these two states in question as APCETS states based on two states in ^{8}Be.

C. ^{14}N

The nucleus nitrogen-14 has been studied for excitation energies above 7.0 MeV through the reactions ^{13}C + p and ^{12}C + d (e.g., [Co68],[Ge66],[Ro64]). The levels in ^{14}N above E_x = 11.6 MeV can be formed by alpha particle bombardment of ^{10}B and resonances have been observed in the reactions $^{10}B(\alpha,\alpha'\gamma)^{10}B$, $^{10}B(\alpha,n)^{13}N$, $^{10}B(\alpha,p\gamma)^{13}C$, and $^{10}B(\alpha,p)^{13}C$; see [Ga69],[Bo56],[Sh53],[Gi59],[Wi75]. The elastic scattering of alpha particles by ^{10}B has been studied for E_α = 2.0 to 4.3 MeV [Mo73] and for E_α = 5 - 30 MeV [Ga69], [Da72].

This odd-odd nucleus has also been the object of many theoretical calculations of the shell model type [Tr63], Nilsson model [So67], and others (e.g., [Co68], [Gl65], [Ri66], [Pa66]. Most of the theoretical calculations have dealt with levels in ^{14}N below E_x = 10.5 MeV because of the increasing complexity of the states higher in energy. So, as with the experimental results, few states observed above E_x = 14.5 MeV have been assigned values for spin and parity.

In the elastic scattering of alpha particles from ^{10}B for $E_\alpha < 4.2$ MeV, four states were required in the R-matrix analysis of the excitation curves [Mo73]; the parameters of these states are listed in Table 5. The first two states have spins of 3^+ and 1^+, respectively, as determined by the R-matrix analysis. Since the ground state of $^{10}B(J^\pi = 3^+)$ and the first excited state ($J^\pi = 1^+$) are separated by 0.72 MeV, the observation of the two states in ^{14}N separated by a nearly equal amount (0.53 MeV) suggests that the APCETS model might be applicable. This possibility is enhanced by the fact that there is a resonance at E_α = 2.95 MeV in the $^{10}B(\alpha,\alpha'\gamma)^{10}B$ channel [Ga69], indicating that this state might be interpreted as an L = 0 alpha particle coupled to the first excited state of ^{10}B. This state apparently has a considerable amount of the ground state plus L = 2 alpha particle configuration mixed in since it is observed in the elastic alpha channel. Because of the possibility of applying the APCETS model to this non-multiplet (L_α = 0) case, two further experiments were undertaken. The $^{10}B(\alpha,\alpha')^{10}B^*$ reaction was performed around the energy of the reported $(\alpha,\alpha'\gamma)$ resonance, and the elastic scattering measurements were extended from E_α = 4.0 MeV to E_α = 9.0 MeV.

The results of the $^{10}B(\alpha,\alpha')^{10}B^*$ reaction are shown in Figure 21. There is obviously a resonance observed in this channel with a resonance energy of E_α = 2.95 MeV. [The

TABLE 5

$^{10}B(\alpha,\alpha_0)^{10}B$ Level Parameters, E_α = 2.0 to 4.0 MeV

E_α (MeV)	E_x (MeV)	J^π	ℓ	γ_α^2 (MeV)	Θ_α^2 (%)	Γ_{α_0}(c.m.) (keV)	$\Gamma_{c.m.}$ (keV)
2.21±0.01	13.19	3^+	0	0.121	15.1	65±10	65±10
2.95±0.05	13.72	1^-	2	0.368	46.0	160±20	180±20
3.69±0.05	14.25	3^+	0	0.145	18.1	360±50	420±100
4.26±0.01	14.66	2^-	3	0.169	21.1	100±20	100±20

$\Theta^2 .= \gamma_\alpha^2/\gamma_{s.p.}^2$

Figure 21. Measured Cross-Section Excitation Curve for the $^{10}B(\alpha,\alpha_1)^{10}B^*$ Reaction for Laboratory Alpha Energies of 2.7 MeV to 3.3 MeV at two Laboratory Angles. Statistical errors are shown. Solid lines are to guide the eye.

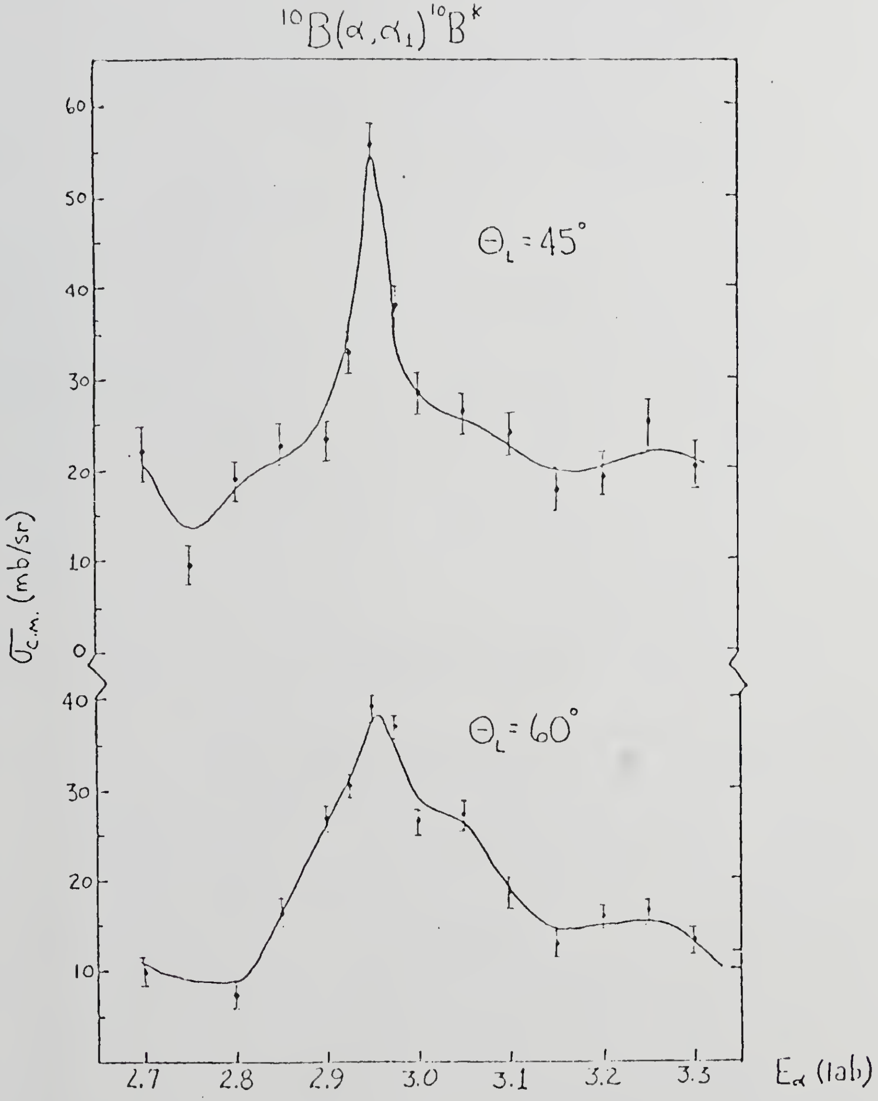
$^{10}B(\alpha,\alpha_1)^{10}B^*$
$\sigma_{c.m.}$ (mb/sr)
60
50
40
30
20
10
0
40
30
20
10
$\Theta_L = 45°$
$\Theta_L = 60°$
2.7
2.8
2.9
3.0
3.1
3.2
3.3
E_α (lab)

background in the energy region of the inelastic alphas in the experimental spectra was significant, and, along with the small yield, resulted in the large statistical errors of the data. The yield at back angles (>90°) was not measurable above the background.]

If this state has a spin of 1^+ (as the APCETS model would predict), it could decay to the first excited state of $^{10}B(J^\pi = 1^+)$ by either $\ell = 0$ or $\ell = 2$ alpha particles. The data did not allow a thorough analysis of the situation; the separation of the resonance from the possible background effects was not carried out and a determination of the ℓ-values comprising the spin of this resonance was not made. No conclusive statement can be made from our data as to the spin of this resonance, but 1^+ is not ruled out.

The R-matrix fit to the previous data [Mo73] indicated that the maximum total width of this 1^+ state was 200 keV and that the minimum partial width, Γ_{α_0}, was 140 keV (Table 5). If the rest of the total width, 60 keV, is in the α_1 channel, the ratio of partial widths might be as large as 0.42 (60/140); this is also the maximum value for the ratio of reduced widths since the penetrabilities are approximately the same in the two channels. In the present measurement, we find the reduced width ratio closer to one. Although we have some good indications that this 1^+ state at E_x = 13.72 MeV in ^{14}N might be an APCET state, there is a slight discrepancy in the experimentally determined widths. This discrepancy is probably the result of the difficulty in extracting $\Gamma_{\alpha 0}$ from the elastic data since this resonance is quite weak in the elastic channel. An additional source of difficulty could lie in the presence of another resonance near this energy. Some evidence for a second resonance is shown in Figure 21 by the apparent "shoulder" in the cross-section around E_d = 3.05 MeV, especially evident at Θ_L = 60°.

The 3^+ state at E_x = 13.19 MeV also has been interpreted as a possible APCET state; no evidence for or against this assignment was obtained in the present experiment. The other two states found at E_α = 3.69 MeV and 4.26 MeV (Table 5) do not fall into the APCETS scheme.

The extension in energy of the elastic scattering of alpha particles from ^{10}B is shown in Figure 22. These data were used as a basis for another R-matrix calculation. In order to lend continuity to the calculation, the parameters of the states previously detremined by Mo and Weller [Mo73] were used in the calculation, as was the same value for the radius parameter, r_0 = 1.4 fm. Because of the obvious complexity of the structures occurring above E = 5.5 MeV, only the region below that point was fitted using the R-matrix calculation. Energy independent boundary conditions were again used (see Sect. III, A. and Appendix A).

The levels used in the final fit are listed in Table 6. We again see a level at E_α = 4.15 MeV as did Mo and Weller. We found their parameters for this two-state reproduced our data as well. The difference in the energy of the resonance used in the calculation results from the boundary

Figure 22. Measured Cross-Section Excitation Curve for the $^{10}B(\alpha,\alpha_0)^{10}B$ Reaction for Incident Alpha Laboratory Energies of 4.0 MeV to 9.0 MeV at Four Laboratory Angles. Solid lines are the R-matrix calculation. Representative statistical errors are shown.

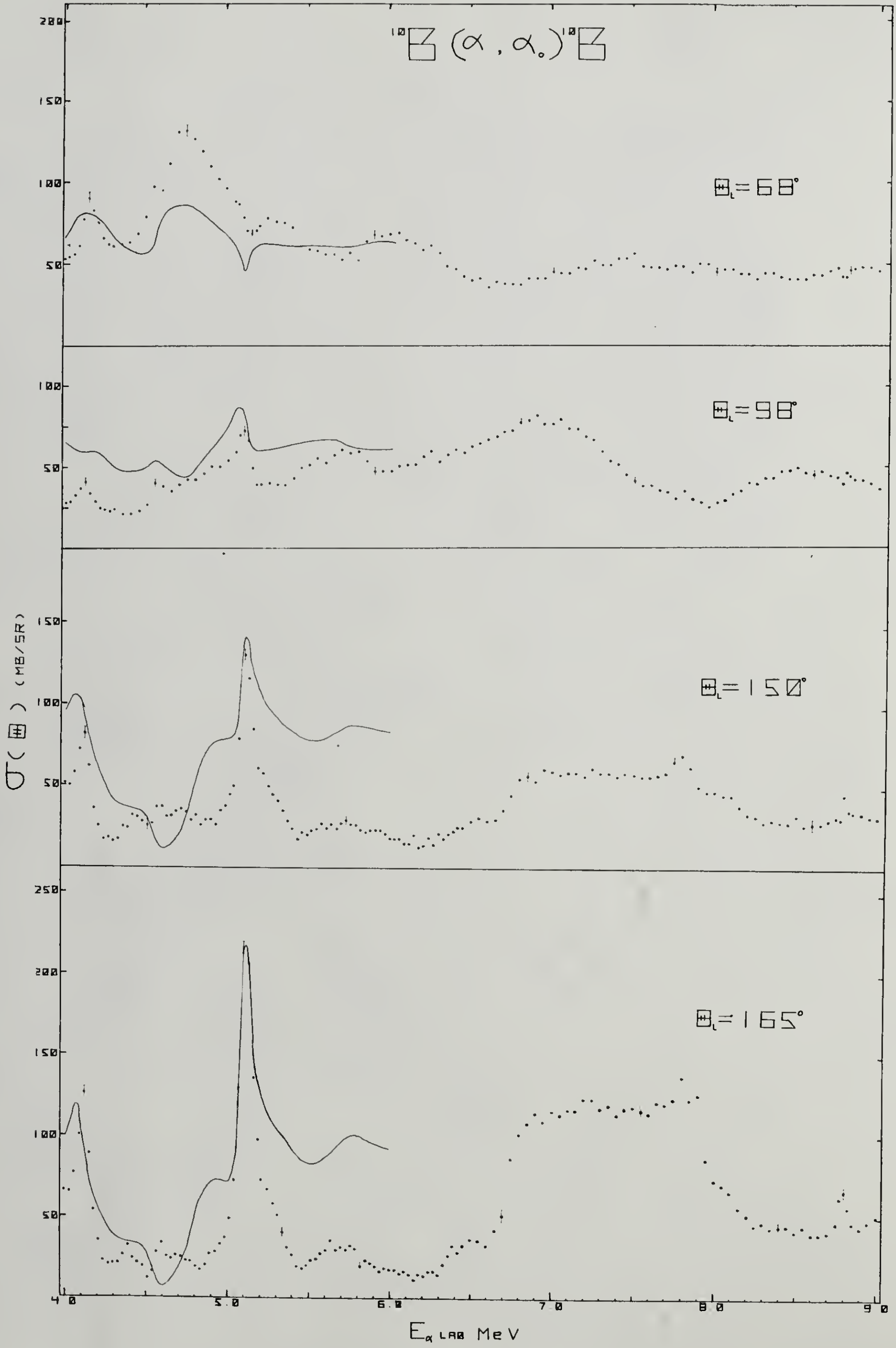
10B (α , α0)10B
ΘL=68°
ΘL=98°
ΘL=150°
ΘL=165°
200
150
100
50
100
50
150
100
50
250
200
150
100
50
σ(Θ) (MB/SR)
4.0
5.0
6.0
7.0
8.0
9.0
Eα LAB MeV

TABLE 6

Resonance Parameters Used in the Analysis of Elastic Scattering of α Particles by ^{10}B in the Energy Region $4.0 < E_\alpha < 5.7$ MeV

E_α(MeV)	E_x(MeV)	J^π	ℓ	γ_α^2(MeV)	Θ_α^2(%)	$\Gamma^\alpha_{c.m.}$(keV)	$\Gamma^{TOT}_{c.m.}$(keV)
3.9±.05	14.4	2^-	3	.188	22.7	75±10	100±10
4.3±.05	14.7	3^+	0	.012	1.4	40±10	200±10
4.55±.02	14.86	4^+	2	.013	1.6	25±5	45±10
4.75±.03	15.0	4^-	1	.078	9.4	250±10	250±20
5.03±.01	15.2	6^+	4	.124	14.9	40±5	60±10
5.25±.02	15.36	4^-	3	.077	9.3	100±10	150±20
5.45±.02	15.5	2^+	2	.011	1.3	30±5	200±10
5.70±.05	15.68	4^+	4	.069	8.3	40±10	200±20

condition; the evaluation of the shift function is made at a different average energy. In their calculations over the energy region E_α = 2.0 to 4.3 MeV, E_{AVG} = 3.1 MeV, while the present calculation was over the range 4.0 to 7.0 MeV, giving E_{AVG} = 5.5 MeV. There is little physical significance in the resonance energy difference.

The 68° yield curve exhibits a strong resonance near E_α = 4.75 MeV, corresponding to an excitation energy in ^{14}N of 15.0 MeV. A state near this energy has been reported in the neutron [Va73] and proton [Bo56] exit channels. A shell model calculation has predicted a 6^- state near this energy [Pe65, Ri66], but how conclusive this spin assignment is could not be determined. Of the choices of J available using ℓ-values from 0 to 4 inclusive ($J^\pi = 1^-$ to 7^+), it was found that the parameters E_R = 4.75 MeV, $J^\pi = 4^-$ ($\ell = 1$) and $\Gamma_\alpha = \Gamma_{TOT}$ = 250 MeV best reproduced the data in the present experiment; this value for the spin (4^-) is not ruled out by any of the theoretical calculations.

The energy region near E_α = 5.1 MeV is dominated by a large resonance, especially observable at the back angles (150° and 165°). Having the same possibilities as before, the best fit to the data was obtained using parameters for this resonance of E_{RES} = 5.03 MeV, $J^\pi = 6^+$ ($\ell = 4$) and $\Gamma_\alpha = \Gamma_{TOT}$ = 60 keV. As with the previous resonance, the ℓ-value of the alpha particle is fairly well defined, but since the channel spin of the reaction is 3^+, any non-zero ℓ-value will result in a multitude of possible J^π values.

A value of ℓ = 4 can result in J^π values of 1^+ to 7^+ when coupled to the 3^+ channel spin. Of these values, only 6^+ and 7^+ can be formed exclusively by ℓ = 4, although spins 1^+ through 5^+ can be made by ℓ = 2 alphas. The addition of ℓ = 2 amplitudes changes the angular distribution of the resonance cross-section and does not give a good fit. We chose 6^+ over 7^+ because of a slightly better fit to the resonance. No calculations have indicated a 6^+ resonance in this region. The resonance at E_x = 15.24 MeV seen in the $^{10}B(\alpha,p_3)^{13}C$ reaction [We73] with a width of 100 keV might be identified with the state in question; of course, if this identification is correct, all of the reaction width cannot be in the α channel. The decay from a 6^+ state might be more likely for p_3 (to the 3.58 MeV $5/2^+$ state in ^{13}C) than for p_1, p_2, or p_0 because the lower lying levels in ^{13}C necessitate higher ℓ-values for the proton decay. Finally, attempts to fit this 6^+ level into a rotational band model were not successful; the existence of the lower J-value members at lower energies is not obvious.

Both of these states (at E_α = 4.75 MeV and 5.1 MeV) have almost all of their widths in the alpha channel, indicating that these states have a high probability of forming an alpha particle outside the ^{10}B core. Though this may be the case, the spins do not correspond to any known low-lying states in ^{10}B and thus they are not identifiable as simple APCET states. The 6^+ resonance at 15.18 MeV has a reduced width of 124 keV, exhausting approximately 15% of the Wigner single particle limit ($\gamma^2_{s.p.} \approx 3/2 \frac{\hbar^2}{\mu a^2}$) [Wi47].

In order to more fully reproduce the excitation curves, it was necessary to include additional states in the R-matrix calculation. These states are listed in Table 5 along with the previously discussed levels. The $E_\alpha = 4.3$ MeV, $J^\pi = 3^+$ state was necessary to cause a minimum in the excitation curve near 4.5 MeV. The narrow $E_\alpha = 4.5$ MeV, $J^\pi = 4^+$ state was inserted to obtain the small "shoulder" in the 68° curve, but its existence remains somewhat in question. A state at $E_\alpha = 5.25$ MeV ($J^\pi = 4^-$) was used in order to better reproduce the minimum on the higher energy side of the 6^+ resonance. The ℓ-values of these resonances are fairly well determined, but as has been mentioned, the J-values may not be so definite.

In the energy region above $E_\alpha = 6.0$ MeV ($E_X = 15.9$ MeV), numerous levels are seen in both the elastic scattering and other reactions. This region was not fitted using R-matrix theory because of the many overlapping levels. Since there are so many parameters (E_{RES}, J^π, Γ_C, Γ_{TOT}) necessary to be specified for each resonance, the number of combinations is very large when several levels overlap. The R-matrix formalism then becomes unwieldly and another technique to extract descriptive parameters should be employed; this situation is also discussed in [Ra70].

The discrepancies in the complete description of the data for this reaction (see Figure 22) are probably the result of background levels not included in the calculation or the tails of higher energy resonances. The present R-matrix calculation does account for the major effects in this energy region (E_x = 14.5 MeV to 16.0 MeV).

Table 7 gives a relatively complete listing of the states in ^{14}N above 14 MeV. This table is a revision of one given by Wilson [Wi75].

In studying the details of an R-matrix calculation, an investigation of the dependence of the resonance size and shape on the radius parameter r_0 was made; the results are shown in Figure 19. As can be readily seen, the choice of r_0 is important in determining the resonance fit. One would expect that the choice of a too small r_0 would not satisfy the channel orthogonality necessary for the R-matrix calculation (see Sect. III, A.) while a too large r_0 might not be physically reasonable. The ratio of partial widths Γ_C/Γ_{TOT} for any channel is independent of the channel radius $\gamma_{\lambda_C} = (\hbar^2/2M_C r_C)\int \Psi_C^* \chi_\lambda dS$ (see Sect. III, A.) is not. The reduced width is proportional to the overlap between the external wave function Ψ and the internal basis set χ_λ. The values of χ_λ are determined by the radius for each channel, as is the reaction surface, S. For example, increasing r_0 by 14% (from 1.4 fm to 1.6 fm) decreases the reduced width by 60% (from 0.42 MeV to 0.17 MeV).

We therefore see that the details of an R-matrix calculation depend on the choice of r_0, and so the value chosen should be conspicuously specified. The most satisfy-

Figure 23. Results of R-Matrix Calculation of Level Shape Dependence for Four Values of r_0 in the $^{10}B(\alpha,\alpha)^{10}B$ Reaction. Cross-section versus E_α(Lab). Θ_L = 165°.

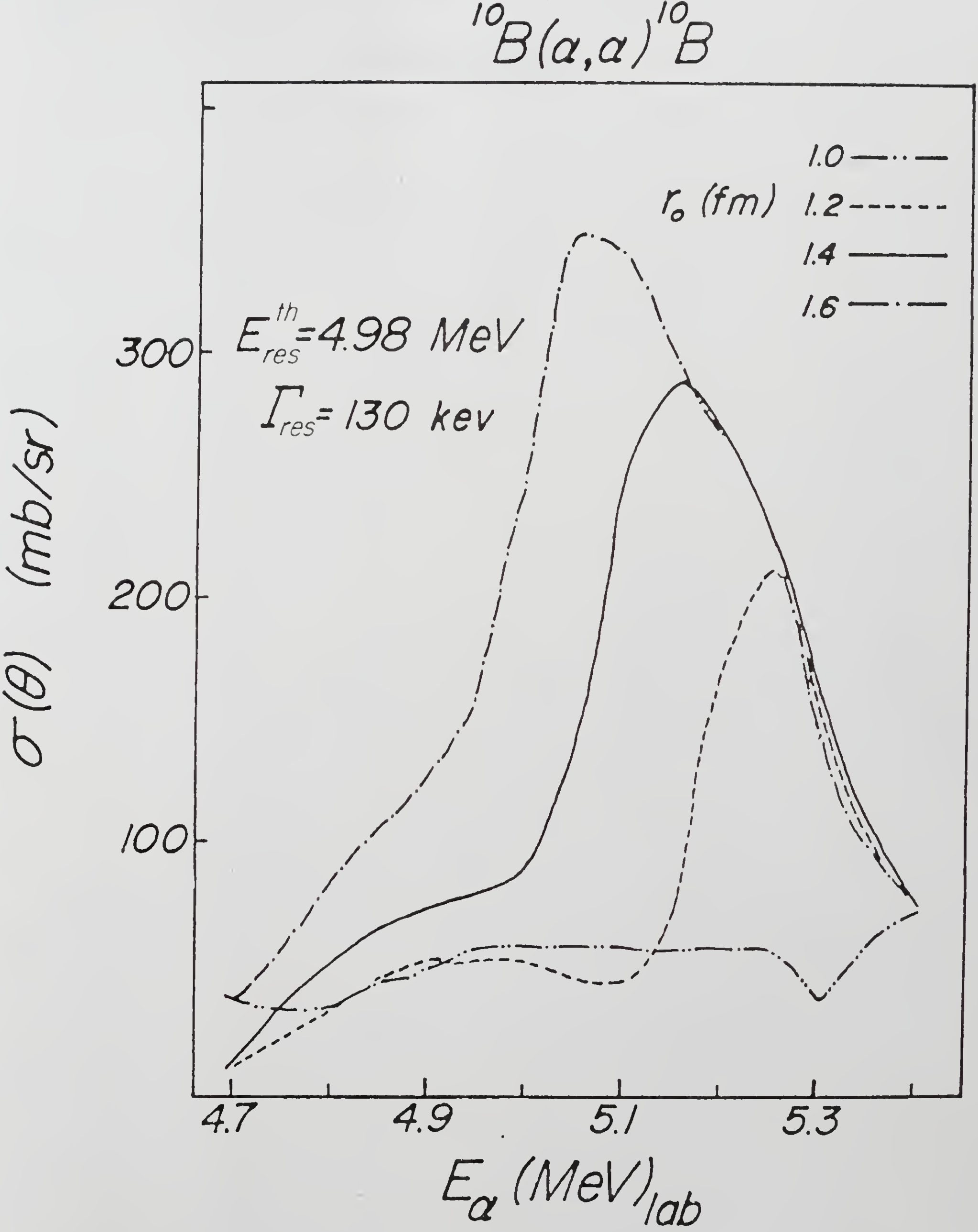
$^{10}B(\alpha,\alpha)^{10}B$
1.0
r_o (fm)
1.2
1.4
1.6
E^{th}_{res}=4.98 MeV
Γ_{res}= 130 kev
300
200
100
$\sigma(\theta)$ (mb/sr)
4.7
4.9
5.1
5.3
E_α (MeV)$_{lab}$

ing choice would be the most physical one, and that choice is made in these calculations; that is, r_0 = 1.4 fm.

TABLE 7

^{14}N Energy Levels E_x = 14.4 to 18.2 MeV

E_x	ENTRANCE CHANNEL	EXIT CHANNEL	Γ_{Obs}	J^π	REFERENCES
14.40	$^{12}C + d$	p_0, p_2	$\sim$120	--	Br66
14.43	$^{10}B + \alpha$	p_γ	$\sim$200	--	Bo56
14.45	$^{10}B + \alpha$	p_0, p_2, n_0	$\sim$100	--	Wi75
14.46	$^{10}B + \alpha$	n_0	$\sim$210	--	Va73
14.40	$^{10}B + \alpha$	α_0	$\sim$100	$2^-(\ell=3)$	a
14.56	$^{10}B + \alpha$	p_0, p_3	50	--	Wi75
14.58	$^{10}B + \alpha$	α_0	100±20	$2^-(\ell=3)$	Mo73
14.58	$^{10}B + \alpha$	n_0	$\sim$180	--	Va73
14.68	$^{10}B + \alpha$	α_0	200	$3^+(\ell=3)$	a
14.70	$^{12}C + d$	d	$\sim$200	--	Br66
14.72	$^{10}B + \alpha$	$p_0, p_1, (p_2), n_0$	125	--	Wi75
14.73	$^{10}B + \alpha$	n_0	100	--	Va73
14.82	$^{12}C + d$	n_0	$\sim$250	--	Da72
14.85	$^{12}C + d$	p_0	200	--	Bo56a
14.85	$^{10}B + \alpha$	n_0, γ_p	200	--	Bo56
14.85	$^{12}C + d$	p_0, p_1, p_2, p_3	100	--	Br66
14.86	$^{10}B + \alpha$	$n_0, (n_{23})$	--	--	Va73
14.86	$^{10}B + \alpha$	α_0	45	$4^+(\ell=2)$	a
14.86	$^{12}C + d$	α_0, d, p_0, p_3	$\sim$100	--	Co69
14.91	$^{10}B + \alpha$	p_0, n_0	90	--	Wi75
14.92	$^{10}B + \alpha$	n_0, n_{23}	43±8	--	Va73

TABLE 7 (continued)

E_x	ENTRANCE CHANNEL	EXIT CHANNEL	Γ_{Obs}	J^π	REFERENCES
15.00	$^{10}B + \alpha$	α_0	$\sim$250	--	a
15.00	$^{13}C + p$	n	50	--	Da61
15.02	$^{10}C + d$	n_0, n_1	$\sim$ 60	--	Va73
15.08	$^{10}B + \alpha$	p,n	$\sim$ 50	--	Bo56
15.09	$^{12}B + \alpha$	p_0	$\sim$350	--	Bo56a
15.12	$^{12}C + d$	p	$\sim$ 50	--	Br66
15.21	$^{10}B + \alpha$	α_0	$\sim$ 60	$6^+(\ell=4)$	a
15.24	$^{10}B + \alpha$	p_3	100	--	Wi75
15.26	$^{12}C + d$	p_1, p_3, d	$\sim$250	--	Br66
15.36	$^{10}B + \alpha$	α_0	150	$(4)^-(\ell=3)$	a
15.43	$^{10}B + \alpha$	p_2, p_3	100	--	Wi75
15.44	$^{10}B + \alpha$	n,p	$\sim$100	--	Bo56
15.45	$^{12}C + d$	α_0	$\sim$150	--	Co69
15.47	$^{12}C + d$	p_1, p_3, d	$\sim$250	--	Br66
15.50	$^{10}B + \alpha$	α_0	200	$(2)^+(\ell=2)$	a
15.58	$^{12}C + d$	p_0, p_3, d	$\sim$200	--	Br66
15.68	$^{10}B + \alpha$	α_0	200	$(4)^+(\ell=4)$	a
15.75	$^{12}C + d$	$\alpha_0, \alpha_1, p_0, d$	100	--	Co69
15.76	$^{12}C + d$	n_0	$\sim$ 50	--	Va73
16.10	$^{12}C + d$	n_0	$\sim$150	--	Va73
16.21	$^{10}B + \alpha$	p_0, p_2, n_0	125	--	Wi75
16.40	$^{12}C + d$	α_0, α_1	$\sim$200	--	Co69
16.40	$^{10}B + \alpha$	p_2	150	--	Wi75

TABLE 7 (continued)

E_x	ENTRANCE CHANNEL	EXIT CHANNEL	Γ_{Obs}	J^π	REFERENCES
16.57	$^{12}C + d$	n_0	∿100	--	Va73
16.91	$^{10}B + \alpha$	p_0	--	--	Wi75
16.95	$^{12}C + d$	n_0	∿150	--	Va73
16.97	$^{12}C + d$	p_0	∿400	--	Co69
17.17	$^{10}B + \alpha$	p_3	50	--	Wi75
17.27	$^{12}C + d$	$\alpha_0, \alpha_1, p_0, p_3, d$	∿300	--	Co69
17.47	$^{12}C + d$	α_1	∿250	--	Co69
17.82	$^{12}C + d$	α_0	∿250	--	Co69
18.02	$^{12}C + d$	α_0	∿100	--	Va73
18.20	$^{12}C + d$	α_0	∿100	--	Va73

a = present work

CHAPTER V

CONCLUSION

The experiments performed in this work were not designed with only the alpha particle core-excited threshold states model in mind; they were performed in an attempt to increase the amount of knowledge concerning three light nuclei. The results of these experiments, when considered along with previous experiments, indicated that a simple description might be appropriate.

Prior experiments on ^{11}C using the $^{10}B(p,\alpha)^{7}Be$ and other reactions (e.g., [Cr56], [Ov62]) indicated the presence of an overlapping doublet near E_x = 10 MeV. The energy separation of these levels indicated that they might be identified as corresponding to the ground and first excited states of ^{7}Be as pictured within the APCETS model. In order to obtain more exact and complete measurements, the reactions $^{10}B(p,\alpha_0)^{7}Be$ and $^{10}B(p,\alpha_1)^{7}Be^*$ were induced for excitation energies of 9.6 to 12.4 MeV.

The results obtained were fairly conclusive. Previous workers had made inconsistent assignments for the spins and parities of these states. In the course of the present work, a Legendre polynomial analysis yielded information which indicated that the APCETS assignments of $3/2^-$ and $1/2^-$ for the two states were not inconsistent with the data. Explanations were also found for some of the previously inconsistent results. The new α_1 results also supported these assignments. For a resonance seen at a higher excitation energy, the results of the present experiment were found to be consistent with previously assigned parameters. Therefore, in the case of ^{11}C, the present results resolved some previous inconsistencies, gave support to a previous set of level parameters for one level, and supported the APCETS picture for two levels at high excitation energies.

The final results for ^{12}C were not as conclusive. At the excitation energies covered by the present $^{10}B + d$ reaction (26 to 28.5 MeV), levels have been observed. Most of the levels in this energy region have been found to have isospin greater than zero; that is, either $T = 1$ or 2. In fact, the lowest lying $T = 2$ level in ^{12}C has been found at 27.6 MeV [Ne71]. The reactions $^{10}B(d,\alpha_0)^8Be$ and $^{10}B(d,\alpha_1)^8Be^*$ cannot populate $T \neq 0$ levels in the absence of isospin mixing. We therefore expect to only see $T = 0$ levels. The excitation curves for the α_0 and α_1 reaction products indicated by both the separation and the widths of the two observed levels that an APCETS identification might be possible. The ground and first excited states of ^8Be have spins 0^+ and 2^+, respectively. The present results were analyzed in order to determine the spins of the states in question. A Legendre polynomial analysis of the measured angular distributions indicated (from the appear-

Figure 24. APCETS Identification of Levels in ^{11}C and ^{12}C

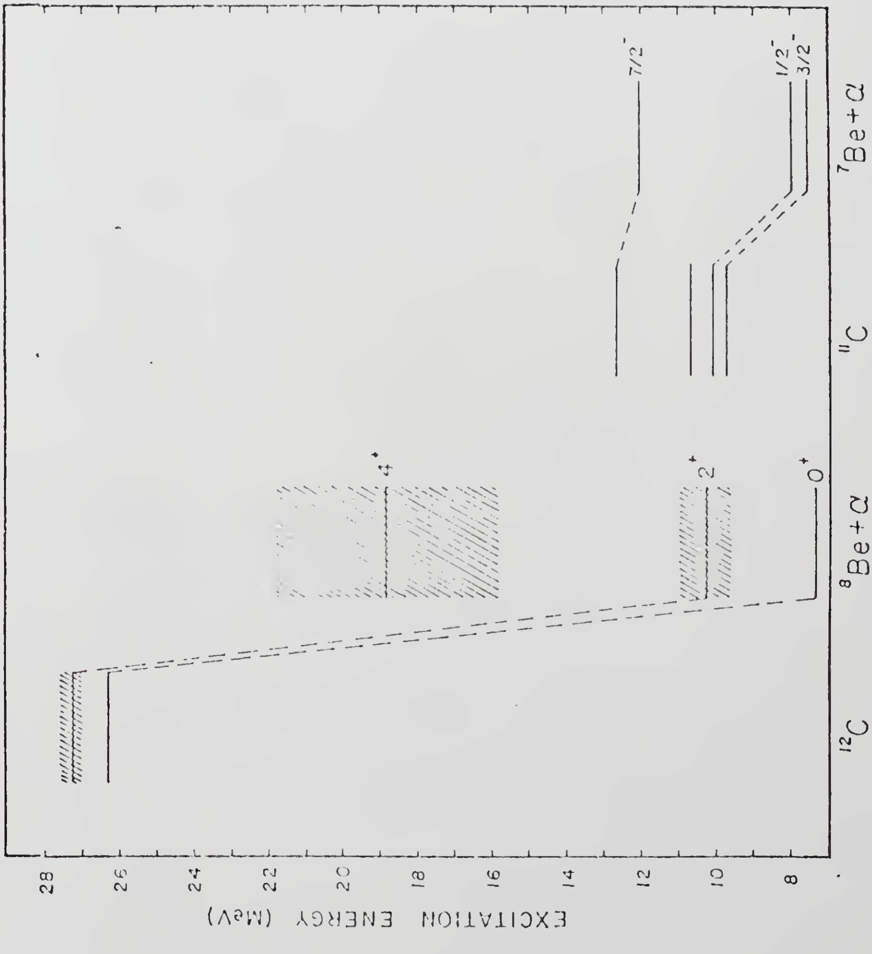
EXCITATION ENERGY (MeV)
8
10
12
14
16
18
20
22
24
26
28
^{12}C
$^{8}Be+\alpha$
^{11}C
$^{7}Be+\alpha$
0^+
2^+
4^+
$7/2^-$
$1/2^-$
$3/2^-$

ance of odd polynomials) that processes other than the formation of two even-parity levels were occurring. The postulation of a higher energy 3^- level (only natural parity levels can decay through the α_0 channel) succeeded in explaining some, but not all, of the results. It was found that although the 0^+ and 2^+ APCETS assignment could not be ruled out, neither could a convincing case for their assignment be developed. It was found though that the relative reduced widths for the proposed 2^+ in the α_0 and α_1 channels did support the APCETS picture in that $\gamma^2_{\alpha_1}$ was much greater than $\gamma^2_{\alpha_0}$ for this state.

At excitation energies of 13.2 MeV and 13.7 MeV, levels were previously found in ^{14}N through the reaction $^{10}B(\alpha,\alpha_0)^{10}B$ which had the same spins and parities as the ground and first excited states of ^{10}B(3^+ and 1^+, respectively) [Mo73]. Measurement of the $^{10}B(\alpha,\alpha_1)^{10}B^*_{2.94}$ reaction cross-section for alpha energies from 2.7 to 3.3 MeV revealed a strong resonance at the same energy as the previously reported 1+ state. This discovery gave stronger support to the APCETS model of this state. Apparent discrepancies concerning the partial widths of this state were found and possible explanations were presented.

For alpha energies of 4.0 to 9.0 MeV, the cross-section was dominated by three large anomalies. Near E_α = 4.75 MeV, a large resonance was found and, using an R-matrix calculation, a set of level parameters was obtained for this region. This 4^- state was previously unreported. Using the same calculation at E_X = 15.2 MeV, a large anomaly was found to be at a 6^+ state with almost its entire width in the alpha channel. This resonance may be correlated with one seen in another reaction [Wi75]. Attempts to fit this 6^+ level into a rotational band scheme were not successful. Assignments for other levels at higher excitation energies were also made (see Sect. IV, C.) None of these assignments were consistent with an APCETS picture for ^{14}N based on the low-lying states in ^{10}B. A higher energy anomaly (near E_α = 8 MeV) was unanalyzed because of the complexity of the excitation curve in this energy region.

A few comments concerning these three particular nuclei and the APCETS model are in order. In ^{11}C, further work seems to be necessary to substantiate the present assignments. A $^{10}B(p,\gamma)^{11}C$ experiment could obtain valuable information on ^{11}C; previous gamma ray experiments were incomplete. For ^{12}C, the present experiment was probably not taken far enough. A more thorough analysis of the alpha particle results (especially the α_1 results) might shed more light on the problem. In the case of ^{14}N, even though the data were not exhaustive, the R-matrix analysis succeeded in giving some level assignments. It has been found that the R-matrix analysis is of limited usefulness in energy regions of many overlapping levels; the number of variable parameters become too large. Some other method may be more useful in these areas.

The present experiments increase by at least one and

Figure 25. Level Diagram of ^{14}N with Possible APCETS Identifications

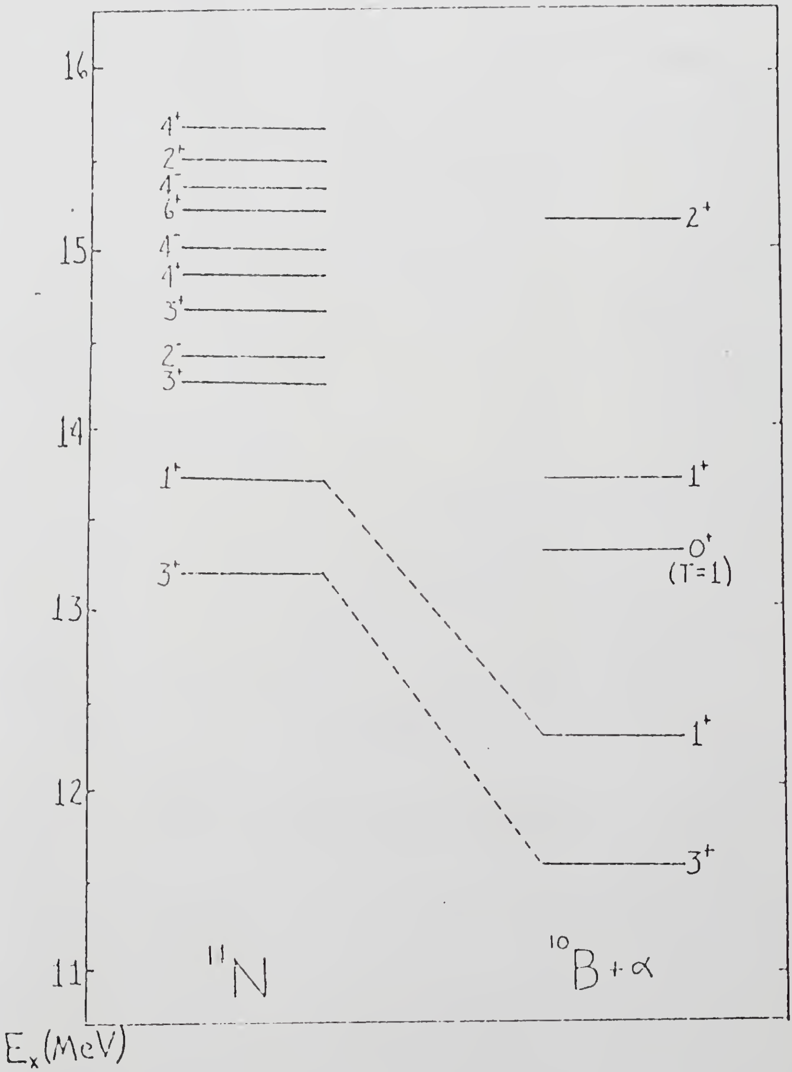
16
15
14
13
12
11
Ex(MeV)
4+
2+
4-
6+
4-
4+
3+
2-
3+
1+
3+
11N
2+
1+
0+
(T=1)
1+
3+
10B+α

possibly two, the number of nuclei where the APCETS model seems to have some utility. Theoretical calculations using the APCETS model have been made on two A = 15 nuclei, ^{15}N and ^{15}O, with some success [Pu74], [Me74]. We now have the case of ^{11}C to consider.

The alpha particle core-excited threshold scheme has so much attraction because of its relative simplicity. Complicated models and theories may be capable of reproducing experimental results but often at the sacrifice of physical "feeling." Any picture which can describe such a complicated object as the atomic nucleus and has a semblence of simplicity, has some advantages. It is much easier to think of some states of ^{11}C as an alpha particle interacting with a ^{7}Be nucleus than to think of 11 separate nucleons interacting. The observation that there is this alpha particle organization in many nuclei (and at various excitation energies) appears to be an important one. It seems that at times the alpha particle is a basic "building block" in the nucleus, and if such is the case, the final description of nuclear processes may be made easier. For it may be said that

> When the answers are simple, then you
> hear God think. [Br73]

Figure 26. Energy Conversion Scales: E_{Lab} to E_x

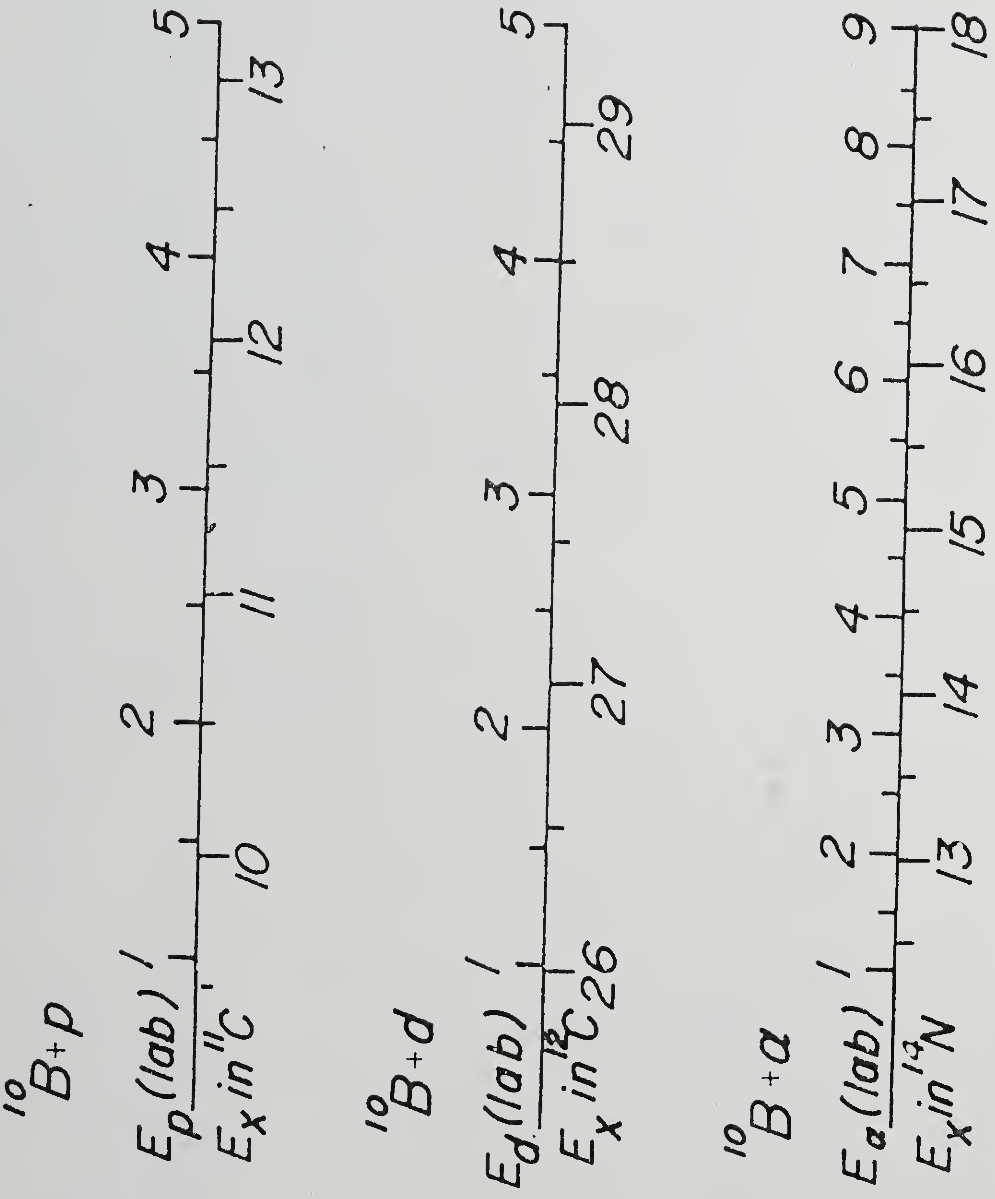
$^{10}B+p$
E_p (lab)
E_x in ^{11}C
$^{10}B+d$
E_d (lab)
E_x in ^{12}C
$^{10}B+\alpha$
E_α (lab)
E_x in ^{14}N

APPENDIX A

MULTI

The computer code MULTI was written by David L. Sellin of Duke University. It computes nuclear reaction cross-sections using a general multi-level, multi-channel R-matrix formalism of the type described by Lane and Thomas [La58]. It is designed to allow for the inclusion of up to 35 channels, 20 levels, 14 different J^{Π} values, and 400 calculation points. A brief description of the formalism used in the calculation follows.

The R-matrix is given by

$$R_{cc'} = \sum_{\lambda} \gamma_{\lambda c} \gamma_{\lambda c'} / E_{\lambda} - E + R_{0_{cc'}}$$

where, in this case, all $R_{0_{cc'}}$'s are set equal to zero. This choice is equivalent to neglecting any background or distant levels other than those explicitly included in the calculation.

The U-matrix is expressed as

$$U = (kr)^{\frac{1}{2}} 0^{-1} (1-RL)^{-1} (1-RL^{*}) I (kr)^{-\frac{1}{2}}.$$

In particular, $(kr)^{\frac{1}{2}}$ and $(kr)^{-\frac{1}{2}}$ are diagonal matrices with components $(k_c r_c)^{\frac{1}{2}}$ and $(k_c r_c)^{-\frac{1}{2}}$ respectively. Here, k is the wave number, 1/ƛ, and r_c is the channel radius. Here, 0 is a diagonal matrix with components 0_c representing the outgoing states; I equals the complex conjugate of 0, 0^{*}; L is the diagonal matrix with components

$$L_c = S_c + iP_c$$

where S_c is the shift function which leads to level shifts and P_c is the penetrability which leads to level widths. In order to calculate U, the matrix (1-RL) must be inverted.

The other quantities of the U-matrix can be rewritten in terms of the regular F_c and irregular G_c Coulomb wave functions, which are solutions to the radial wave equation in the exterior region. Using these functions,

$$I_c = O_c^* = (G_c - iF_c)e^{+i\omega_c}$$

where ω_c is the Coulomb phase shift. This phase shift is related to the orbital angular momentum quantum number ℓ_c and the Coulomb parameter

$$\eta_c = Z_1 Z_2 e^2/hv_c$$

(where Z_1 and Z_2 are the charges on the pair of reaction products, and v_c is their relative velocity) by

$$\omega_c = \sum_{n=1}^{\ell_c} \tan^{-1}(\eta_c/n).$$

The penetrability and shift function can be written as

$$P_c = k_c r_c [F_c^2 + G_c^2]^{-1}$$

and

$$S_c = -b_c + (F_c F_c' + G_c G_c')[F_c^2 + G_c^2]^{-1}$$

where the prime means the derivative $r_c d/dr_c$.

The differential cross-section for the process $\alpha, s \rightarrow \alpha', s'$ is given by

$$d\sigma_{\alpha s, \alpha' s'} = \sum_{\nu, \nu'} (2s+1)^{-1} |A_{\alpha' s' \nu', \alpha s \nu}(\Omega_{\alpha'})|^2 \, \Omega_{\alpha'}$$

where ν' and ν are the z components of s and s' respectively. The matrix A is expressed as

$$A_{\alpha's'\nu',\alpha s\nu}(\Omega_{\lambda'}) = \frac{\Pi^{\frac{1}{2}}}{k_\lambda}[-C_{\lambda'}(\Theta_{\lambda'})\ {}_{\alpha's'\nu',\alpha s\nu}$$

$$+i\Sigma_{Jm\ell\ell'm'}(2\ell+1)^{\frac{1}{2}}(\ell o s\nu|MJ)(\ell'm's'\nu'|MJ)xT^{J}_{\lambda's'\ell',\lambda s\ell}Y^{m}_{\ell'}(\Omega_{\lambda'})]$$

The Clebsch-Gordon coefficients $(j_1m_1j_2m_2|MJ)$ are easily recognized and

$$T^{J}_{\alpha's'\ell',\alpha\ell s} = e^{2i\sigma_{\lambda'}}\delta_{\alpha's'\ell',\alpha s\ell}-U^{J}_{\alpha's'\ell',\alpha\ell s}$$

with the Coulomb (or Rutherford) amplitudes

$$C_\lambda(\Theta_\lambda) = (4\Pi)^{-\frac{1}{2}}\eta_\lambda\mathrm{cosec}^2\frac{\Theta_\lambda}{2}\ \exp[-2i\eta_\lambda\ \ln\ \sin\frac{\Theta_\lambda}{2}].$$

The quantities $Y^{m'}_{\ell'}$ are the usual spherical harmonics.

The cross-sections are obtained by squaring the scattering amplitudes A and summing over projection and spin quantum numbers. The resultant expression is

$$(2s+1)\frac{k_\lambda^{2}}{\pi}d\sigma_{\alpha s,\alpha's'}/d\Omega_{\lambda'} = (2s+1)|C_{\lambda'}(\Theta_{\lambda'})|^{2}\delta_{\lambda's',\lambda s}$$

$$+\pi^{-1}\Sigma_L B_L(\lambda's',\lambda s)P_L(\cos\Theta_{\lambda'})+(4\Pi)^{-\frac{1}{2}}\Sigma_{J\ell\ell'}(2J+1)2\mathcal{R}_e[iT^{J}_{\lambda's'\ell',\lambda s\ell}$$

$$C_{\lambda'}(\Theta_{\lambda'})P_\ell(\cos\Theta_{\lambda'})]$$

where P_L is a Legendre polynomial of order L and B_L is given by

$$B_L(\lambda's',\lambda s) = \frac{1}{4}(-1)^{s-s'}\Sigma_{J_1J_2\ell_1\ell_2\ell_1'\ell_2'}\bar{Z}(\ell_1J_1\ell_2J_2;sL)$$

$$\bar{Z}(\ell_1'J_1\ell_2'J_2;s'L)x(T^{J_1}_{\lambda's'\ell',\lambda s\ell})(T^{J_2}_{\lambda's'\ell',\lambda s\ell})^{*}.$$

The $\bar{Z}$ quantities are discussed in Appendix B.

The cross-sections obtained without a polarized beam or target do not distinguish between the various s and s' values, and therefore are obtained by an appropriate sum over these quantities:

$$\sigma_{\alpha,\alpha'} = \sum_{s,s'} g_s \, \sigma_{\alpha's',\alpha s}$$

where the g's are statistical spin factors and give relative probabilities that the incident particle in an unpolarized beam will have spin s. They are defined as

$$g_s \equiv \frac{(2s+1)}{(2I+1)(2i+1)}$$

where I and i are the target and projectile spins respectively.

This formalism considers only states of positive energy and neglects all electromagnetic (γ) transitions in the compound nucleus. Non-resonant scattering is described by the use of hard-sphere phase shifts calculated by

$$\phi_c = \tan^{-1}(F_c/G_c).$$

Two choices for boundary conditions are also possible in MULTI: energy dependent, when $b_c = \mathcal{S}_c'(E)$ or energy independent, $b_c = \mathcal{S}_c'(E_{AVG})$ where E_{AVG} is the average energy over which the calculation is made. Here, $\mathcal{S}$ is the shift function. (See Chapter III-A). The latter choice is made.

The parameters supplied to the code include the channels to be considered, the boundary condition, and for each resonance, the total width Γ_{TOT}, partial widths for each channel, Γ_c, and energy and J^{π} values. Output is the differential center-of-mass cross-section as a function of laboratory angle and energy, which can then be compared to the experimental data.

APPENDIX B

ZBAR

The $\overline{Z}$ factors appearing in the expression for the angular distribution of the cross-section (see Chapter III-B) are kinematical factors resulting from the coupling of angular moments. A $\overline{Z}(\ell_1 J_1 \ell_2 J_2;sL)$ describes the probability of forming a state of total angular momentum J_1 from orbital angular momentum ℓ_1 and channel spin s or J_2 from ℓ_2 and s. Because of these compositions, the triads (J_1,ℓ_1,s) and (J_2,ℓ_2,s) must satisfy the triangle condition, i.e., the three members must be able to form the sides of a triangle. If these conditions are not met, the $\overline{Z}$ factor vanishes. The same result is valid for the factor $\overline{Z}(\ell_1' J_1 \ell_2' J_2;s'L)$ describing the decay of possible states J_1 and J_2 into channels ℓ_1' and s' or ℓ_2' or s'. To insure that each term in the summation is real, s-s' must be an integer.

Further restrictions on the elements of the Z factors result from the fact that the expression given in ChapterIII-B is the decomposition of the square of a matrix element into Legendre polynomials. For example, the amplitude for the compound system to decay with the emitted particle having orbital angular momentum ℓ_1' will interfere with the amplitude with final orbital angular momentum ℓ_2'. In order for this interference to result in an angular distribution containing $P_L(\cos\Theta)$, the condition

$$\vec{\ell}_1{}' + \vec{\ell}_2{}' = \vec{L}$$

must be satisfied. This condition means ℓ_1', ℓ_2' and L form a triangle. The triads (ℓ_1, ℓ_2, L) and (J_1, J_2, L) must also form triangles. From these criteria, the results

$$L_{MAX} \leq 2\ell_{MAX} \text{ or } L_{MAX} \leq 2\ell'_{MAX}$$

are a consequence. In other words, the maximum order of Legendre polynomical which appears in the description of the angular distribution must be less than or equal to twice the largest value of the initial orbital angular momentum (or final orbital angular momentum), whichever happens to be smaller. Finally, the parity of the states are determined by the ℓ's; therefore, $\ell_1+\ell_2+L$ and $\ell_1'+\ell_2'+L$ are even.

The $\overline{Z}$ coefficients themselves are calculated using an expression given by Rotenberg et al. [Ro59].

$$\overline{Z}(abcd;ef) = [(2a+1)(2b+1)(2c+1)(2d+1)(2f+1)]^{\frac{1}{2}}$$

$$x \begin{Bmatrix} a & b & e \\ d & c & f \end{Bmatrix} \begin{pmatrix} a & c & f \\ o & o & o \end{pmatrix}$$

where $\begin{Bmatrix} a & b & e \\ d & c & f \end{Bmatrix}$ is a 6-j symbol and $\begin{pmatrix} a & c & f \\ o & o & o \end{pmatrix}$ is a 3-j symbol. The $\overline{Z}$ values are calculated by a sub-routine in MULTI and by the code ZBAR.

In computing the values for the $\overline{Z}$ coefficients, the 6-j symbols are evaluated using an expression given by Rotenberg [Ro59].

$$\begin{Bmatrix} a & b & e \\ d & c & f \end{Bmatrix} = (-1)^{a+b+c+d} \Delta(abe)\Delta(cde)\Delta(dbf)\Delta(acf)$$

$$x \sum_k \frac{(-1)^k (a+b+c+d+1-k)!}{k!(a+b-e-k)!(c+d-e-k)!(a+c-f-k)!(d+b-f-k)!(-a-d+e+f+k)!(-b-c+e+f+k)!}$$

where $\Delta(xyz) = [\frac{(x+y-z)!(x-y+z)!(-x+y+z)!}{(x+y+z+1)!}]^{\frac{1}{2}}$ and the summation index k ranges over all values which do not result in negative factorial.

The 3-j symbols are calculated using an expression given by Messiah [Me58]:

$$\begin{pmatrix} a & c & f \\ o & o & o \end{pmatrix} = (-1)^p \Delta(acf) \frac{p!}{(p-a)!(p-c)!(p-f)!}$$

where $2p = a+c+f$.

A listing of the code ZBAR follows this appendix.

```
CCCCCCCC      CALCULATION OF ZBAR COEFFICIENTS
CCCCCCCC      INPUTS

  2 READ (5,500) A,B,C,D,E,F
500 FORMAT (6F1.0)
    ZB=ZBAR(A,B,C,D,E,F)
 99 WRITE (6,600) A,B,C,D,E,F,ZB
600 FORMAT (3X,6F2.0,'Z',1X,F6.3)
    IF (A) 5,2,2
  5 STOP
    END




    FUNCTION ZBAR(A,B,C,D,E,F)
    REAL N1,N2,N3,N4,N5,N6,N7,N8
    DIMENSION S(12),R(8)
    N=A+C+F
CCCCCCCC      TEST IF A+C+F IS EVEN
    IF(N-(N/2)*2) 1,2,1
  1 ZB=0.0
    GO TO 900
CCCCCCCC      TRIANGLE EQUALITIES
  2 IF(A+B-E) 1,3,3
  3 IF(A-B+E) 1,4,4
  4 IF(B-A+E) 1,5,5
  5 IF(C+D-E) 1,6,6
  6 IF(C-D+E) 1,7,7
  7 IF(D-C+E) 1,8,8
  8 IF(A+C-F) 1,9,9
  9 IF(A-C+F) 1,10,10
 10 IF(C-A+F) 1,11,11
 11 IF(B+D-F) 1,12,12
 12 IF(B-D+F) 1,13,13
 13 IF(D-B+F) 1,14,14
CCCCCCCC      CALCULATION OF 6-J SYMBOL
 14 S(1)=A+B-E
    S(2)=C+D-E
    S(4)=B+D-F
    S(5)=E+F-A-D
    S(6)=E+F-B-C
CCCCCCCC      FIND VALUES FOR SUMMATION INDEX
    MIN=S(1)
    DO 402 I=1,4
    IF(MIN-S(I)) 402,402,401
401 MIN=S(I)
402 CONTINUE
    NZMAX=MIN+1
    R(1)=-S(5)
    R(2)=-S(6)
    R(3)=0.0
    MAX=R(1)
    DO 602 I=2,3
    IF (MAX-R(I)) 601,602,602
601 MAX=R(I)
602 CONTINUE
    NZMIN=MAX+1
    IF(NZMIN-NZMAX) 403,403,1
403 ZB=0
CCCCCCCC      SUMMATION FOR 6-J SYMBOL
    DO 20 N=NZMIN,NZMAX
    Z=N-1
```

```
      N1=(A+E+F[illegible]
      N2=(S(1)-Z+1.)
      N3=(S(2)-Z+1.)
      N4=(S(3)-Z+1.)
      N5=(S(4)-Z+1.)
      N6=Z+1.
      N7=(S(5)+Z+1.)
      N8=(S(6)+Z+1.)
      T=(FAC(N1)/(FAC(N2)*FAC(N3)*FAC([illegible] 5)*FAC(N6)*FAC(N7)*FAC(N[illegible]
      IF(M-(M/2)*2) 20,19,20
 19   T=-T
CCCCCCCC      ZB IS 3-J VALUE
 20   ZB=ZB+T
CCCCCCCC      COMPUTATION OF DELTAS
      N1=A+B-E+1.
      N2=A-B+E+1.
      N3=-A+B+E+1.
      N4=A+B+E+2.
      DEL1=(FAC(N1)*FAC(N2)*FAC(N3))/FAC(N4)
      N1=C+D-E+1.
      N2=C-D+E+1.
      N3=-C+D+E+1.
      N4=C+D+E+2.
      DEL2=(FAC(N1)*FAC(N2)*FAC(N3))/FAC(N4)
      N1=A+C-F+1.
      N2=A-C+F+1.
      N3=-A+C+F+1.
      N4=A+C+F+2.
      DEL3=(FAC(N1)*FAC(N2)*FAC(N3))/FAC(N4)
      N1=B+D-F+1.
      N2=B-D+F+1.
      N3=-B+D+F+1.
      N4=B+D+F+2.
      DEL4=(FAC(N1)*FAC(N2)*FAC(N3))/FAC(N4)
      ZB=ZB*SQRT(DEL1*DEL2*DEL3*DEL4)
CCCCCCCC      COMPUTATION OF 3-J SYMBOL
      T=((A+C+F)/2.)+1.
      N1=T-A
      N2=T-C
      N3=T-F
      M=T+F-1.0
      DF=T
      T=SQRT((2.*F+1.)*DEL3)*FAC(DF)/(FAC(N1)*FAC(N2)*FAC(N3))
      IF(M-(M/2)*2) 22,23,22
 22   T=-T
 23   ZB=SQRT((2.*A+1.)*(2.*B+1.)*2.*C+1.)*(2.*D+1.))*ZB*T
CCCCCCCC      FINAL VALUE
900   ZBAR=ZB
      RETURN
      END



      FUNCTION FAC(V)
CCCCCCCC      FACTORIALS
      I=V
      FAC=1.0
      IF (I-2) 103,103,131
131   DO 102 J=2,I
      XI=J-1
102   FAC=XI*FAC
103   CONTINUE
      RETURN
      END
```

APPENDIX C

The self-supporting foils of enriched ^{10}B which were necessary for the experiments were made by evaporation techniques. The evaporation of boron required the use of electron bombardment so as to reach a temperature near its melting point of 2300°C. The mounting of the foils onto target frames was also difficult and tedious. In order to facilitate the process for anyone who might desire boron foils for experimental purposes, a few production details are given.

(1) New, unused glass microscope slides were used as the base onto which the boron was evaporated. Previously used, cleaned slides did not provide much success.

(2) The boron powder used in the electron gun apparatus was "packed" before bombardment by dousing it with alcohol and allowing the alcohol to evaporate.

(3) Boron has a great tendency to sputter when heated; this sputtering can damage the slides. To eliminate the possibility of damage, the boron being heated was shadowed from the slides by a shutter until the boron had melted and sputtering ceased.

(4) A very thin film of boron was evaporated onto the slides and was allowed to oxidize in air for approximately one hour. The oxidized boron acted as a release agent. An alternate release agent which was used with some success was a very thin layer of LiF evaporated onto the slides.

(5) After oxidation of the intital layer, more boron was evaporated onto the slides until a visible brown layer was observed. The vacuum chamber was purged with dry nitrogen to minimize oxidation of the prime boron layer.

(6) The thin foils were floated off the base layer on the surface of a container of warm, still water. The foils were then mounted on target frames, allowed to dry, and used as targets.

BIBLIOGRAPHY

Aj68 F. Ajzenberg-Selove and T. Lauritsen, Nucl. Phys. A114, 1 (1968).

Aj75 F. Ajzenberg-Selove, unpublished.

Al56 A. Allen, L. Govindjee and J. Saima, Proc. Phys. Soc. 69A, 350 (1956).

An73 K. Anathanarayanan, M. Best and S. Das Gupta, Phys. Rev. C7, 1760 (1973).

Be63 J. A. Becker and J. D. Fox, Nucl. Phys. 42, 669 (1963).

Be65 E. M. Bernstein, Nucl. Phys. 59, 525 (1965).

Bl70 J. L. Black, M. A. Nagarajan and R. Pollard, Nucl. Phys. A13, 190 (1970).

Bl52 J. M. Blatt and L. C. Biedenharn, Rev. Mod. Phys. 24, 258 (1952).

Bl72 S. L. Blatt, K. J. Moon and D. Kohler, Phys. Rev. C6, 1536 (1972).

Bo56 T. W. Bonner, A. A. Kraus, Jr., J. B. Marion, and J. P. Schiffer, Phys. Rev. 102, 1348 (1956).

Bo56a T. W. Bonner, J. T. Eisinger, A. A. Kraus, Jr., and J. B. Marion, Phys. Rev. 101, 209 (1956).

Br51 A. B. Brown, C. W. Snyder, W. A. Fowler, and C. C. Lauritsen, Phys. Rev. 82, 159 (1951).

Br66 D. M. Brink, "Proceedings of the International School of Physics, Enrico Fermi, Course XXXVII," ed. C. Bloch, North Holland, Amsterdam (1966).

Br73 J. Bronowski, The Ascent of Man, Little, Brown and Co. (1973).

Br66a G. Bruno, J. Decharge, A. Perrin, and G. Surget, J. Phys. C1, 151 (1966).

Ce56 M. Cerineo, Nucl. Phys. 2, 113 (1956).

Ch56 G. B. Chadwick, T. K. Alexander, and J. B. Warren, Can. J. Phys. 34 381 (1956).

Co69 H. Cordes, G. U. Din and B. A. Robson, Nucl. Phys. A127, 95 (1969).

Co68 R. L. Cottrell, J. C. Liste, and J. O. Newton, Nucl. Phys. A109, 288 (1968).

Cr56 J. W. Cronin, Phys. Rev. 101, 295 (1956).

Da72 J. R. Davis and G. U. Din, Nucl. Phys. A127, 95 (1972).

Da54 R. B. Day and T. Huus, Phys. Rev. 95, 1003 (1954).

Di67 G. U. Din, M. A. Nagarajan and R. Pollard, Nucl. Phys. A93, 190 (1967).

Fe49 S. Fernbach, R. Serber and T. B. Taylor, Phys. Rev. 75, 1352 (1949).

Fe60 H. Feshbach, Nuclear Spectroscopy, Part B, p. 625, Academic Press, N.Y. (1960).

Fe66 H. Feshbach, "Doorway States," Nuclear Structure Study with Neutrons, North-Holland, Amsterdam (1966).

Fr68 E. Fredland and H. Verlager, Z. Phys. 211, 373 (1968).

Ga69 A. Gallman, F. Gibou and P. Fentz, Nucl. Phys. A123, 27 (1969).

Ge66 L. B. Geesaman, H. B. Knowles and J. B. Mead, Nucl. Phys. 88, 177 (1966).

Gi59 J. H. Gibbs and R. L. Macklin, Phys. Rev. 114, 571 (1959).

Gi64 V. Gillet and N. Vinh-Mau, Nucl. Phys. 54, 321 (1964).

Gl65 N. K. Glendenning, Phys. Rev. 137, B102 (1965).

Go74 D. R. Goosman, D. F. Geesaman, F. E. Cecil, R. L. McGrath, and P. Paul, Phys. Rev. C10, 1525 (1974).

Ho63 P. E. Hodgson, The Optical Model of Elastic Scattering, Oxford, G.B. (1963).

Hu54 R. Huby, Proc. Phys. Soc., A67, 1103 (1954).

Hu57 S. E. Hunt, R. A. Pope and W. W. Evans, Phys. Rev. 106, 1012 (1957).

Ja71 R. F. Jackson and H. R. Weller, Nucl. Phys. A160, 247 (1971).

Ja61 A. N. James, Nucl. Phys. 24, 675 (1961).

Je64 J. G Jenkin, L. G. Earwaker and E. W. Titterton, Nucl. Phys. A50, 516 (1964).

Ka38 P. L. Kapur and R. E. Peierls, Proc. Roy. Soc. [London] A166, 377 (1938).

La58 A. M. Lane and R. G. Thomas, Revs. Mod. Phys. 30, 257 (1958).

La57 R. D. Lawson and J. L. Uretsky, Phys. Rev. 108, 1300 (1957).

Le52 R. E. LeLevier and D. S. Saxon, Phys. Rev. 87, 40 (1952).

Lo69 J. M. Lombaard, E. Friedland and H. Verleger, Z. Phys. 219, 124 (1969).

Mc68 I. E. McCarty, Introduction to Nuclear Physics, J. Wiley and Sons, N.Y. (1968).

Me74 M. R. Meder and J. E. Purcell, Phys. Rev. C10, 84 (1974).

Me58 A. Messiah, Quantum Mechanics, Vol. II, North-Holland, Amsterdam (1958).

Mo73 T. Mo and H. R. Weller, Phys. Rev. C8, 972 (1973).

Ne71 P. H. Nettles, C. Barnes, D. Hensley, and C. Goodman, Bull. Am. Phys. Soc. 16, 489 (1971).

Ot71 W. R. Ott, Ph.D. dissertation, University of Florida (1971).

Ov62 J. C. Overley and W. Whaling, Phys. Rev. 128, 315 (1962).

Ov63 J. C. Overley, Nucl. Phys. 49, 537 (1963).

Pa66 L. Parish, J. Rawlins and Y. Shin, Bull. Am. Phys. Soc. 11, 27 (1966).

Pa68 J. Y. Park, Nucl. Phys. A111, 433 (1968).

Pe65 R. H. Pehl, E. Rivet, J. Cerney, and B. G. Harvey, Phys. Rev. 137, B114 (1965).

Pu74 J. E. Purcell and M. R. Meder, Phys. Rev. C10, 89 (1974).

Pu63 K. N. Purser and B. H. Wilderthal, Nucl. Phys. 22, 44 (1963).

Ra70 J. J. Ramirez, Ph.D. dissertation, University of Florida (1970).

Ra72 G. H. Rawitscher, Phys. Rev., C6, 1212 (1972).

Ri66 E. Rivet, R. Pehl, J. Cerny, and B. G. Harvey, Phys. Rev. 141, 1021 (1966).

Ro64 H. J. Rose, F. Riess and W. Trost, Nucl. Phys. 52, 481 (1964).

Ro59 M. Rotenbert, N. Metropolis, R. Bivens, and J. K. Wooten, Jr., The 3-j and 6-j Symbols, Technology Press, Mass. (1959).

Se70 D. L. Sellin, private communication.

Sh53 E. S. Shire, J. R. Wormald, G. Lindsay-Jones, A. Lunden, and A. G. Stanley, Phil. Mag. 44, 1197 (1953).

So67 A. Soga, Bull. Am. Phys. Soc. 12, 501 (1967).

Ta65 T. Tamura, Revs. Mod. Phys. 37, 679 (1965).

Ta67 T. Tamura, Oak Ridge National Laboratory publication 4152 (1967).

Th65 V. K. Thankappan and W. W. True, Phys. Rev. 137, B793 (1965).

Th66 V. K. Thankappan, Phys. Rev. 41, 957 (1966).

Tr63 W. W. True, Phys. Rev. 130, 1530 (1963).

Va73 L. Vander Zwan and K. W. Geiger, Nucl. Phys. A216, 188 (1973).

Vi62 N. Vinh-Mau and G. E. Brown, Nucl. Phys. 29, 89 (1962).

Vo62 E. Vogt, Revs. Mod. Phys. 34, 723 (1962).

Wa59 A. H. Wapstra, G. J. Nygh, R. van Lieshout, Nuclear Spectroscopy Tables, p. 16, North-Holland, Amsterdam (1959).

Wa68 H. R. Weller, Ph.D. dissertation, Duke University (1968).

We69 H. R. Weller, Phys. Lett. 30B, 409 (1969).

We72 H. R. Weller, Phys. Rev. Lett. 28, 247 (1972).

Wi47 E. P. Wigner and L. Eisenbud, Phys. Rev. 72, 29 (1947).

Wi66 K. Wildermuth and W. McClure, Springer Tract in Modern Physics, Vol. 41, Springer-Verlag, N.Y. (1966).

Wi75 S. L. Wilson, Phys. Rev. C11, 1071 (1975).

Wo54 R. D. Woods and D. S. Saxon, Phys. Rev. 95, 577 (1954).

BIOGRAPHICAL SKETCH

David Ronald Griggs was born on April 19, 1950, in Jacksonville, Florida. He graduated from N.B. Forrest High School in 1967 as valedictorian. Mr. Griggs received a B.S. degree with high honors from the University of Florida in 1971 and began graduate school that same year. While doing his graduate studies, he was supported by both teaching and research assistantships and received a University of Florida Graduate School Fellowship for two years. He is still alive.

I certify that I have read this study and that in my opinion it conforms to acceptable standards of scholarly presentation and is fully adequate, in scope and quality, as a dissertation for the degree of Doctor of Philosophy.

Henry R Weller

Henry R. Weller, Chairman
Associate Professor of Physics
and Astronomy

I certify that I have read this study and that in my opinion it conforms to acceptable standards of scholarly presentation and is fully adequate, in scope and quality, as a dissertation for the degree of Doctor of Philosophy.

Richard A Blue

Richard A. Blue
Associate Professor of Physics
and Astronomy

I certify that I have read this study and that in my opinion it conforms to acceptable standards of scholarly presentation and is fully adequate, in scope and quality, as a dissertation for the degree of Doctor of Philosophy.

F. E. Dunnam, for

Charles F. Hooper
Professor of Physics and
Astronomy

I certify that I have read this study and that in my opinion it conforms to acceptable standards of scholarly presentation and is fully adequate, in scope and quality, as a dissertation for the degree of Doctor of Philosophy.

E D Adams

Earnest D. Adams
Professor of Physics and
Astronomy

I certify that I have read this study and that in my opinion it conforms to acceptable standards of scholarly presentation and is fully adequate, in scope and quality, as a dissertation for the degree of Doctor of Philosophy.

Luis J Muga

for David A. Micha
Professor of Chemistry

This dissertation was submitted to the Graduate Faculty of the Department of Physics and Astronomy in the College of Arts and Sciences and to the Graduate Council, and was accepted as partial fulfillment of the requirements for the degree of Doctor of Philosophy.

August, 1977

Dean, Graduate School

#544. [illegible] Bd (137)

OM33 7.7. 3.104.